UNIVERSITY OF ILLINOIS
URBANA

AERONOMY REPORT NO. 80

ROCKET OBSERVATIONS OF ELECTRON-DENSITY IRREGULARITIES IN THE EQUATORIAL IONOSPHERE BELOW 200 KM

by
D. E. Klaus
L. G. Smith

June 1, 1978

Library of Congress ISSN 0568-0581

Supported by
National Aeronautics and Space Administration
Grant NGR 14-005-181

Aeronomy Laboratory
Department of Electrical Engineering
University of Illinois
Urbana, Illinois

CITATION POLICY

The material contained in this report is preliminary information circulated rapidly in the interest of prompt interchange of scientific information and may be later revised on publication in accepted aeronomic journals. It would therefore be appreciated if persons wishing to cite work contained herein would first contact the authors to ascertain if the relevant material is part of a paper published or in process.

UILU-ENG 78 2502

A E R O N O M Y R E P O R T
N O. 80

ROCKET OBSERVATIONS OF ELECTRON-DENSITY IRREGULARITIES IN THE EQUATORIAL IONOSPHERE

by

D. E. Klaus
L. G. Smith

June 1, 1978

Supported by
National Aeronautics and
Space Administration
Grant NGR 14-005-181

Aeronomy Laboratory
Department of Electrical Engineering
University of Illinois
Urbana, Illinois

ABSTRACT

Three Nike Apache rockets carrying instrumentation to measure electron density and its fine structure in the equatorial ionosphere were launched from Chilca, Peru in May and June 1975. The fine structure experiment and the data reduction system are described. Results obtained from this system are presented and compared with those obtained by VHF radar and from other rocket studies. A description of the equatorial ionosphere and its features is also presented.

TABLE OF CONTENTS

Page

LIST OF TABLES

LIST OF FIGURES

1. INTRODUCTION

The equatorial ionosphere is particularly interesting for the presence of irregularities in electron density. These occur over a wide range of sizes; some give rise to the characteristic equatorial sporadic-*E* echoes on ionograms; others produce spread-*F* echoes. Important studies of these phenomena have been conducted using ground-based radio experiments. Rockets, however, provide a method of making *in situ* observations, thus complementing the radio experiments.

Until recently the principal systematic investigations had been VHF radar experiments conducted at Jicamarca, Peru, and rocket launches from Thumba, India. In 1973 a rocket launch site was developed at Chilca, Peru, slightly south of the geomagnetic equator (magnetic dip 0.8°N). The location of this site is shown, in Figure 1.1, in relation to metropolitan Lima and to the radio observatory at Jicamarca. The geographic coordinates of the launch site are 12.5°S and 76.8°W. The site is sometimes called the Punta Lobos range.

The Chilca range was first used in 1974 for an investigation of equatorial spread-*F*. The project, sponsored by the U.S. Air Force, was given the code name Equion.

The following year a more comprehensive program was undertaken under NASA sponsorship. The operation carried the code name Antarqui. Twenty-two sounding rockets were launched during the period 23 May to 7 June 1975, as indicated in Table 1.1. This study of the structure included rocket measurements of the neutral and ionized atmosphere, electron density and temperature, energetic particles, fields and wind. Measurements were also made from balloons. Many of the observations were coordinated with ground-based experiments and with the Atmospheric Explorer-C satellite.

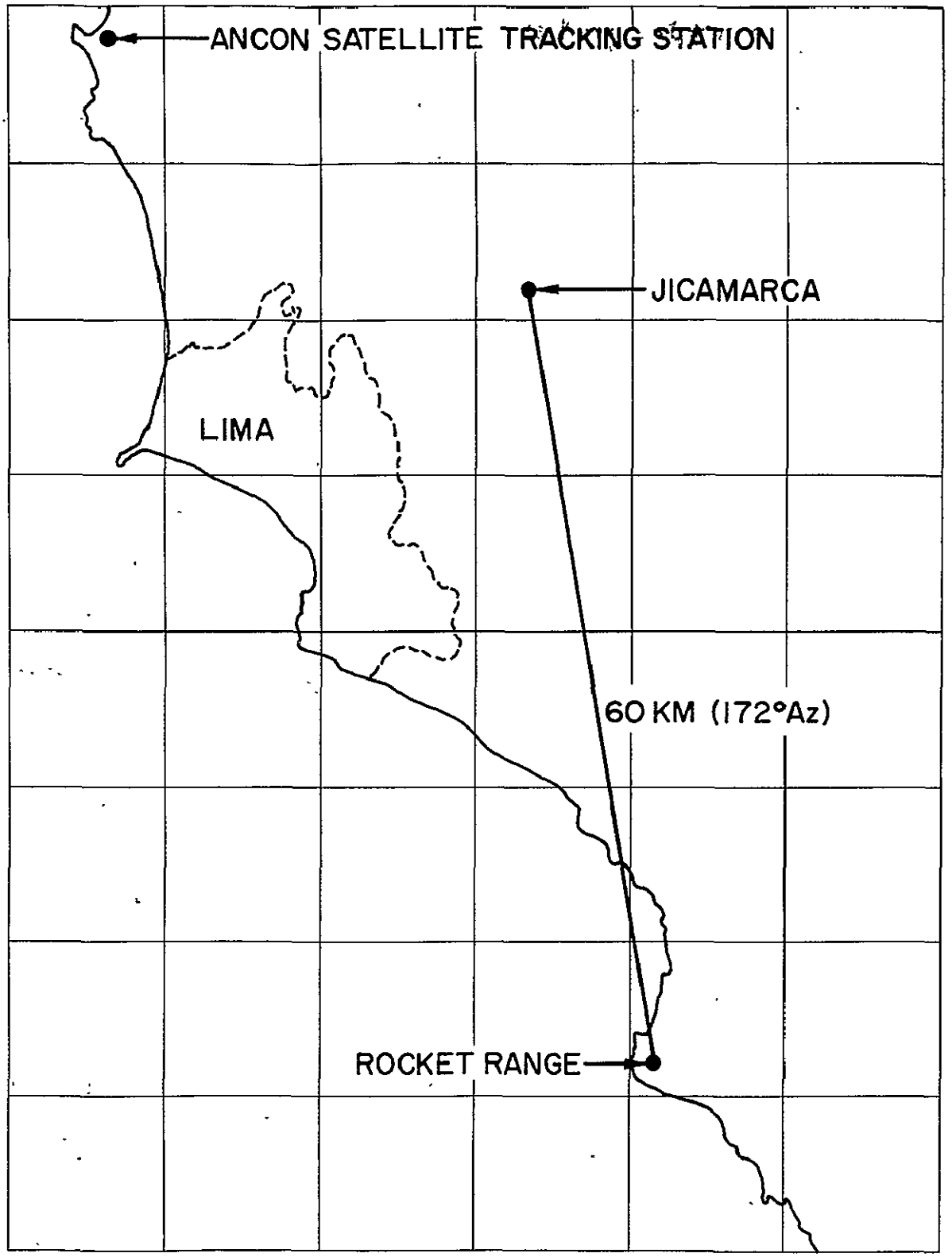

Figure 1.1 Location of the Chilca rocket range in relation to metropolitan Lima, the radio observatory at Jicamarca and the satellite tracking station at Ancon.

Table 1.1

Sounding Rockets Launched during Project Antarqui 1975

Date	LST	Rocket	Experiment	Project Scientist
23 May	2000	18.170	Energetic particles	R. A. Goldberg
23 May	2005	15.139	Ion conductivity	L. C. Hale
23 May	2052	15.133	Ozone	E. Hilsenrath
24 May	0155	18.171	Energetic particles	R. A. Goldberg
24 May	0205	15.140	Ion conductivity	L. C. Hale
24 May	0244	15.134	Ozone	E. Hilsenrath
24 May	0342	15.135	Ozone	E. Hilsenrath
24 May	0924	1-7743	Ozone	A. J. Krueger
24 May	1400	1-7742	Ozone	A. J. Krueger
25 May	1444	1-7744	Ozone	A. J. Krueger
27 May	0301	14.530	Particulates	C. L. Hemenway
27 May	1402	14.531	Particulates	C. L. Hemenway
28 May	1430	15.142	Ion conductivity	L. C. Hale
28 May	1526	14.532	Ionosphere	L. G. Smith
28 May	1616	15.141	Ion conductivity	L. C. Hale
29 May	2336	14.524	Ionosphere	L. G. Smith
31 May	2255	14.538	Neutral composition	E. C. Zipf, Jr.
02 June	0011	14.525	Ionosphere	L. G. Smith
03 June	1114	18.149	Fields	N. C. Maynard
03 June	1141	14.540	Neutral winds	J. F. Bedinger
07 June	1107	18.150	Fields	N. C. Maynard
07 June	1145	14.541	Neutral winds	J. F. Bedinger

Vehicle identification: 1- Super Loki; 14. Nike Apache; 15. Super Arcas; 18. Nike Tomahawk.

The Aeronomy Laboratory, Department of Electrical Engineering, University of Illinois at Urbana-Champaign, participated in three Nike Apache rocket launches. One, launched in the daytime, carried instrumentation to measure electron density, electron-density fine structure and electron temperature. The latter quantity was measured by two independent probes, one an RF resonance probe prepared by K. Hirao and K. Oyama, University of Tokyo. A satisfactory comparison of data from the two probes with each other and with data from Jicamarca has been made [*Smith et al.*, 1978].

The other two payloads were instrumented for measurement of energetic particles in place of the electron temperature experiments and were launched near local midnight. These particle measurements have been the subject of another study [*Voss and Smith*, 1977].

In the present report the observations obtained of electron density and its fine structure will be presented, including data from the daytime flight and the two nighttime flights. These are compared with earlier data from rockets launched at Thumba and with VHF radar data from Jicamarca.

Chapter 2 of this report describes the equatorial ionosphere and its features. The electrojet is discussed in connection with experimental studies such as ground-based, rocket, and satellite measurements. Equatorial sporadic *E*, an effect of the electrojet, and investigations into its structure are described. VHF radar studies and *in-situ* rocket measurements of irregularities are also presented.

The experimental technique used to measure the electron density and fine structure is discussed in Chapter 3. It is based on the Langmuir probe, the theory of which is presented. The fine structure experiment is described in some detail including the circuit design and performance characteristics. Each section of the data reduction process is discussed as to its function

and features. The calibration procedure followed to achieve accuracy and uniformity is explained at the end of the chapter.

Chapter 4 presents the electron-density profiles for all three flights including related material from ionograms and f-plots. The results of the fine structure experiment are presented and discussed.

Chapter 5 consists of a summary of the report and suggestions for possible improvements in the fine structure experiment. The conclusions of this study are presented.

2. EQUATORIAL IONOSPHERE

The ionosphere refers to the region of the earth's upper atmosphere in which free electrons exist in such amounts so as to significantly affect the propagation of radio waves. The ionosphere extends upwards from an altitude of approximately 50 km in the daytime and 80 km at night until it merges with the magnetosphere. The ionosphere is conventionally divided into three parts: the *D* region (below 90 km), the *E* region (between 90 and 160 km), and the *F* region (above 160 km).

The equatorial ionosphere is unique because it is here that the earth's magnetic lines of force are nearly horizontal. The result is an anomaly in the dynamo-generated electric current system. This is the equatorial electrojet and in the daytime flows eastward in an approximately 700-km wide band centered on the magnetic equator. The equatorial electrojet is contained in the *E* region and has a maximum current in the altitude range 105 to 110 km.

2.1 *Equatorial Electrojet*

2.1.1 *Ground-based magnetic field measurements.* The history of the atmospheric dynamo dates from 1722 when Graham discovered certain regular daily variations in a compass needle. In 1922 a geomagnetic observatory was constructed at Huancayo, Peru, near the dip equator, and it was found that the diurnal range in the horizontal magnetic field component (*H*) was abnormally large there. Further investigations were carried out by *Egedal* [1947, 1948] who made observations of *H* at six stations located near the equator. These observations when plotted against dip latitude showed a sharply peaked curve about the dip equator. Egedal attributed this enhancement to a 300-km wide electric current flowing in a very narrow zone near the dip equator. Subsequent measurements were made in Uganda, Togo, Peru, Sudan, and India which proved that the enhancement could be found anywhere near the dip equator.

Chapman [1951] coined the term "equatorial electrojet" to describe the phenomenon. Much of the work done on the electrojet has dealt with ground-based magnetic field measurements. A typical example of these results is illustrated with Peruvian data in Figure 2.1. Here observations by *Forbush and Casaverde* [1961] are compared with a calculation by *Richmond* [1973]. The peak in ΔH occurs at the dip equator.

The electrojet current generally increases from sunrise, reaching a maximum at noon and then decreases until sunset (Figure 2.2). Large daily changes in intensity, position, and width are found with no apparent correlation between them. An experiment demonstrating the variability was performed by *Burrows* [1970] who used a latitude spread of seven magnetometers located close to the dip equator in Peru. The magnetic H variation was from 41γ to 198γ with an average value of 103γ. [$1\gamma \equiv 10^{-5}$G $\equiv 10^{-9}$T; the earth's total magnetic field $\approx$ 0.5G] The average width defined by values of ΔH of magnitude 0.75 of the peak (ΔH_{max}) is approximately 600 km. *Forbush and Casaverde* [1961] estimated a total width of 6° or about 660 km.

2.1.2 *Rocket measurements of magnetic field.* The ground-based magnetic field measurements provide much insight into the electrojet but cannot provide any information as to the vertical structure. Information on the vertical structure of the electrojet current has been obtained through measurements made by rocket-borne magnetometers [*Singer et al.*, 1951; *Cahill*, 1959]. The magnetometers measure the earth's magnetic field as the rocket flight progresses and simultaneously telemeter the information back to the ground where it is interpreted as the effect of an electric current superimposed on the geomagnetic field.

As part of NASA Mobile Launch Expedition to the coastal waters of Peru, *Maynard* [1967], *Davis et al.* [1967], and *Shuman* [1970] conducted rocket

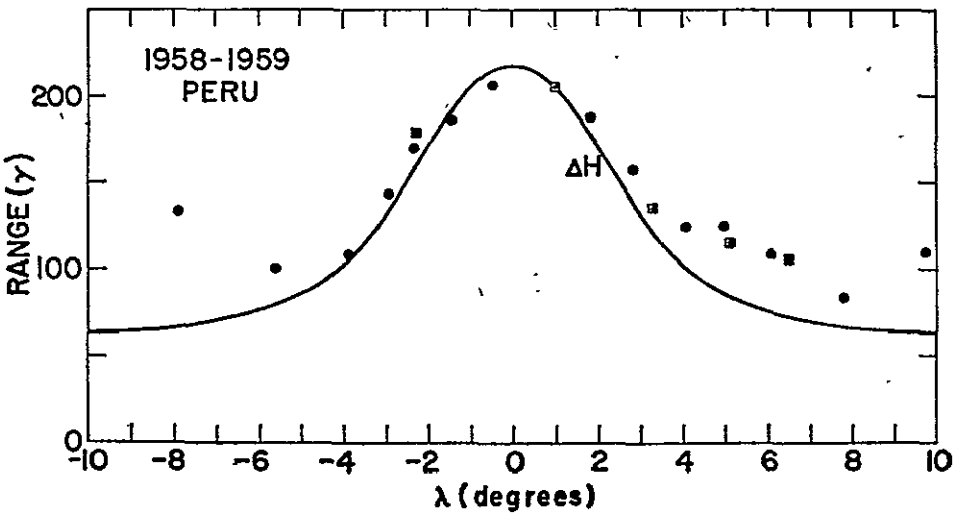

Figure 2.1 Observed (points) and computed (solid line) variations in H around midday in Peru, for equinox conditions in 1958 and 1959, as a function of geomagnetic latitude [after *Richmond*, 1973].

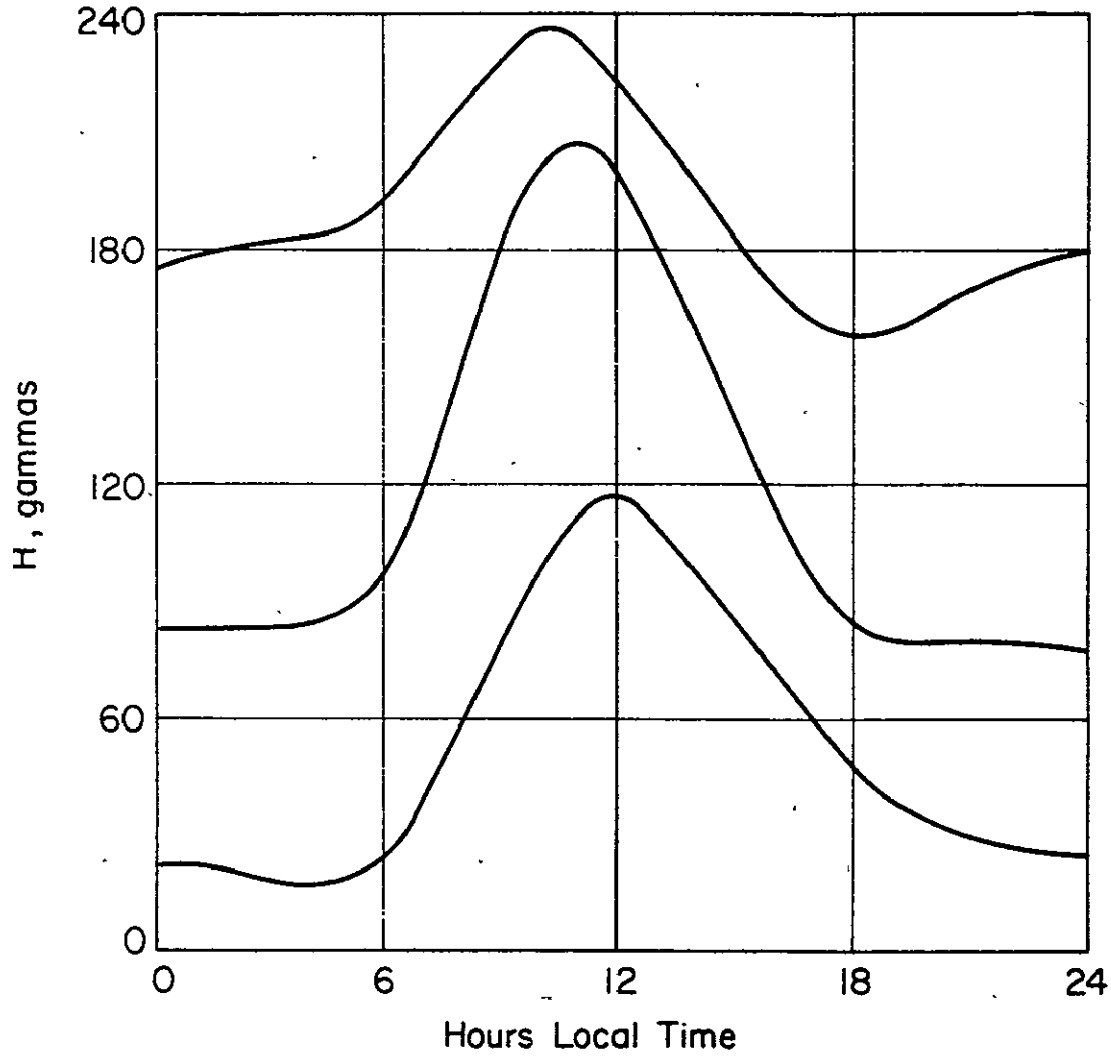

Figure 2.2 Three types of the diurnal variation of H observable near the electrojet on quiet days [after *Onwumechilli*, 1967].

flights to measure current density as a function of altitude. *Maynard* [1967] launched four rockets off the USNS Croatan--two near the magnetic dip equator and two to the north. His experiments showed an intense layer of current centered at 109 km with a more diffuse current up to about 140 km. The maximum altitude of the electrojet was observed to depend on the intensity.

Eight Nike Apache rocket flights conducted by *Davis et al.* [1967] in the same campaign showed a lower boundary of 87 km with a maximum current of 10 A km^{-2} at 107 km. A very small ionospheric current was also seen at night in the opposite direction from the eastward daytime current.

Shuman [1970] also launched four Nike Apache rockets in March 1965 from the USNS Croatan but found no evidence of current at night. The result of an equatorial launch during maximum electrojet showed 13.5 A km^{-2} at an altitude of 106 km. A plot of current versus altitude for six selected flights together with an average curve is shown in Figure 2.3 [*Richmond*, 1973], which also includes a computed curve. Two flights by *Burrows and Sastry* [1976] during a normal and an intense electrojet showed that total current increases in proportion to the magnetic effects observed on the ground. They also showed that the shape of the electrojet current profile does not change much when the intensity doubles.

2.1.3 *Satellite observations.* Between 1967 and 1970, the POGO-4 and 6 satellites made over 2000 transversals over the electrojet in an altitude range between 400 and 800 km when local times were near the electrojet maximum. These spacecraft carried total field magnetometers capable of making measurements to an accuracy of 2γ. The deviations of these measurements from an internal reference model were computed and were plotted for a 30° range of latitude about the geographic equator. The results showed a sharp negative V-signature some 16° to 19° in width and variable in amplitude with position

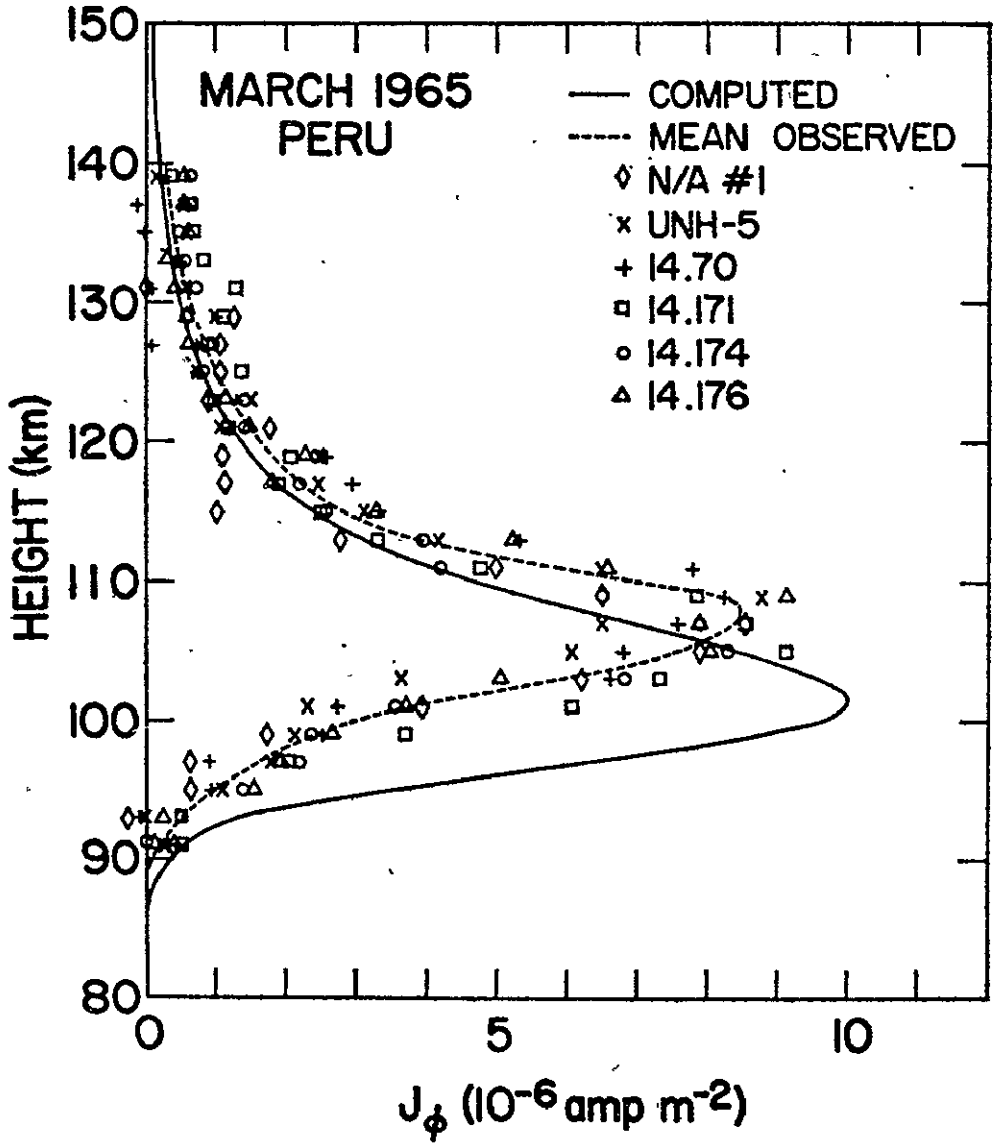

Figure 2.3 Computed eastward current density profile near noon at the dip equator compared with observations from six rocket flights. The currents are normalized to correspond to 100 γ variation in H at Huancayo [*Richmond*, 1973].

and time (Figure 2.4). The position of the minimum (corresponding to current maximum) was found to lie within 0.5° of dip equator [*Cain and Sweeney*, 1973]. A comparison of scatter diagrams of POGO amplitudes and surface data for India, Africa, South America and the Phillipines show a very good correlation on the average but also numerous exceptions [*Cain et al.*, 1973].

2.1.4 *Cause and parameters.* A world-wide system of electric fields and currents exists in the ionosphere driven by the dynamo action of the atmospheric tides acting in the presence of the geomagnetic field. Charged particles are dragged across the lines of forces and a resulting charge separation creates electric fields. The horizontal current is essentially restricted to the *E* region where the conductivity is the greatest. The *E* region currents are particularly intense at the geomagnetic equator and in the auroral zone. At the dip equator an east-west electric field tries to create a vertical current but is prevented from doing so by the insulating layers above and below where the conductivity is small. This creates a vertical polarization field which now drives a strong horizontal Hall current; this is the electrojet. The properties of the equatorial electrojet are summarized in Table 2.1, from *Farley* [1971].

2.2 *Equatorial Sporadic* E

Sporadic *E* is a phenomenon seen in ionograms in which a strong echo is returned from an altitude of about 100 km. Its principal characteristic is that the virtual height is essentially independent of the frequency of the probing radio wave over a large range of frequency. The phenomenon is observed at all latitudes but three zones are defined which are now known to be different causes; midlatitude sporadic *E* results from concentration of metallic ions in thin layers under the action of a shear in the neutral wind; sporadic *E* in the auroral zone is an effect of particle precipitation;

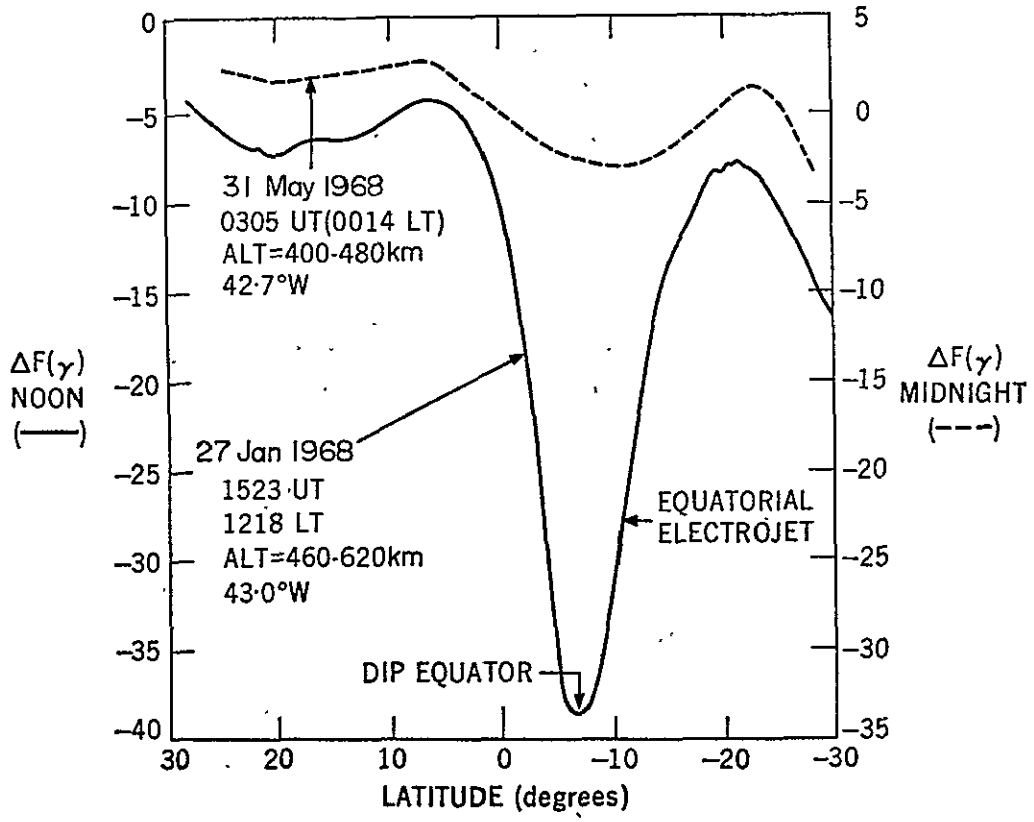

Figure 2.4 'Ideal' ΔF variation of observed field after subtracting an internal reference model. Shown are two separate traversals over the middle Atlantic and eastern Brazil. Solid curve is a daytime pass showing the 'V' signature due to the equatorial electrojet; the dotted curve is from a near midnight traversal showing no electrojet. [*Cain and Sweeney*, 1973]

Table 2.1

Average Characteristics of the Equatorial Electrojet

Electron density:	10^{5} cm^{-3}
Magnetic field:	0.3 G
E-W electric field:	10^{-3} V m^{-1}
Electron drift velocity:	500 m s^{-1}
Ion thermal velocity:	350 m s^{-1}
Current density:	10^{-5} A m^{-2}
Height-integrated current density:	10^{2} A km^{-1}

equatorial sporadic *E* is the radio-wave scattering phenomenon occurring in the *E* region due to electron-density irregularities.

Equatorial sporadic *E*, termed *Es-q*, is found in the electrojet region and is readily distinguishable from other types of sporadic *E*. Equatorial sporadic *E* is largely transparent to probing radio waves and rarely blankets waves reflecting from higher regions; midlatitude sporadic *E* usually obscures part of the higher layers. An ionogram taken in Huancayo, Peru (Figure 2.5) illustrates the various features of *Es-q*. This *Es-q* is seen as a well-defined lower edge at around 100 km with diffuse echoes appearing above this sharp lower boundary. The ionogram also shows an example of equatorial slant sporadic *E* designated *Es-s*. This results from oblique reflections from the layer.

The observation of equatorial sporadic *E* has been suggested as being related to the presence of the equatorial electrojet [*Matsushita*, 1951]. *Knecht and McDuffie* [1962] conducted an experiment which verified this relationship. In the period of July 1957 to June 1959 seven closely-spaced ionospheric vertical sounding stations were operated near the magnetic equator in Peru and Bolivia. Figure 2.6 shows the average percentage occurrence of *Es-q* during daylight hours at each of the stations. These data show a full width at half maximum of about 11° in dip angle, or about 700 km, essentially the same width obtained for the electrojet from magnetometer data. This study also showed that blanketing sporadic *E* of the midlatitude type occurred in an equatorial zone even narrower than the electrojet.

A further verification of the relationship between *Es-q* and the electrojet was given by *Bowles and Cohen* [1962] with a radio-wave forward scattering experiment in South America. A continuous wave of 50 MHz was scattered from the ionosphere at locations at magnetic dip angles of 8°N, 1°N (Huancayo), and 8°S. Strong scatter propagation was observed during

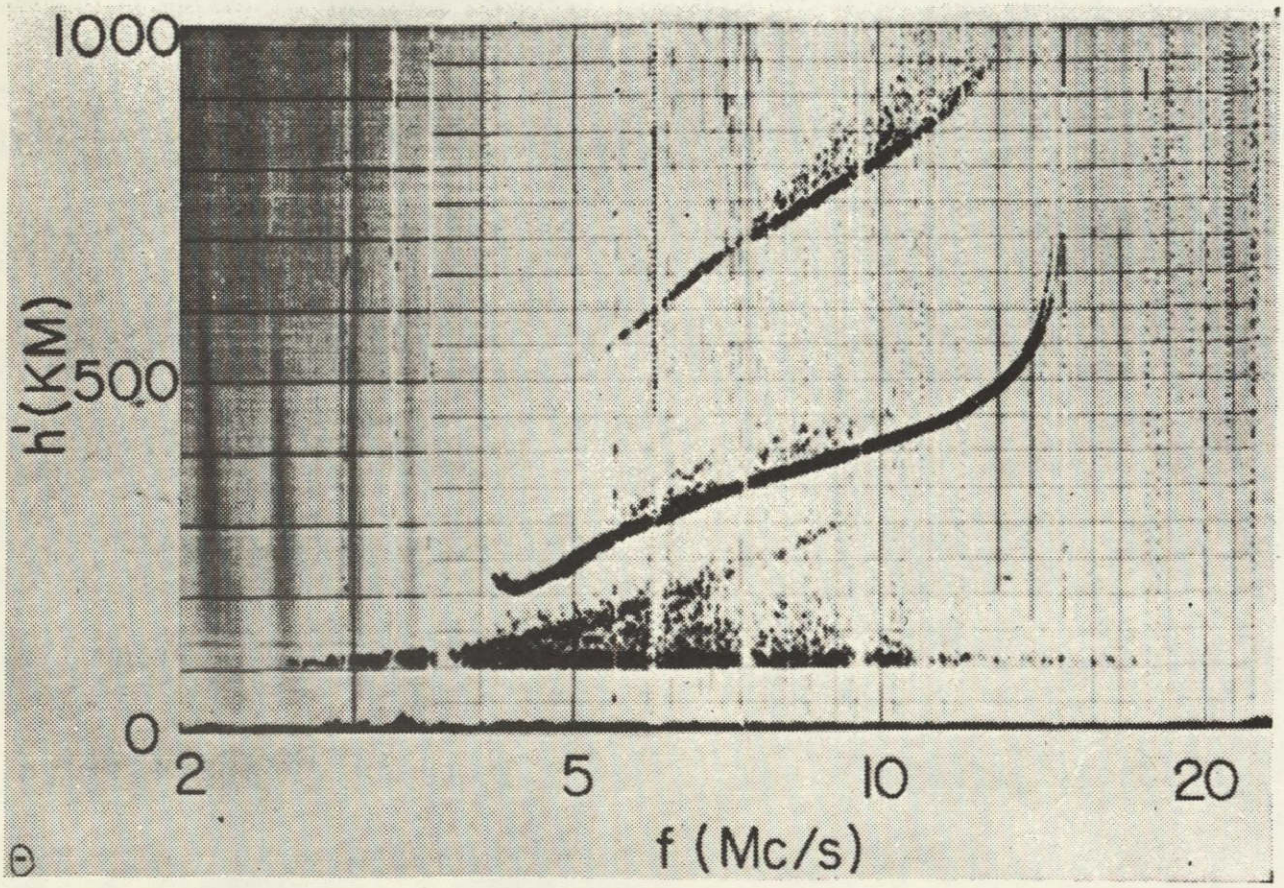

Figure 2.5 Ionogram recorded at Huancayo at 1229 EST on 19 April 1960 showing equatorial sporadic *E* and equatorial slant sporadic *E* [*Bowles and Cohen*, 1962].

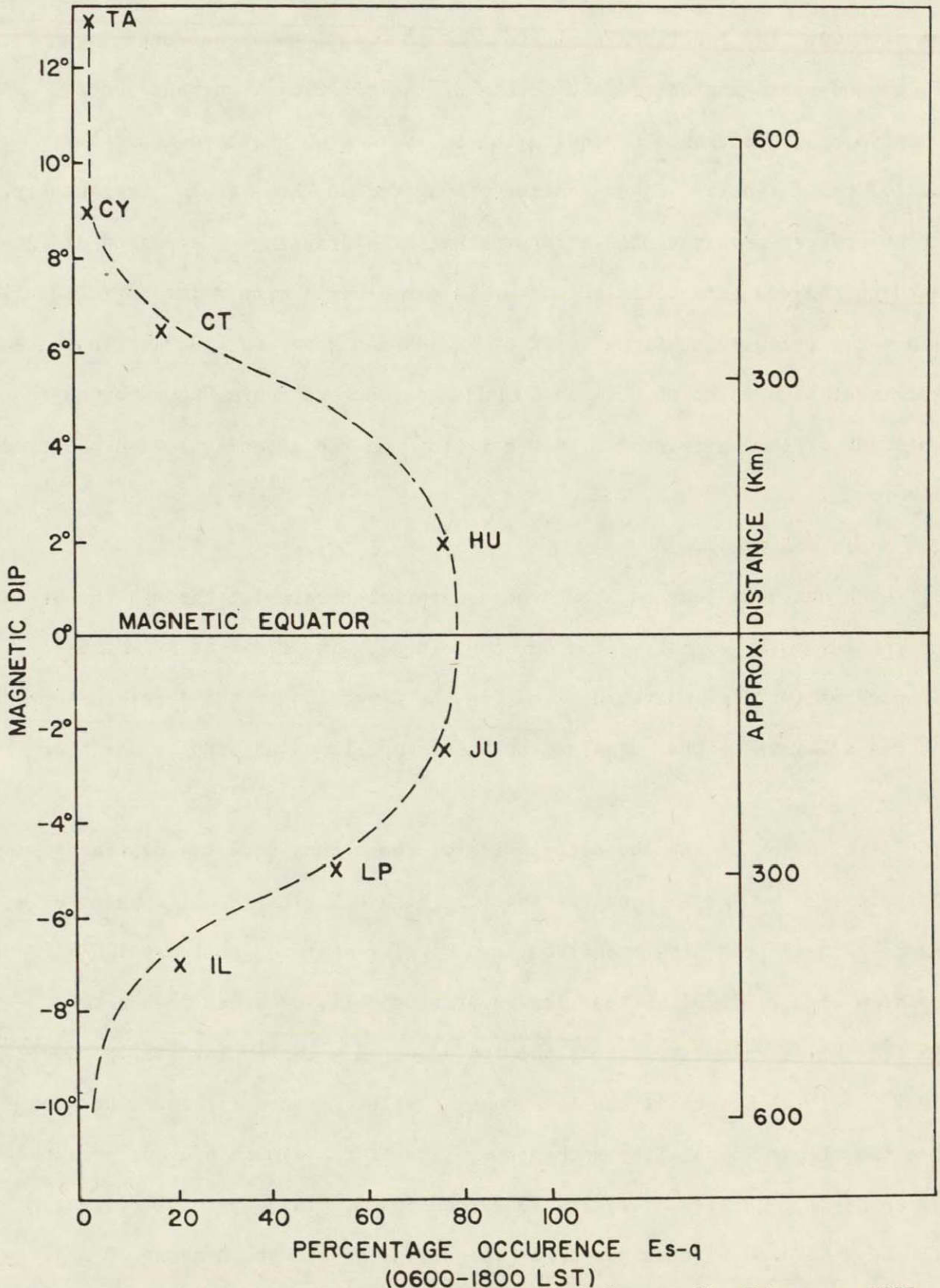

Figure 2.6 Percentage occurrence of equatorial sporadic *E* between 0600 and 1800 LST along a chain of vertical sounding stations [*Knecht and McDuffie*, 1962].

the daytime. The experiments showed a close relationship between: (1) ground-based magnetic measurements of the electrojet current above Huancayo, (2) occurrence of equatorial sporadic *E* on Huancayo ionograms, and (3) the intensity of the scatter-propagated 50 MHz signals. Frequently, strong scatter propagation similar to that of blanketing *Es* appeared at the northern and southern sites but never in the central site. This agrees well with the previously mentioned work of *Knecht and McDuffie* [1962]. In another experiment a correlation between 50 MHz radar echoes above Huancayo and the amplitude of the horizontal magnetic field *H* on the ground was also observed (Figure 2.7).

2.3 *Radar Observations*

Much has been learned about the equatorial electrojet through the use of VHF radar [*Bowles et al.*, 1963; *Balsley*, 1969]. The radar at 50 MHz is directed eastward or westward, i.e., in the direction of the electric current, and the scattered signal examined both for amplitude and Doppler shift of frequency.

Examination of the characteristics of the echoes show two distinct types characterized by the VHF Doppler spectra (Figure 2.8). Type I appears as a sharp spectral peak displaced from zero Doppler shift by at least 125 Hz [*Balsley et al.*, 1976]. These irregularities: (1) occur only when the electron drift velocity exceeds the ion-acoustic velocity (typically about 360 m s^{-1}); (2) travel at the ion-acoustic velocity; and (3) are generated by a two-stream instability mechanism. Type II has a much broader symmetrical spectrum generally averaging less than 50 Hz. These irregularities: (1) are generated by electron drift velocities greater than about 30 m s^{-1}; (2) move with the electrons; and (3) are produced by the gradient drift instability in regions of steep density gradients.

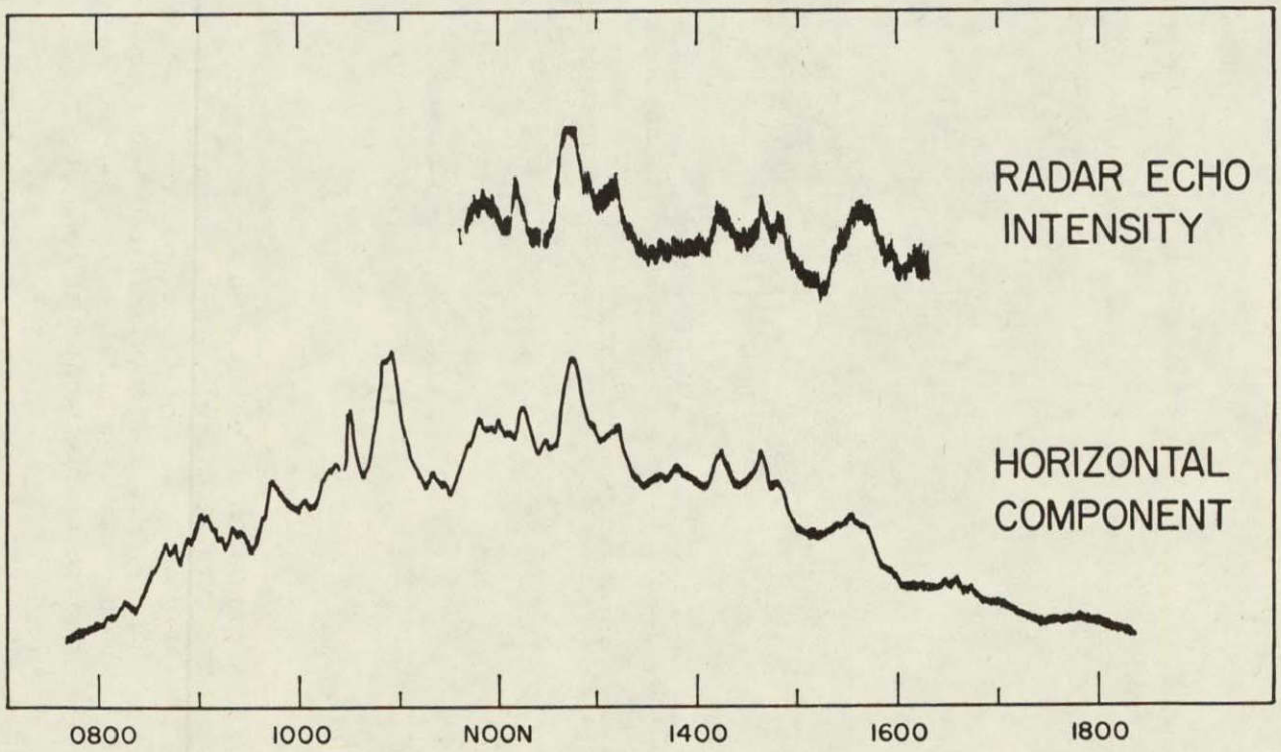

Figure 2.7 The intensity of 50 MHz radio echoes at vertical incidence from equatorial electrojet irregularities compared with *H* at Huancayo, 17 March 1960. The ordinates are nearly linear. [*Bowles and Cohen*, 1962]

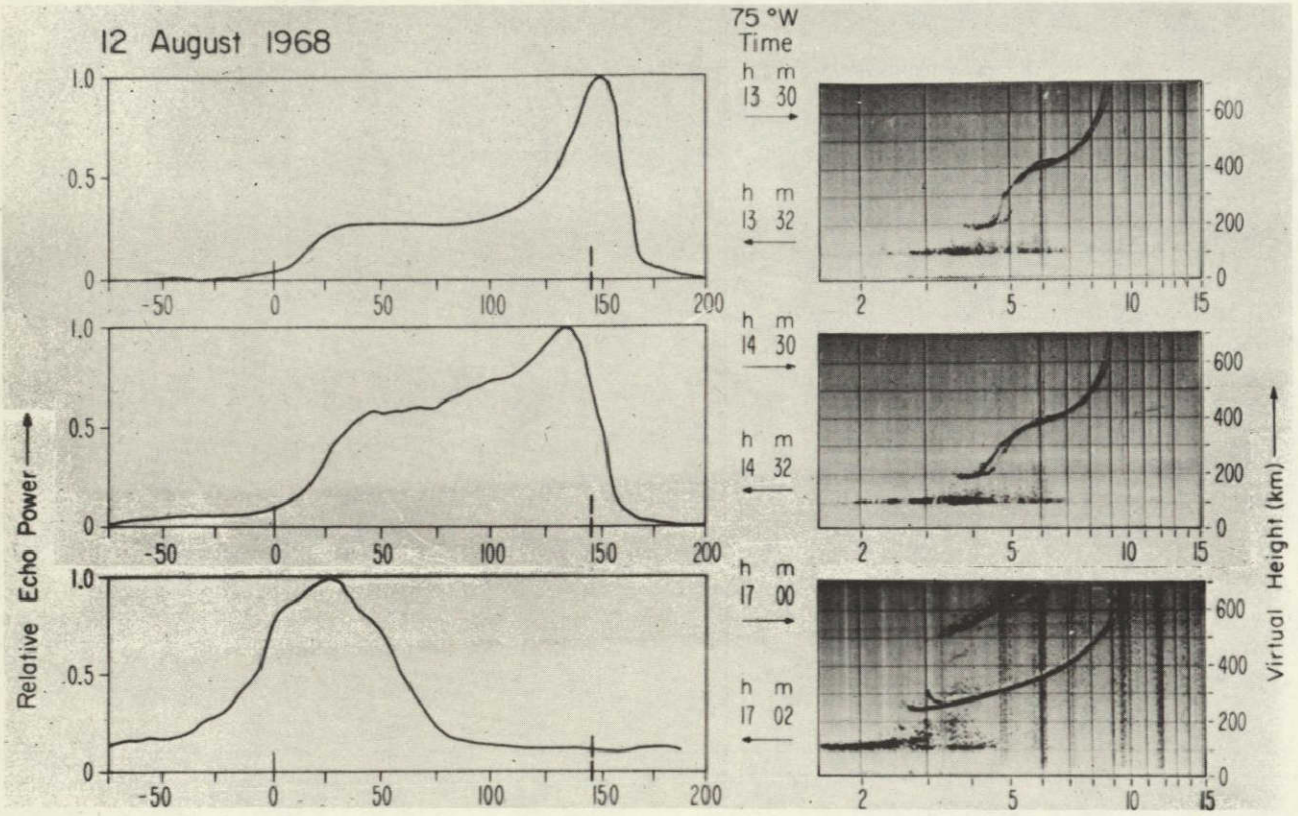

Figure 2.8 Comparison of oblique 50 MHz *E* region power spectra at Jicamarca with simultaneous ionograms at Huancayo. The first spectrum shows predominantly type I irregularities, the second includes both types; the third shows the presence of type II irregularities [after *Balsley et al.*, 1976].

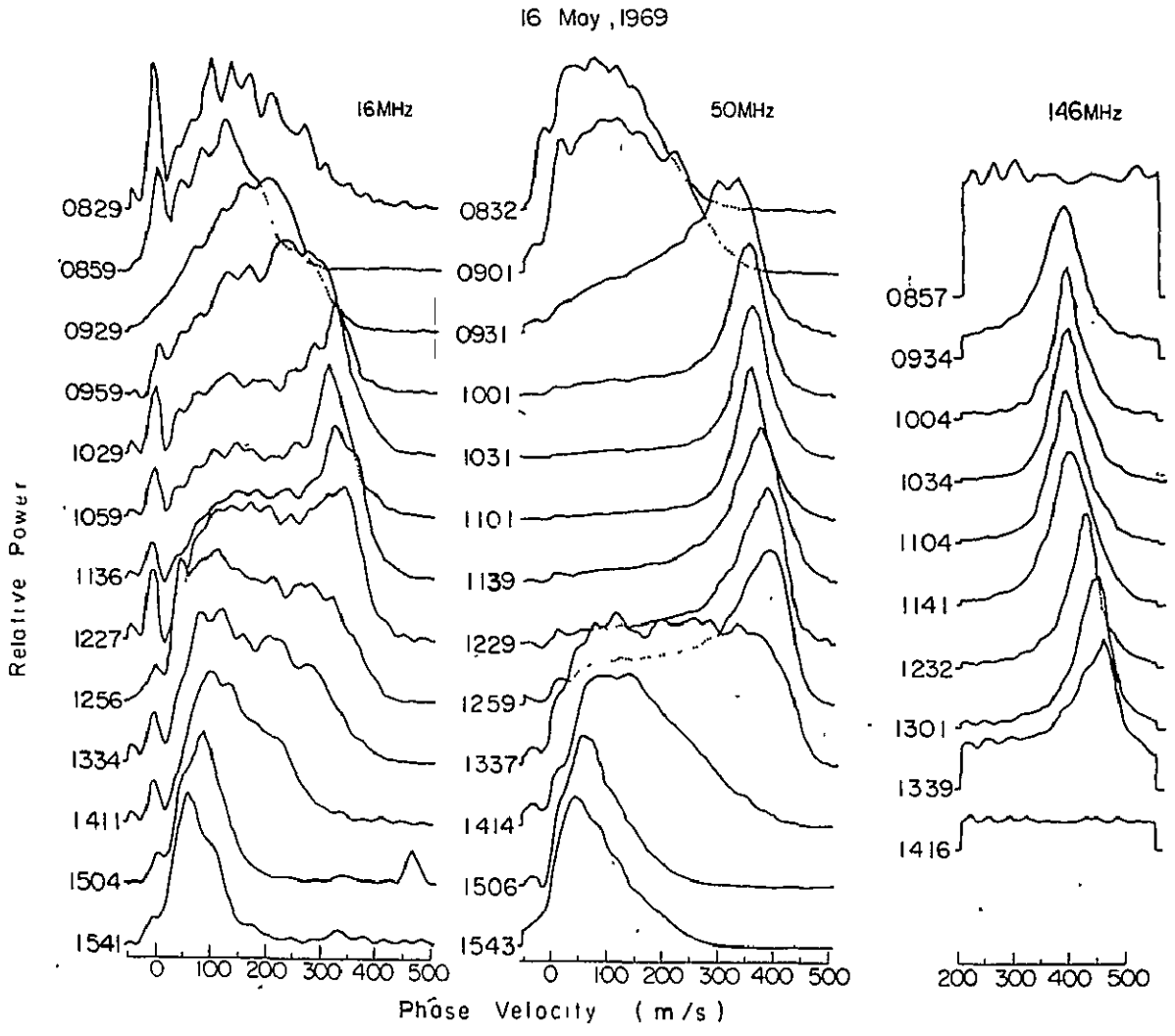

Figure 2.9 Doppler spectra from the equatorial electrojet obtained nearly simultaneously at three frequencies [*Balsley and Farley*, 1971].

Table 2.2

Rocket Launches from Thumba Investigating
Electron-Density Irregularities in the Equatorial Ionosphere

Vehicle	Date	Time (IST)	References
10.11	12 Mar 1967	1857	1,3,6
10.13	2 Feb 1968	1856	2,3,6,7,8,9,10
20.07	29 Aug 1968	1415	5,10
20.08	29 Aug 1968	2300	4,6,7,9,10
10.37	28 Jan 1971	1040	8,9,10
10.38	28 Jan 1971	1110	8,9,10
C05.16	17 Aug 1972	1532	11
10.44	13 Oct 1972	1259	10
10.45	3 Mar 1973	1220	10

Data from above flights contained in:

1. *Prakash et al.* [1968]
2. *Prakash et al.* [1969a]
3. *Prakash et al.* [1969b]
4. *Prakash et al.* [1970]
5. *Prakash et al.* [1971a]
6. *Prakash et al.* [1971b]
7. *Prakash et al.* [1971c]
8. *Prakash et al.* [1971d]
9. *Prakash et al.* [1972]
10. *Prakash et al.* [1973]
11. *Prakash et al.* [1976]

2.4.1 *Measurement technique*. To determine the various parameters associated with the irregularities, the following techniques were utilized [*Prakash et al.*, 1973]:

(1) Rocket-borne Langmuir probe

(2) Rocket-borne resonance probe

(3) Rocket-borne proton precession magnetometer

(4) Ground-based VHF backscatter radar

(5) Ground-based ionosonde and magnetometer

The Langmuir probe has been used to study the gradients in electron density and also the shape, size, and amplitude of the irregularities. This rocket-borne probe was developed at the Physical Research Laboratory, Ahmedabad, India [*Prakash and Subbaraya*, 1967]. The probe system itself was a modification of the original system conceived by *Smith* [1967]. The Langmuir probe system and its operation will be discussed in greater detail in Section 3.2.

A resonance probe experiment was utilized in order to determine absolute values of electron density. In this technique, developed by *Prakash et al.* [1972], an RF signal of varying frequency is applied to an exciter antenna located at the fins of the rocket. The received signal at the nose shows amplitude variations and several plasma resonances can be detected. From this information, the ambient electron density can be derived.

Current density was measured using a magnetometer similar to that used in the rocket flights discussed in Section 2.1. The rocket-borne magnetometer measures the resultant field due to the earth's magnetic field and the electrojet. When the effects of the earth's main magnetic field are eliminated, the slope of the resulting curve can be used to obtain a vertical

profile of ionospheric current density.

In order to compare the rocket measurements with ground observations, VHF backscatter radar and ionosonde measurements were concurrently made. These experiments were based on those used in the ground studies (i.e., Jicamarca radar) discussed previously. A ground-based magnetometer was also employed to measure ground effects due to the overhead electrojet.

2.4.2 *Observations of irregularities.* Based on observations from numerous rocket flights, *Prakash et al.* [1973] have classified the irregularities in the following manner:

(1) Type L: Large-scale irregularities

These irregularities have scale sizes of up to a few kilometers in the vertical direction and more than 40 km horizontally in the east-west direction. These irregularities were found only during nighttime flight 20.08 at 2300 hr IST in a region between 90 and 125 km. Early that evening sporadic *E* similar to that observed in the daytime was seen on Thumba ionograms whereas this was not the case on other nights. No suitable theory to explain type L irregularities has been found although cross-field instability and wind shears are two conjectures.

(2) Type Mc: Medium scalesize irregularities with vertical scalesizes of 30 to 300 m due to cross-field instability

These irregularities were observed in all rocket launches except one. They were found only in regions exhibiting a gradient in background electron density and have amplitudes of $\Delta N/N$ ranging from a few percent up to about 30%. During daylight and evening twilight hours the irregularities are found in regions of positive electron-density gradient while at night they occur in areas of negative electron-density gradients. In the day, type Mc

irregularities show a large amplitude (≈ 20%) around 85 km and then decrease with height to about 5% at 95 km. Rapid decrease in amplitude above this height is observed. A sawtooth-like vertical structure in irregularities is also seen giving the irregularities some definite shape (Flight 10.45). At night and twilight, the irregularities can be as large as 30% but are over a much larger region, typically from around 85 or 90 km to about 130 km. Generation of type Mc irregularity appears to be due to cross-field instability.

(3) Type Sc: Irregularities in 1 to 15 meter scalesize range due to cross-field instability

These irregularities generally co-exist with type Mc however their amplitudes are much smaller and reach a maximum amplitude of only a few percent. Some correlation appears between the characteristics of type Sc and type II irregularities observed with radar and it is thought that these might be the same. Type Sc irregularities, like type Mc, are also thought to be created by cross-field instability.

(4) Type Ss: Irregularities in 1 to 15 meter scalesize range due to two-stream instability

These irregularities are of the same size as those of type Sc but are only observed in the 105 km region around noontime at peak of electrojet. The spectrum of these irregularities is flat indicating that the various size Sc irregularities are of about the same amplitude. Thus these irregularities cannot be created through the decay of larger irregularities. The result is that type Ss irregularities appear to be caused by the streaming of electrons possibly in the form of the two-stream instability. Many similarities exist between type Ss and the type I irregularities observed with radar.

(5) Type Mn: Medium size 30 to 300 meter irregularities due to neutral turbulence

These irregularities occur only during the daytime and even then not on every flight. The amplitude of type Mn is larger at lower altitudes (10 to 15% at about 60 to 70 km) and then decreases as altitude increases (4 to 7% at 80 km). These irregularities of type Mn are probably due to neutral turbulence and wind shears.

(6) Type Sn: Small size 1 to 15 meter irregularities due to neutral turbulence

These irregularities are found with type Mn but have much smaller amplitudes--on the order of a few percent at maximum. The generating mechanism of these irregularities also appears to be neutral turbulence and wind shears.

2.5 *Equatorial Spread* F

2.5.1 *Ionosonde and radar observations.* Ionograms throughout much of the world have shown an evening and night phenomena in which the normally smooth *F* layer trace becomes diffused or spread (Figure 2.10). This feature is spread *F* and is due to electron-density irregularities in the *F* region which cause radio-wave scattering. Apparently two distinct types of spread *F* occur--one type with maximum occurrence at high latitudes and the other occurring mainly in the equatorial region. The area between 20° and 40° geomagnetic latitude rarely develops spread *F*. This discussion will be limited to the equatorial type of spread *F*.

Spread *F* is almost exclusively a nighttime phenomena, as can be seen in the graphs of Figure 2.11 [*Clemesha and Wright*, 1966], although irregularities sometimes exist for a short time after sunrise. After sunset, the *F* layer usually rises rapidly: in part only apparent and due to the loss of bottom-

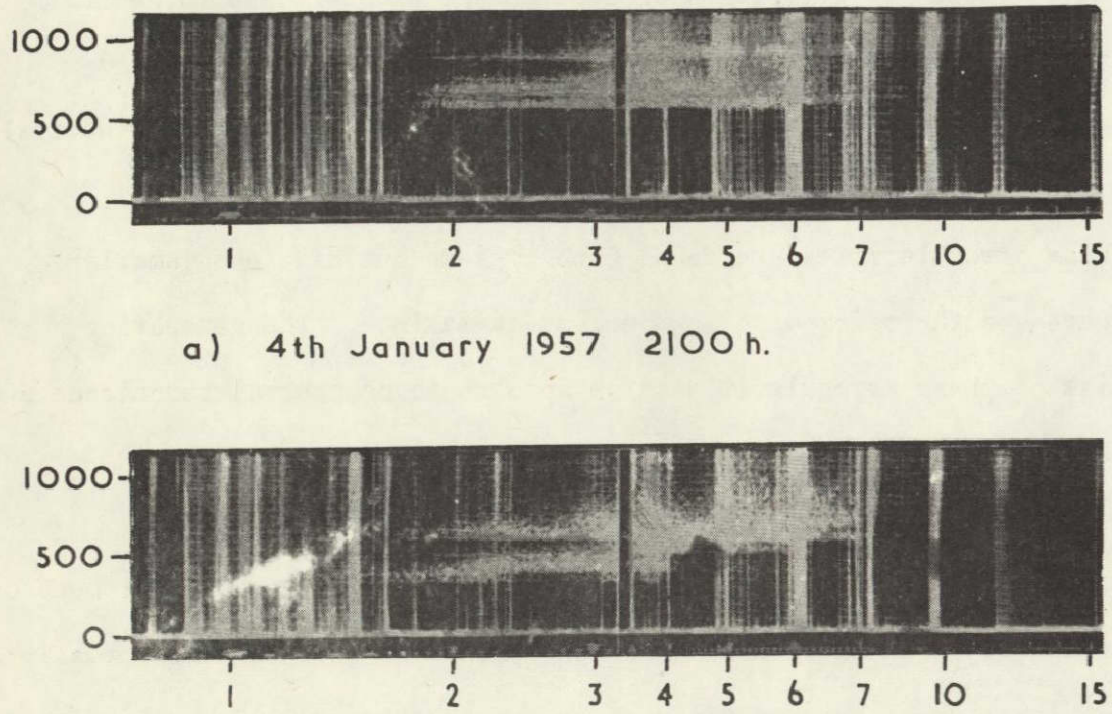

Figure 2.10 Examples of ionograms showing spread *F*, Ibadan [*Clemesha and Wright*, 1966].

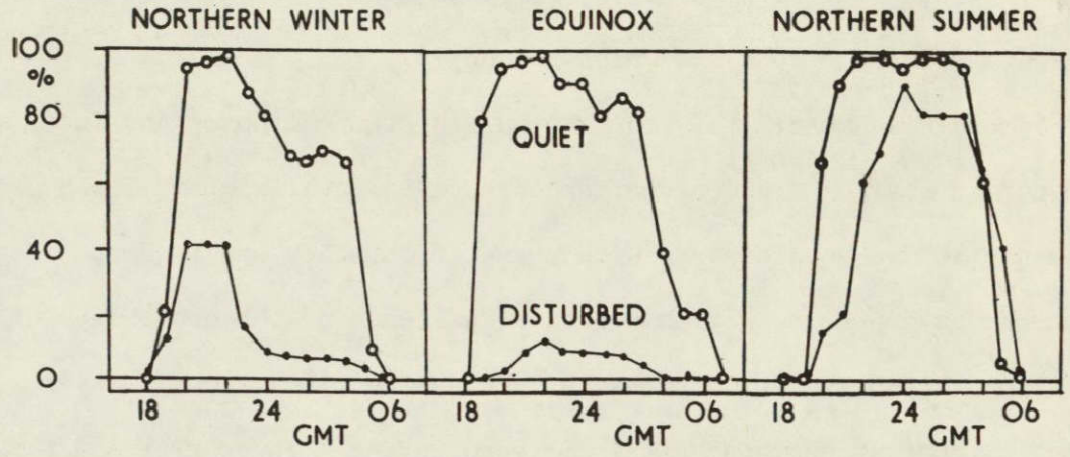

Figure 2.11 Percentage occurrence of spread *F*, Ibadan, 1957-8 [*Clemesha and Wright*, 1966].

side ionization through recombination and diffusion. A true upward velocity of the layer can also exist which can be as large as 60 m s^{-1}. Spread *F* usually appears within an hour or two of this rise although this depends on many factors such as season, solar activity, and magnetic disturbances [*Farley et al.*, 1970]. Ionograms illustrating the rapid development of spread *F* taken in Ibadan, Nigeria (very near the magnetic equator) are shown in Figure 2.12 [*Clemesha and Wright*, 1966].

Spread *F* is most likely to occur during the equinoxes and local summer with a much smaller frequency of appearance in local winter if the geographic and magnetic dip equators are widely spaced, as they are in Peru. Magnetic disturbances appear to have a negative influence on the occurrence of spread *F*. Also, this magnetic disturbance reduces the rise in the *F* layer after sunset further strengthening the tie between the *F* layer rise and the development of spread-*F* irregularities.

A strong correlation exists between the appearance of spread *F* on bottomside and topside ionograms, the scintillation of radio star and satellite signals, and with HF and VHF forward scatter and backscatter in the *F* region. The radio-wave measurements indicate that the electron-density irregularities are aligned with the earth's magnetic field lines with lengths of several km or more. The width of the irregularities perpendicular to the field ranges from a few meters to a few km. These irregularities usually seem to occur in patches having east-west dimensions in the range of 100 to 1000 km and thicknesses between 1 km, or less, and 100 km. The patches themselves drift to the east at a rate of about 100 to 200 m s^{-1} [*Farley et al.*, 1970]. Radar studies by *Farley et al.* [1970] using the 50 MHz Jicamarca radar indicate that the 3-m irregularities detected in the nighttime *F* region are closely associated with larger irregularities

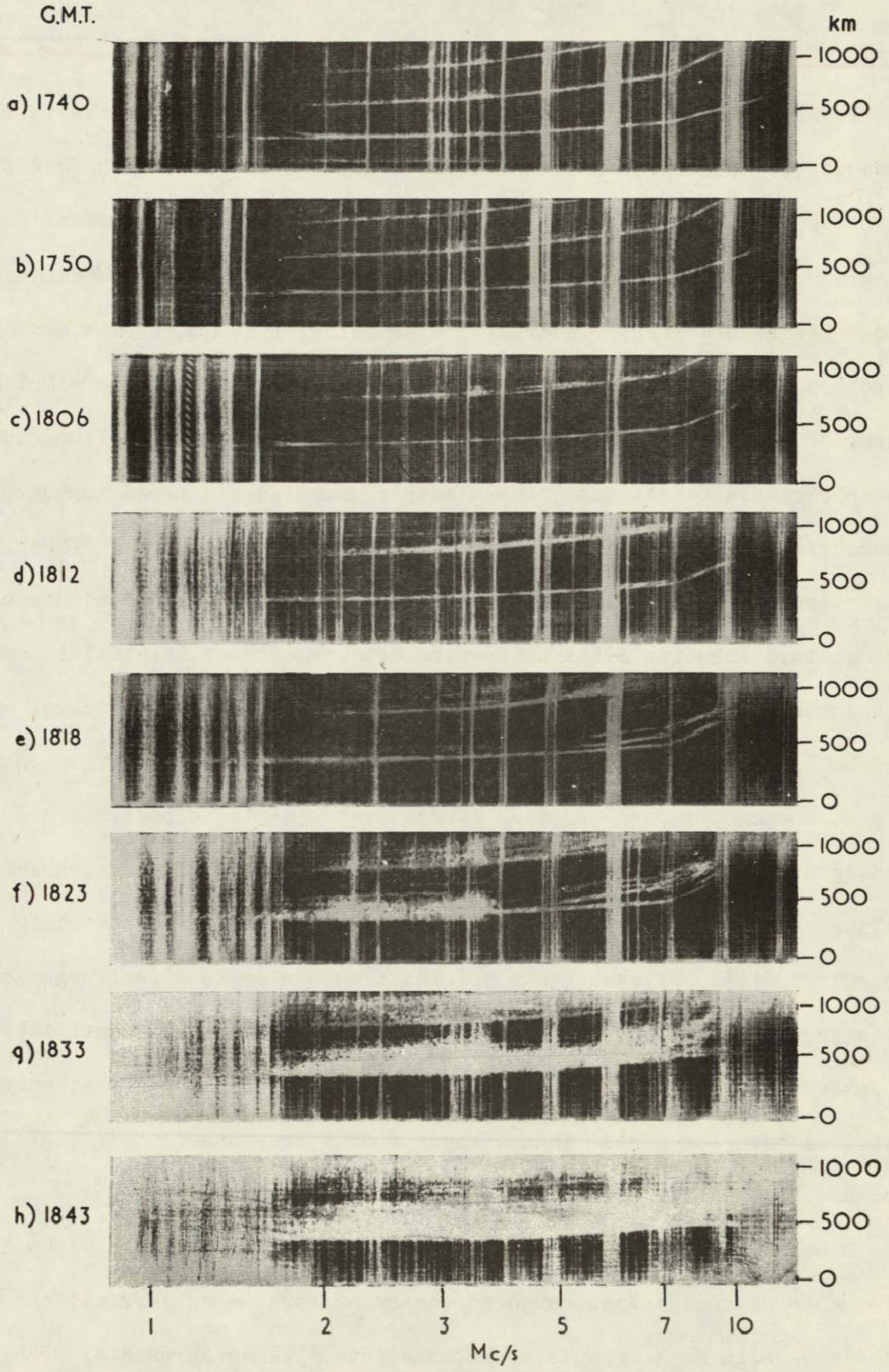

Figure 2.12 Sequence of ionograms showing the rapid development of spread *F*, Ibadan sunspot maximum [*Clemesha and Wright*, 1966].

which are responsible for spread *F* and scintillations.

2.5.2 *Rocket observations*. As in the case of the equatorial electrojet, ground-based observations can be effectively supplemented with *in situ* measurements. *Morse et al.* [1977] conducted an extensive coordinated rocket- and ground-based study called Equion in 1974 in order to further investigate spread-*F* irregularities. A Bristol Black Brant IVB rocket launched from Punta Lobos (Chilca), Peru carried a payload which intended to simultaneously measure the vertical profile of energetic particles well into the topside ionosphere, ion composition, the electric and magnetic field components, atmospheric emissions, and the electron-density fluctuations. These *in situ* measurements were then compared with data taken from the Ancon, Huancayo, and Jicamarca Observatories concerning measurements of scintillations, radar backscattered power and spectra, ionosonde reflections, and optical emissions.

Several conclusions on spread *F* resulted from this experiment. First of all, the experiments verified the existence of large positive and negative gradients in electron density which seem to be responsible for enhanced backscatter radar power returns. The data also verify the postulate of *Farley et al.* [1970] that radar returns from 3-m scale-size irregularities are a good indication of large irregularities which cause scintillations and ionogram spread echoes. Some earlier reports had indicated that energetic particles may play a role in causing spread *F* but *Morse et al.* [1977] conclude that particles are not part of the natural background.

2.5.3 *Theories*. Many theories exist which attempt to explain the phenomenon of spread-*F* although no theory appears to satisfy all the details made through ground, rocket and satellite measurements. The theories basically agree that spread *F* is due to electron-density irregularities which are aligned with the earth's magnetic field. It seems that

3. EXPERIMENTAL TECHNIQUE

3.1 *Introduction*

Twenty-six sounding rockets were launched from Chilca, Peru during the period 20 May to 10 June 1975 by the United States National Aeronautics and Space Administration. The Aeronomy Laboratory of the Department of Electrical Engineering of the University of Illinois at Urbana-Champaign built three of the payloads flown on Nike Apache rockets. These payloads were designed to investigate the anomalous properties of the equatorial ionosphere with one daytime and two nighttime launches.

All three payloads carried the two radio propagation experiments operating at 3.145 MHz and 2.114 MHz respectively. A continuous wave is transmitted to the payload from a ground-based station. The electron density is determined by the method of Faraday rotation [*Fillinger et al.*, 1976]. Each payload also contained a dc/Langmuir probe using a nose-tip electrode for measuring in electron density. Also included in each of the payloads was a spin magnetometer and a 210 kHz tone-ranging receiver and filter.

Nike Apache 14.532 was planned for launch during the daytime and in addition included two experiments to measure electron temperature. One of these duplicated the boom-mounted probe flown successfully on Nike Apaches 14.475/6 and 14.513/4 [*Schutz et al.*, 1975]. The other was an RF resonance probe prepared at the University of Tokyo [*Hirao and Oyama*, 1970].

Nike Apaches 14.524 and 14.525 were to be launched at local midnight, one with quiet geomagnetic conditions and the other with disturbed geomagnetic conditions. Instead of the electron temperature experiments these payloads each carried an energetic particle spectrometer [*Voss and Smith*, 1974; 1977] for investigation of nighttime ionization sources.

3.2 *Langmuir Probe*

The instrumentation used to measure electron-density irregularities is essentially that of *Prakash et al.* [1972], which is itself an adaptation of the dc probe experiment developed by *Smith* [1967]. The arrangement is shown in Figure 3.1. The nose-tip electrode is insulated from the body of the rocket and, in the fixed-voltage mode, is held at a potential of 4.05 V. The current is measured by an electrometer with a logarithmic scale of six decades (10^{-10} A to 10^{-4} A). The output of the electrometer is telemetered and used in conjunction with the propagation experiment to obtain the electron-density profile.

3.2.1 *Theory of Langmuir probe.* In the Langmuir probe technique, an electrode is inserted into the ionospheric plasma and the current to it is determined as a function of the potential of the electrode. The electron temperature and electron density are then determined from the resulting current-voltage characteristic.

When the electrode is exactly at the potential of the plasma the electron current to it is determined by the random thermal motions of the electrons in the gas. From kinetic theory the number of electrons striking unit area per second is $N\bar{v}/4$ where N is the electron density and $\bar{v}$ the mean electron velocity. Since each electron carries a charge e, the electron random current density j_o is given by

$$j_o = Ne\bar{v}/4 \tag{3.1}$$

The mean electron velocity $\bar{v}$ is related to the electron temperature T by

$$\bar{v} = (8kT/\pi m)^{1/2} \tag{3.2}$$

where k is the Boltzmann constant and m is the electron mass. The use here of

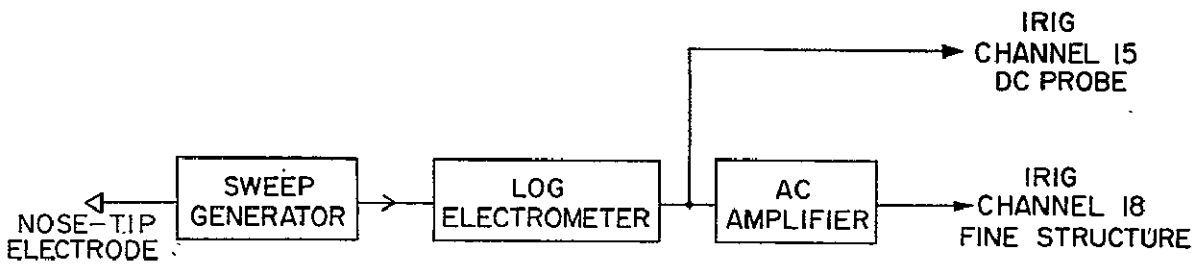

Figure 3.1 Block diagram of dc probe and fine structure experiment. Sweep generator is held at 4.05 V for electron-density fine structure observations.

electron temperature implies a Maxwellian energy distribution, i.e., thermal equilibrium.

As the electrode is made negative with respect to the plasma, only those electrons with energies greater than the retarding potential can strike the electrode. For retarding potentials on the electrode the electron current density j is given by

$$j = j_o \exp(eV/kT) \tag{3.3}$$

where V is the retarding potential. It is from a semi-log plot of j versus V (V less than plasma potential) that the electron temperature is obtained.

For positive electrode potentials the electron current is dependent on the shape of the electrode. A very small spherical electrode at a positive potential has an electron current density given by

$$j = j_o(1 + eV/kT) \tag{3.4}$$

When the probe is at a constant positive potential V with respect to the rocket body (4.05 V in this experiment), the probe current is proportional to the ambient electron density. The main assumption here is that electron temperature remains constant over short periods. Therefore fluctuations in probe current are proportional to fluctuations in the ambient electron density. This is the basis of the fine-structure experiment.

The current to the electrode is the sum of currents due to positive ions as well as electrons (negative ions are absent in the E region). Equations of the same general form of the previous equations are used but due to the much greater mass of the positive ion, the positive ion random current density is smaller than the electron random current density by a factor of about 170. The result is that correction of the observed current to obtain

electron current involves a small quantity, negligible in the fine-structure experiment.

3.2.2. *Probe current calibration.* Variations of electron concentration with altitude are believed to be accurately represented by changes in probe current [*Mechtly et al.*, 1967]. However, exact equations giving electron concentration as a function of probe current, collision frequency, rocket velocity, and other parameters do not exist. For this reason, the dc probe current is calibrated by values of electron concentration from the radio-propagation experiment. These are averages over about 1 km.

In the typical radio-propagation experiment, radio waves of both characteristic modes (ordinary and extraordinary) are radiated from a pair of ground-based transmitters. A power ratio of 10 dB at the rocket is maintained by a servoloop that includes the transmitters, the rocket-borne receiver, and the telemetry system. At the geomagnetic equator, however, linearly-polarized modes of equal amplitudes are transmitted in order to maximize Faraday amplitudes. These two modes are 500 Hz apart and are centered at 2.114 MHz and 3.145 MHz. The propagation data is analyzed to find the Faraday rotation rate which results from the changing phase characteristics between the two propagating modes. Another quantity typically measured is differential absorption which is characterized by a difference in the attenuation rates of the two modes. However, at the geomagnetic equator the system sensitivity is so low that the differential absorption cannot be measured with sufficient accuracy to be useful in calibrating the probe.

When both Faraday rotation and differential absorption are used together, it is possible to independently determine electron concentrations and electron collision frequency. With only Faraday rotation data available, a model for the collision frequency must be used. With this information, an iterative

computer algorithm based on the Sen-Wyller equations [*Mechtly et al.*, 1970] calculates the electron densities. From these data and the appropriately averaged probe current a calibration curve for the probe is obtained. Finally this calibration is applied to the unsmoothed probe current to obtain the electron-density profile.

3.3 *Fine-Structure Experiment*

3.3.1 *Principle of measurement.* The highly compressed scale required by the large range of electron density in the *D* and *E* regions of the ionosphere permits direct observation of only the major features of fine structure, for example sporadic-*E* layers. To examine the structure with greater resolution, both in altitude and in electron density the ac component of the electrometer output signal is amplified and telemetered on a separate channel, Figure 3.1. Since the electrometer output is proportional to probe current on a logarithmic scale, the amplitude of this signal is proportional to the fractional change in electron density ($\Delta N/N$). In this manner small irregularities in density can be measured, limited mainly by the capabilities of the telemetry system of the payload.

3.3.2 *Circuit design and characteristics.* The design of the log electrometer is shown in Figure 3.2. The electrometer (Keithley 302) is used with diodes in the feedback loop to achieve its logarithmic characteristics. The actual electrometer on Nike Apache 14.532 has an output of 0.80 V per decade of current from the probe. A 1% change in current then corresponds to (0.8) (ln 1.01)/(ln 10) = 3.5 mV which is fed to the ac amplifier with a nominal gain of 100. Full scale (±2.5 V) on the telemetry channel thus corresponds to ±7.1% in current. The smallest signal that can be measured is about 0.2% of full scale so that the smallest value of $\Delta N/N$ that can be detected is about 0.015%.

The high frequency response of the electrometer was measured as it could

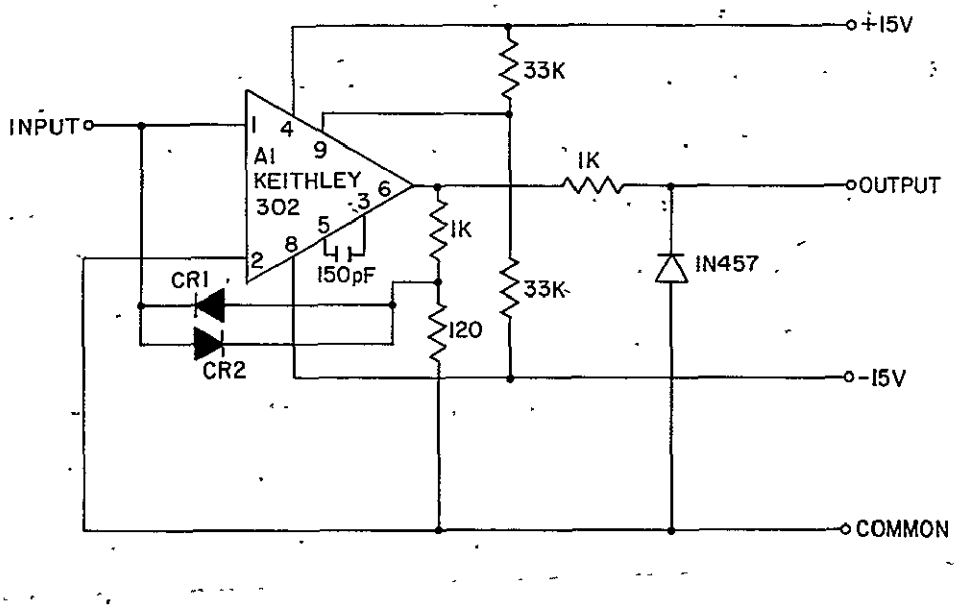

Figure 3.2 Schematic of log electrometer. CR1 and CR2 are diode-connected transistors (2N929).

be a limiting factor in the high frequency response of the system. The test set-up is shown in Figure 3.3. A dc bias current was inserted into the electrometer upon which was superimposed squarewaves of displacement current. This displacement current was generated using a triangular voltage waveform and capacitor differentiation. The amplitude of the squarewave at the electrometer output was adjusted to 50 mV and the rise time measured to 90% of steady value for various dc bias currents. It was found that for steady currents greater than 10^{-8} A (which is equivalent to an electron density of about 10^{2} cm^{-3} in the ionosphere) the rise time is less than 150 μs. Thus the electrometer would not limit the system high frequency response.

The circuit of the ac amplifier used in the Peru launches is shown in Figure 3.4. The mid-range gain, determined by the four 1% resistors, is 100. The bandpass characteristics of the three flight units have been recorded by examining the response to a step-function at the input (actually the leading edge of a square-wave). The 90% rise and fall times are given in Table 3.1 together with 3-dB points f_H and f_L calculated from the rise and fall times. These are in agreement with the expected values based on the capacitors used and their tolerances. Data from this experiment was corrected using this measured frequency response.

It is characteristic of the measured current that a modulation of up to 2% of the average current is imposed at the spin rate of the rocket (typically between 4 and 6 Hz). This contains harmonics and effectively prohibits useful measurements of ambient irregularities in the frequency range from 4 to about 90 Hz. The low-frequency cutoff of the amplifier was chosen to avoid overloading resulting from this modulation. With a rocket velocity of 1.4 km s^{-1} this limits the size of irregularities that can be reliably observed to greater than 350 m (for the output of the electrometer) and to less than 15 m (for the

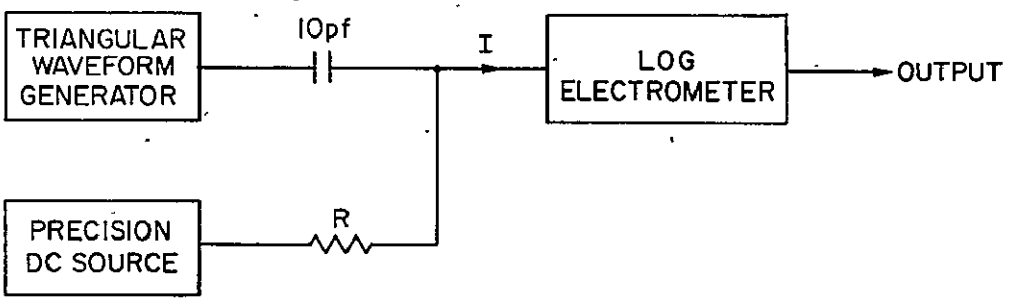

Figure 3.3 Arrangement for obtaining frequency response of log electrometer.

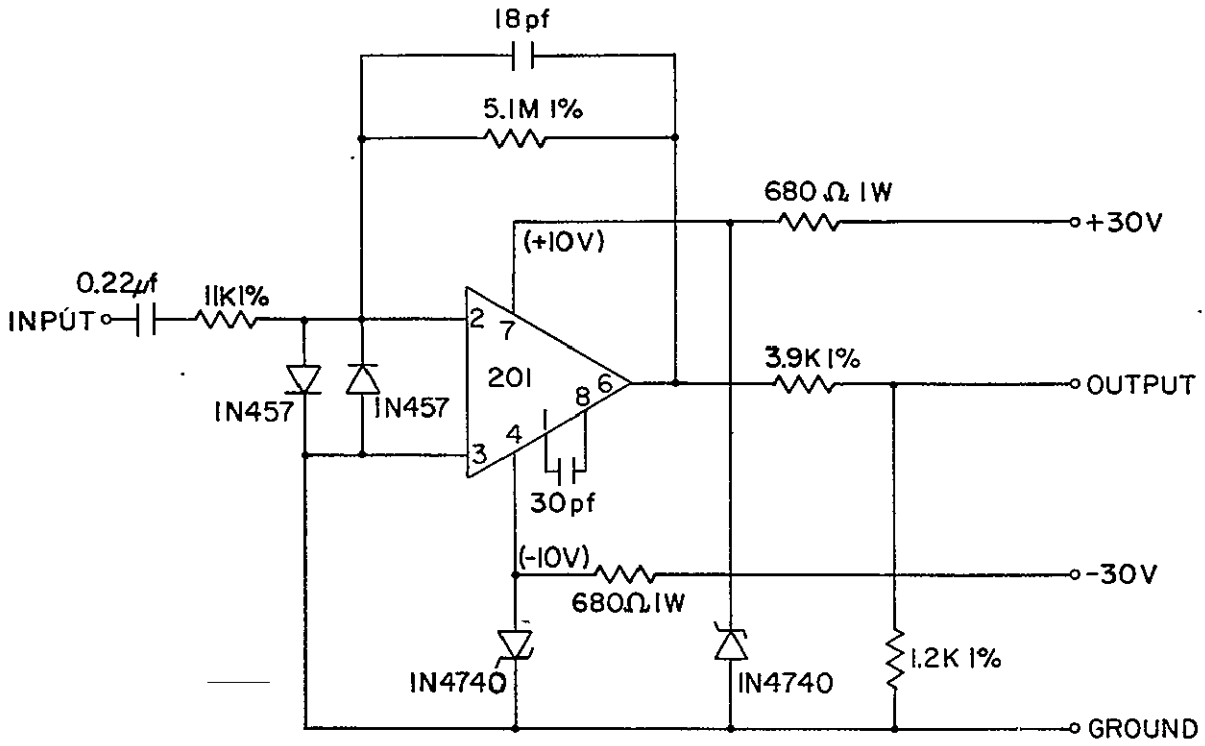

Figure 3.4 Amplifier for electron-density fine structure experiment. Together with the 1 K output resistor of the log electrometer, the four 1% resistors give a gain of 100.

Table 3.1

Frequency Response of ac Amplifiers

Rocket	Rise Time (μs)	Fall Time (ms)	f_H (Hz)	f_L (Hz)
14.524	190	7.4	1929	49.5
14.525	185	6.0	1981	61.1
14.532	195	6.8	1880	53.9

output of the ac amplifier).

3.3.3 *Integration into rocket payload.* The three payloads utilize a standard IRIG FM-FM telemetry system for transmission of experimental data to the ground. In this proportional bandwidth system, data is assigned to various subcarrier channels depending on bandwidth required. A voltage-controlled oscillator converts the data signal to a subcarrier frequency with 7.5% deviation. The resultant subcarriers are then frequency modulated and transmitted at 240.2 MHz. The log electrometer was assigned to IRIG channel 15 with an effective data cutoff of 450 Hz. IRIG channel 18 carried the fine structure data. A low-pass filter in the discriminator of the ground-based data-processing system provided the data cutoff points which could be extended if necessary. This was the case for the fine structure data as information was desired to 2300 Hz.

3.4 *Data Reduction Technique*

3.4.1 *General arrangement.* The processing of the irregularity data was accomplished using an analog system, shown in Figure 3.5. The signal from the magnetic tape is played back through a discriminator with tape speed compensation. This signal is then passed to an adjustable narrow-band filter and the output fed to a full-wave rectifier. The output of the rectifier is recorded on a chart recorder. The spectral nature of the signal is determined by making separate runs for each of the eight selected frequency bands between 90 and 2307 Hz. These eight bands were chosen with a geometrically increasing bandwidth ratio of 1.5 and basically the same as those used by *Prakash et al.* [1972] in his analysis. However, due to a slowing of rocket velocity with altitude, the actual size of the irregularities measured changes as given by $\lambda = v/f$ (Figure 3.6). At 95 km the irregularities measured vary between 0.6 and 15 m while at 160 km the range is only from 0.35 to 9 m.

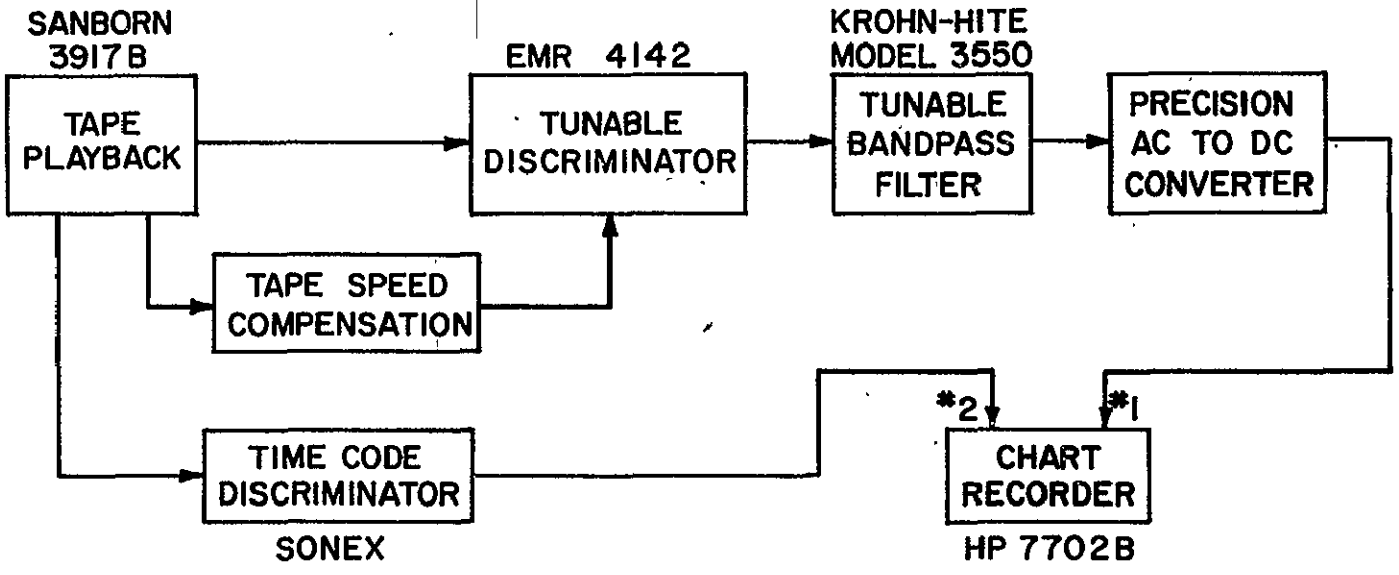

Figure 3.5 Analog data reduction system for equatorial irregularities.

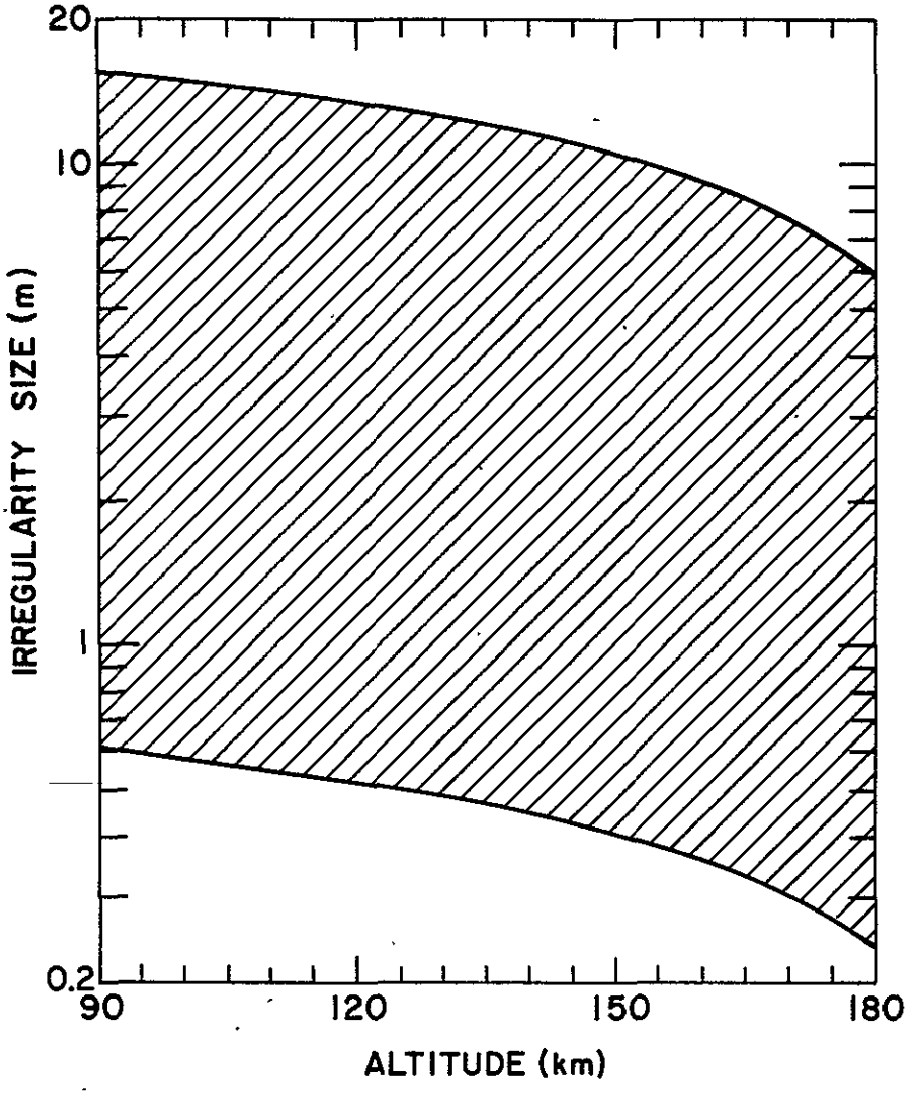

Figure 3.6 The range of size of irregularities corresponding to the frequency range 90 to 2307 Hz, as a function of rocket altitude.

These data may be represented by a spectral index n such that $E(f) \propto f^n$ where $E(f)$ is the rms amplitude of $\Delta N/N$ in the specified band, divided by the bandwidth. Since the frequency (f) is related to the wave number (k) of the irregularities by $k = (2\pi/v)f$; where v is the rocket velocity, it follows that n is also the wave number spectral index. On a log-log plot of the irregularity amplitudes at their respective band centers, the slope of the line obtained by means of a least-squares-fit computer program gives the spectral index n.

3.4.2 *Tape recorder and discriminator.* The magnetic tape playback unit used in this analysis is a Sanborn 3917B capable of playing back 7-track, 0.5 inch tapes at a speed of 60 inch/sec. A proportional bandwidth tuneable-discriminator, EMR model 4142, demodulates the fine structure data from the multiplexed video track. The discriminator is adjusted to a center frequency of 70 kHz to decode the IRIG channel 18 fine structure data. To avoid discriminator attenuation of the data, the low pass filter is set at 5 kHz instead of 1.05 kHz for the normal modulation index equal to 5.

Tape speed compensation for differences in the record and playback speeds was accomplished by means of a recorded 100 kHz reference signal on a track of the telemetry tape. This signal is demodulated by a 100 kHz reference discriminator, VIDAR 302, to produce a voltage error signal which is then directed to the EMR discriminator. Circuitry internal to the EMR discriminator sums the data signal and the error signal to correct for the error in tape speed. A 75 μs delay unit, VIDAR 4303, is inserted between the tape playback and the EMR discriminator on the data line so that the data signal is synchronous with the tape speed compensation signal.

To calibrate the discriminator, a dc signal was applied to a calibrated IRIG channel 18 voltage-controlled oscillator (VCO). The VCO had a center

frequency voltage of 2.5 V which corresponded to an output of 0.0 V from the discriminator. 5.0 V and 0.0 V to the VCO produced the ±5.0 V discriminator output. In this manner the EMR discriminator was kept in calibration.

3.4.3 *Filter characteristics.* Bandpass filtering of the data signal is accomplished by an adjustable multifunction analog filter, Krohn-Hite model 3550. The filter consists of a low pass section in series with a high pass section. At this point in the data reduction process the frequency band of interest is selected. The low pass section is adjusted for the higher bandedge and the high pass section for the lower bandedge to achieve the bandpass function. Tests show that the filter frequency response is down from midband approximately 2 dB at the bandedges. Attenuation is 24 dB per octave outside the bandedges, equivalent to a four-pole filter. A typical plot of response for a frequency band is shown in Figure 3.7. Though the filter response is not ideal, the bandpass characteristics are sufficient to attenuate most of the signal from adjoining bands. It will be shown in Section 4.2.2 that for the spectrum being analyzed the error in amplitude is moderate and the error in the spectral index is negligible.

3.4.4 *Signal detection.* In order to produce an rms voltage, the fluctuating data signal is applied to a precision ac to dc converter, Figure 3.8 [*National Semiconductor*, 1972]. This precision converter is required because of the very small amplitudes of the signals, typically less than 100 mV. A diode rectifier could not convert these signals due to the 0.7 V typical diode drop. Using diode feedback in an operation amplifier circuit, this voltage drop is reduced by the amplifier gain (approximately 10^5) to an insignificant amount.

The circuit performance was tested and found to be linear down to approximately 1.0 mV, Figure 3.9. Low pass filtering occurs as a result of

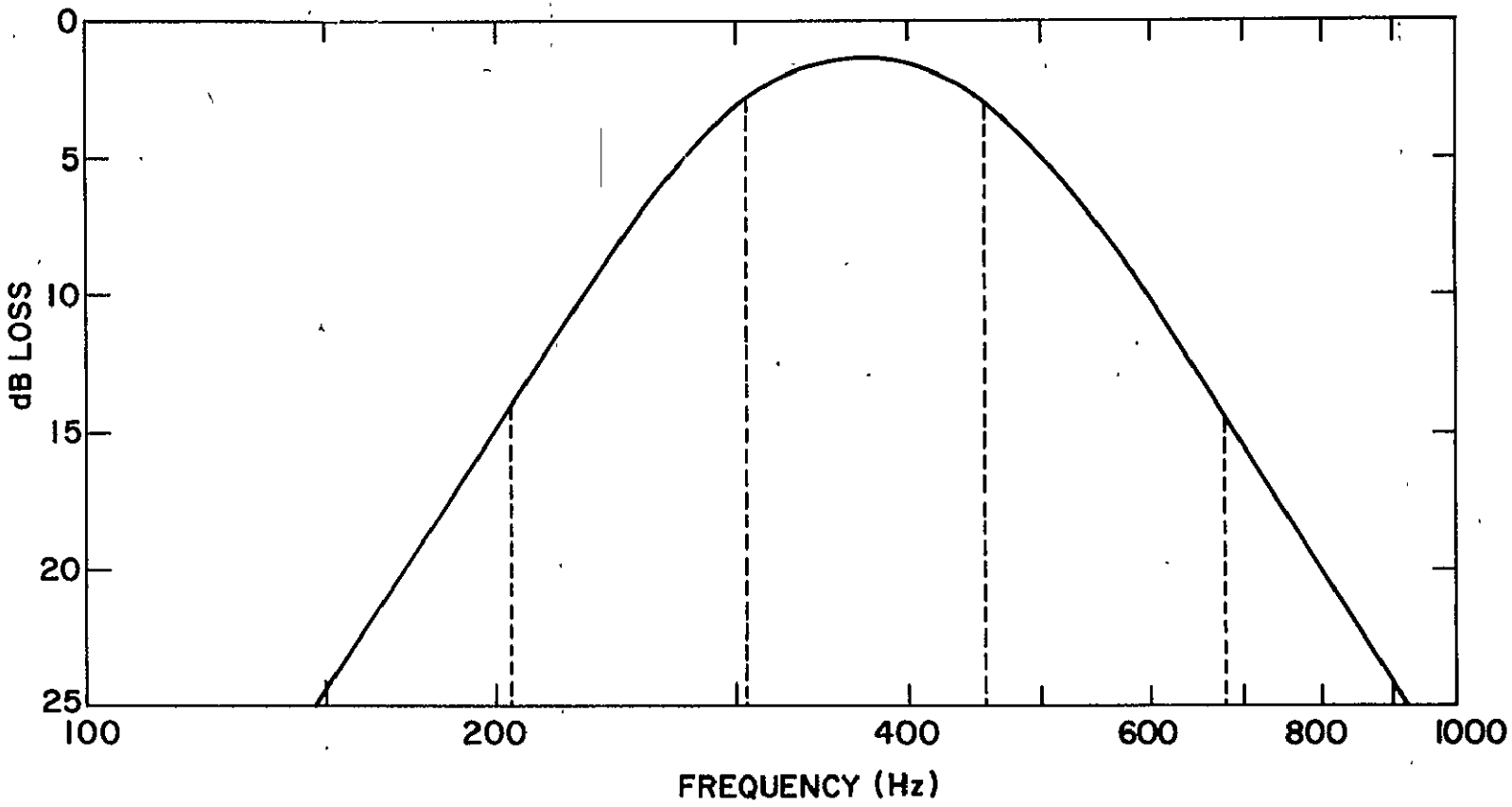

Figure 3.7 Measured response of the filter when set for the frequency band 304 to 456 Hz. The input signal was 50 mV rms.

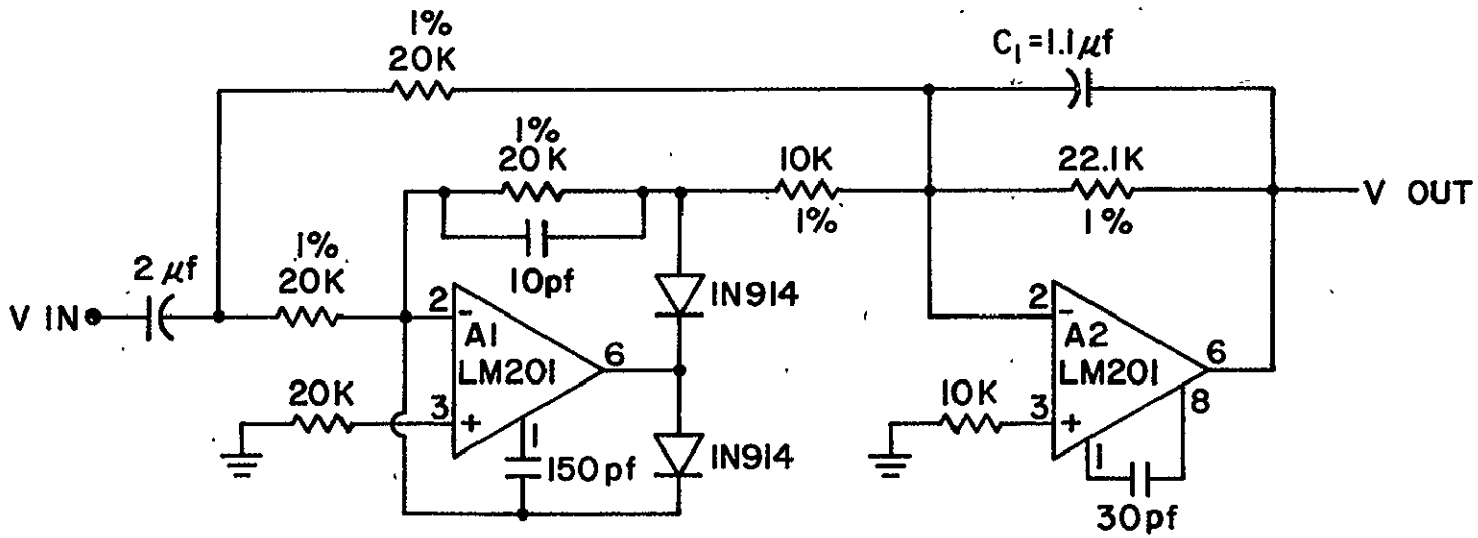

Figure 3.8 Precision ac to dc converter [adapted from *National Semiconductor Corporation*, 1972].

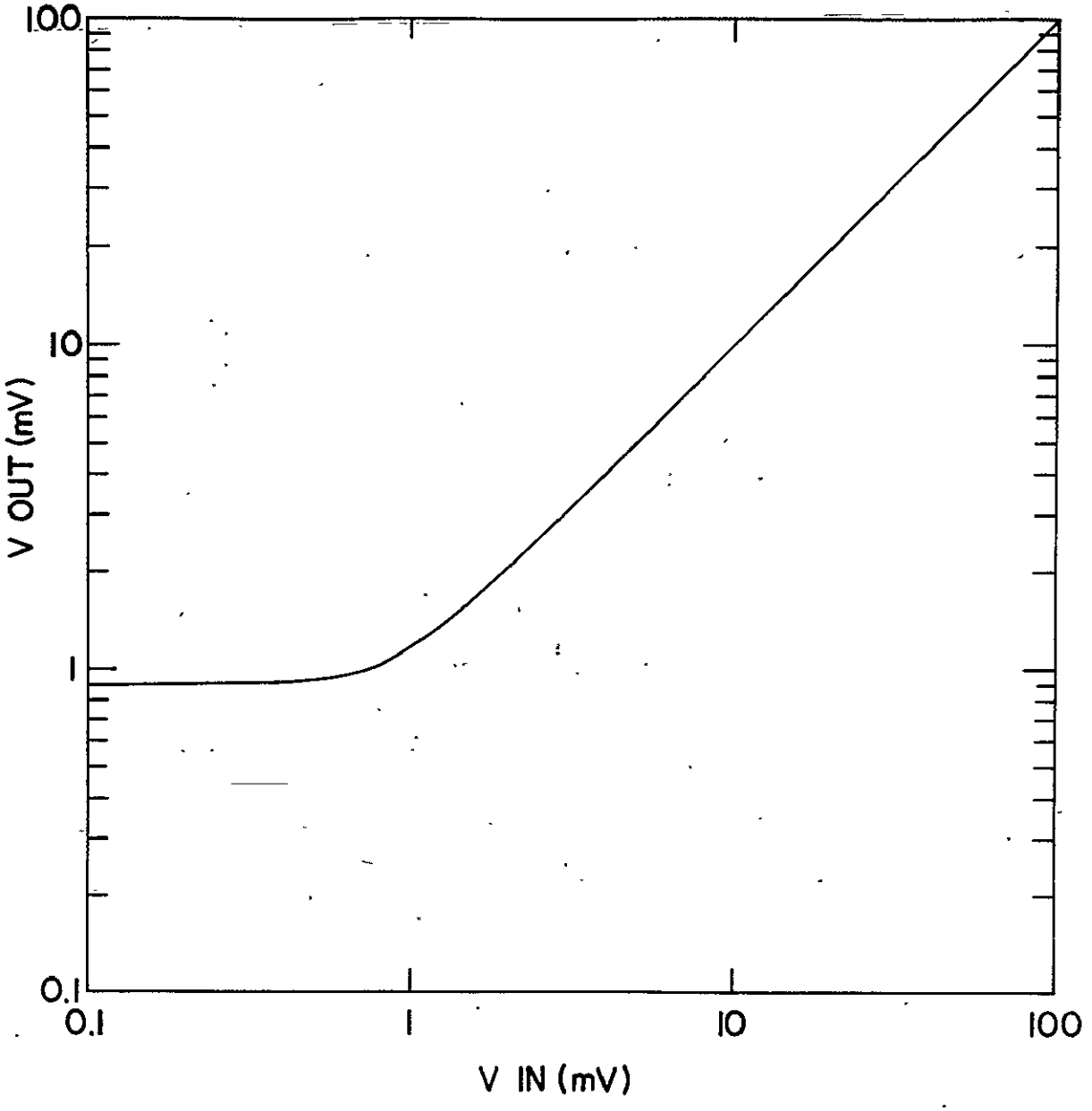

Figure 3.9 Transfer characteristics of the precision ac to dc converter.

the converter output stage and this action can be adjusted by means of C_1. Several values of C_1 were tested (1.1 μF, 3.3 μF, 6.8 μF) and it was found that a value of 1.1 μF provided the optimum amount of filtering for accurate chart record analysis. The output of the filter was originally direct-coupled to the converter and as a result any dc level on the filter output could give a false dc level at the converter output. To alleviate this problem, a 2.0 μF blocking capacitor was inserted on the input of the converter to give a 25 Hz corner frequency which produced negligible attenuation in the frequency bands of interest.

3.4.5 *Chart recorder.* To record the data signal at the output of the converter, a dual channel Hewlett-Packard 7702B chart recorder was utilized. This instrument was equipped with two low-level pre-amp plug-ins capable of handling inputs as low as 1 μV. Six chart speeds were available; the 5 mm s^{-1} setting was used almost exclusively due to ease of data analysis. On channel 1 the fine structure data was displayed while simultaneously recorded on channel 2 was a NASA 28 bit time code derived from the flight tape with a Sonex discriminator. This time code was essential in determining the altitude of the data points on the chart record.

3.4.6 *System calibration.* A system calibration procedure was established and followed for each data run. The arrangement is shown in Figure 3.10. A sinewave of known amplitude corresponding in frequency range to the irregularity scale sizes under investigation was inserted into the calibrated IRIG channel 18 VCO along with the required +2.5 V bias. This portion of the setup simulated the rocket-borne fine structure experiment and telemetry system and replaces the tape playback unit in the previously described data reduction system. The output of the precision converter was monitored by a dc voltmeter and the input frequency to the VCO from the sinewave generator

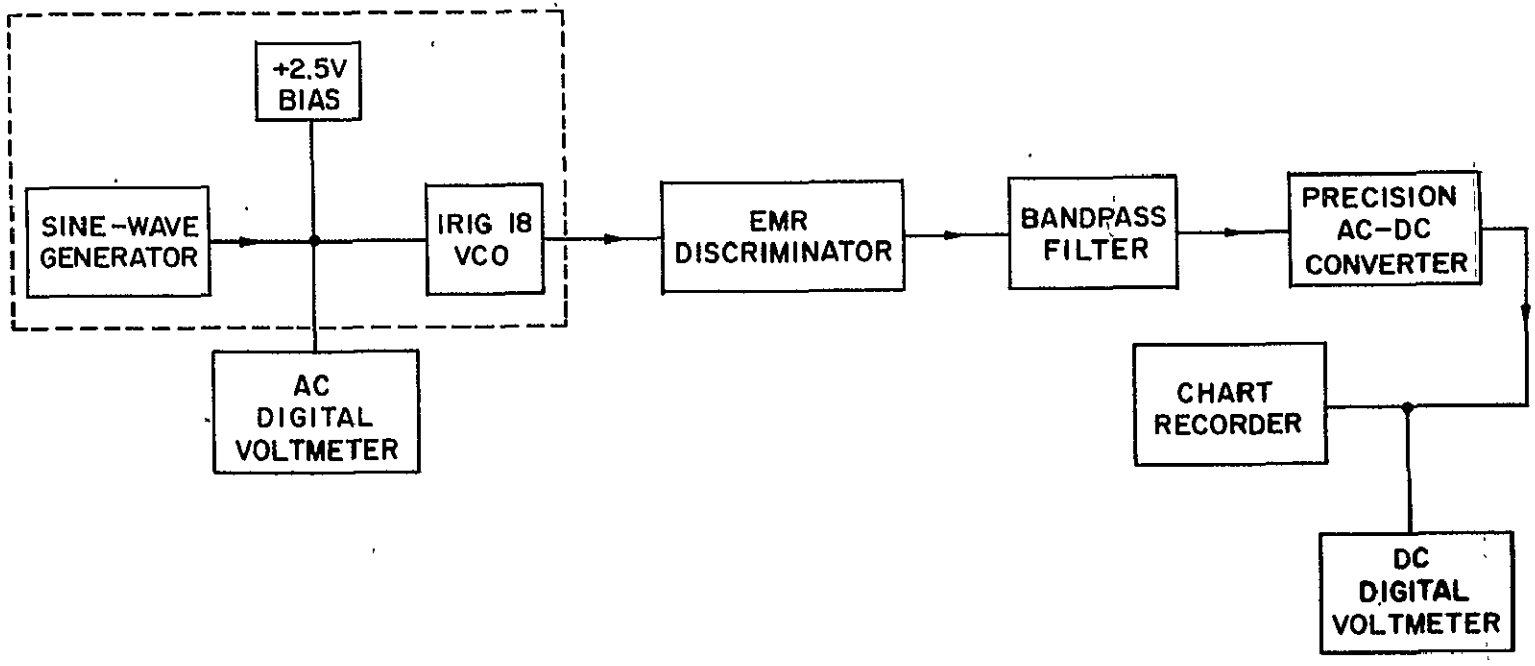

Figure 3.10 Block diagram of the arrangement used for calibrating the data reduction system. The instrumentation within the dashed line simulates the rocket-borne portion of the fine structure experiment.

adjusted within the selected filter band to give maximum output. By adjusting the input voltage to the VCO to a specific value, a reference level of irregularity amplitude would be marked at the beginning of the chart record. The relationship between the input to the VCO (analogous to the ac amplifier output) and $\Delta N/N$ amplitudes is described in Section 3.3.2. After several iterative runs of adjusting the chart recorder sensitivity an optimum setting for the band under investigation would be found. The input calibration voltage level would then be adjusted for that chart sensitivity. Typically 35 mV was used corresponding to an irregularity amplitude of 0.1%. The irregularity amplitudes could then be accurately measured from the calibration level.

4. OBSERVATIONS

4.1 *Launch Operations*

The times and geophysical conditions for the three launches were selected on the basis of a number of scientific objectives. One launch, Nike Apache 14.532, was to be an investigation of the daytime equatorial ionosphere. The time of day was selected for a solar zenith angle of 60° in the afternoon. This would allow comparison of the principal features of the electron-density profile with others obtained at midlatitudes at the same solar zenith angle. A second objective was the intercomparison of two rocket-borne electron temperature probes and separate comparisons with data obtained at Jicamarca by incoherent scatter. The third objective of the daytime flight was the study of the fine structure of the electron-density profile: the irregularities occurring in the electrojet which produce strong radiowave echoes.

The other two launches, Nike Apaches 14.524 and 14.525 were to be launched near midnight, local time. This time was selected because of the desire to compare the electron-density profile with a group of profiles obtained at Wallops Island, Virginia, near midnight. Whereas for the daytime flight there was no reason to expect the equatorial ionosphere up to, say, 180 km to be different from the midlatitude ionosphere, significant differences were anticipated for the nighttime flights. This follows from the much greater role at night of neutral winds in the vertical motion of ionization. This process, known as the wind-shear mechanism, is important at midlatitudes and produces the intermediate layer, with its peak near 150 km at midnight. At the geomagnetic equator, because the magnetic field lines are horizontal, the wind-shear mechanism is ineffective and there is no vertical transport except for that produced by electric fields. Electric fields, however,

cannot produce convergence of the ionization, thus no layering would be expected.

In addition to observing the large-scale features of the electron-density profile a further objective of the nighttime flights was to observe the small-scale structure, particularly that associated with spread *F*. Finally, again because of the interest in comparison with observations from Wallops Island it was decided to measure particle precipitation at the equator.

Because both the occurrence of spread *F* and the intensity of particle precipitation are known to be correlated with geomagnetic activity, it was decided that one of the nighttime launches would be a time of quiet geomagnetic activity while the other would be a relatively disturbed time.

In the following sections of this chapter the observations from the three launches relating to the electron-density profile and its large- and small-scale structure are presented.

4.2 *Daytime Observations*

4.2.1 *Electron-density profile.* Nike Apache 14.532 was launched at 1526 LST (2026 UT) on 28 May, 1975 at a solar zenith angle of 60°. The Kp index was 2-. The probe current was measured from approximately 55 km to rocket apogee at 191 km. The probe data were calibrated to 139 km by the on-board propagation experiment. The propagation experiment used Faraday rotation and the reflection points for the two frequencies: 2.114 MHz at 100.6 km and 3.145 MHz at 139.1 km. Through analysis of this data the calibration factors (N/I) below 139 km were calculated. Above this height a true-height analysis* of ionograms from the Huancayo Observatory gave an

---

*These data were obtained from WDC-A for Solar-Terrestrial Physics.

electron-density profile which was used to establish an N/I ratio.

Ionograms taken at Huancayo shortly before and after launch, Figure 4.1, show a normal ionosphere with equatorial sporadic *E* just above 100 km. Another perspective of conditions is given by the Huancayo *f*-plots for 28 and 29 May 1975 shown in Figure 4.2. At launch time, three open circles are apparent as the chart is followed vertically from 1530 LST on the horizontal scale. The lowest circles indicate the critical frequency of the *E* layer while the one above indicates the *F*-layer critical frequency [*Piggott and Rawer*, 1972]. No major differences are apparent when this *f*-plot is compared with other adjacent days.

Figure 4.3 shows the profile of electron concentration obtained from the rocket-borne experiments. The calibration procedure suppresses features smaller than about 0.3 km. The *D* region can be seen from about 56 km to the mesopause at about 86 km. It is here at the base of this steep gradient that the *E* region begins and extends upward to the *F* region at approximately 160 km. Looking closely at the plot it is apparent that the *E*-region curve is fairly smooth with some small irregularities appearing between 98 and 110 km. Above 110 km, the profile is smooth with little variation in electron concentration. The gaps in the profile above 128 km result from the voltage sweeps of the dc probe used in determination of electron temperature.

In Figure 4.4, electron concentration data obtained independently from the incoherent scatter facility at Jicamarca [*C. Calderon*, private communication] is shown along with the rocket and true-height analysis data illustrating the compatibility of the methods.

4.2.2 *Electron-density irregularities.* As previously noted, few large-scale irregularities (>300 m) can be observed on the daytime electron-density profile. However analysis of the fine structure data shows smaller

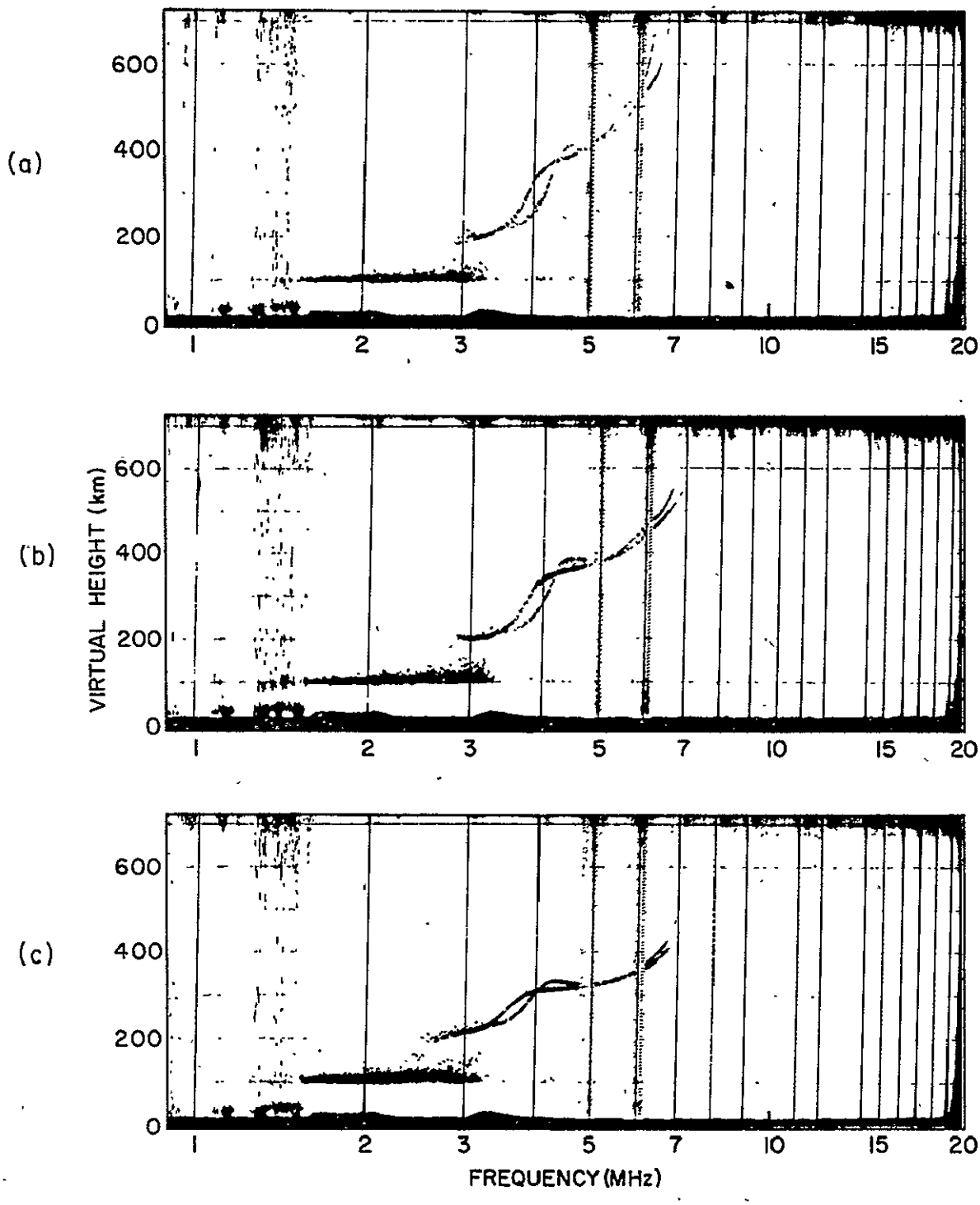

Figure 4.1 Ionograms recorded at (a) 1500, (b) 1530, and (c) 1600 LST, 28 May 1975 at Huancayo. Nike Apache 14.532 was launched at 1526 LST from the Chilca rocket range. [Data obtained from WDC-A for Solar Terrestrial Physics].

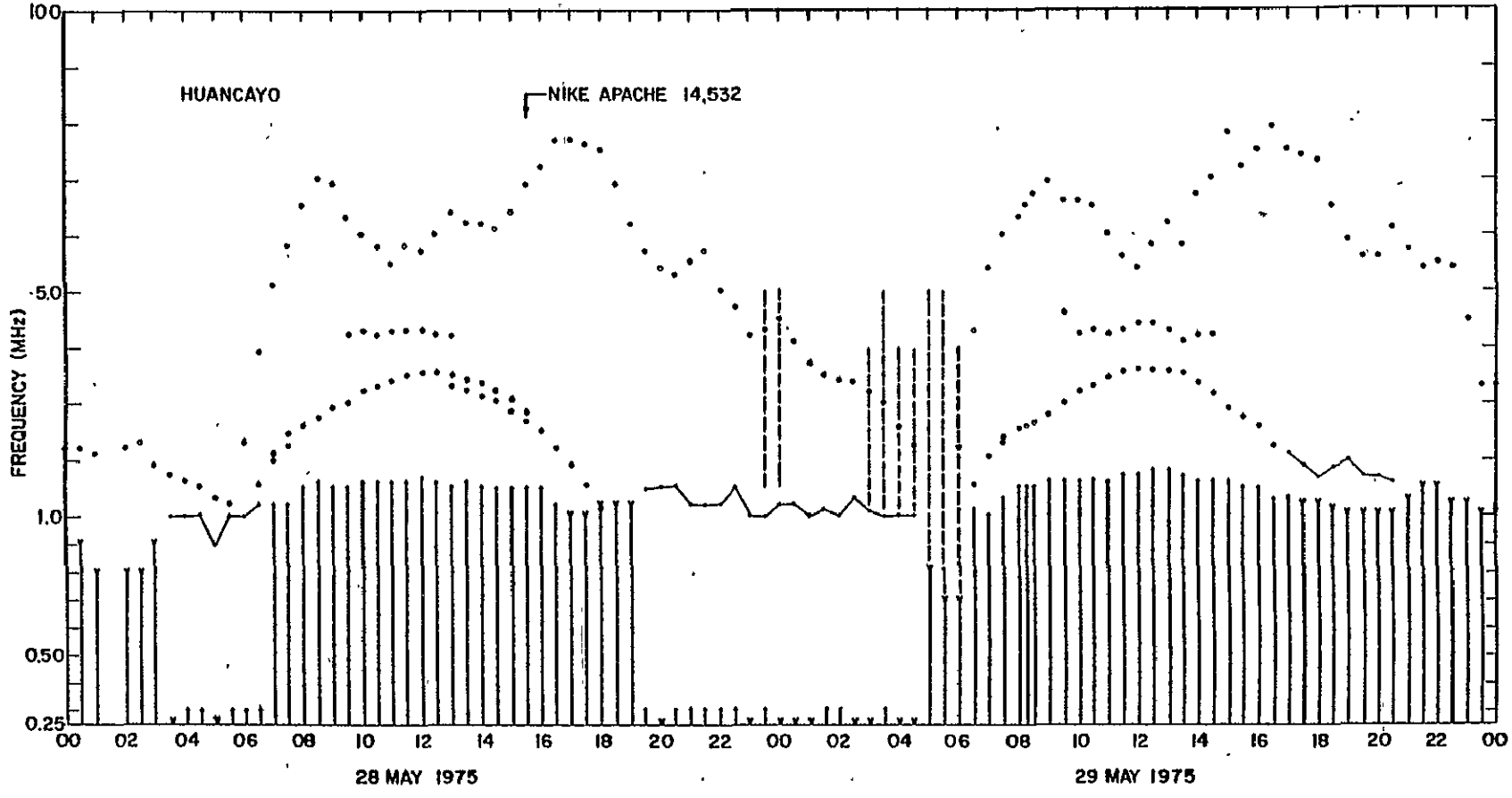

Figure 4.2 Huancayo *f*-plots for 28 and 29 May 1975. The launch time of Nike Apache 14.532 is indicated. [Data obtained from WDC-A for Solar-Terrestrial Physics].

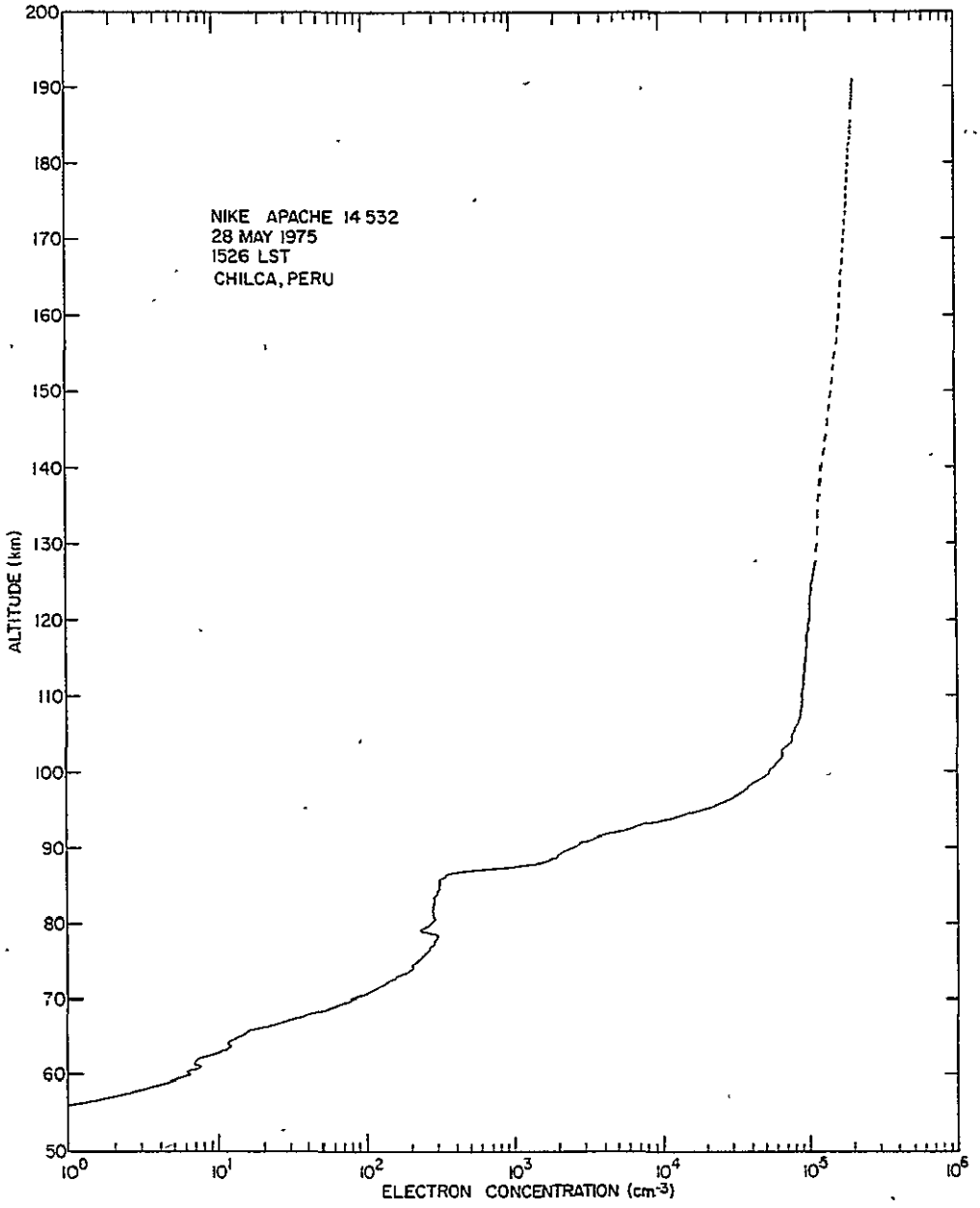

Figure 4.3 Electron concentration profile from Nike Apache 14.532. Above 128 km the probe experiment is interrupted at two-second intervals.

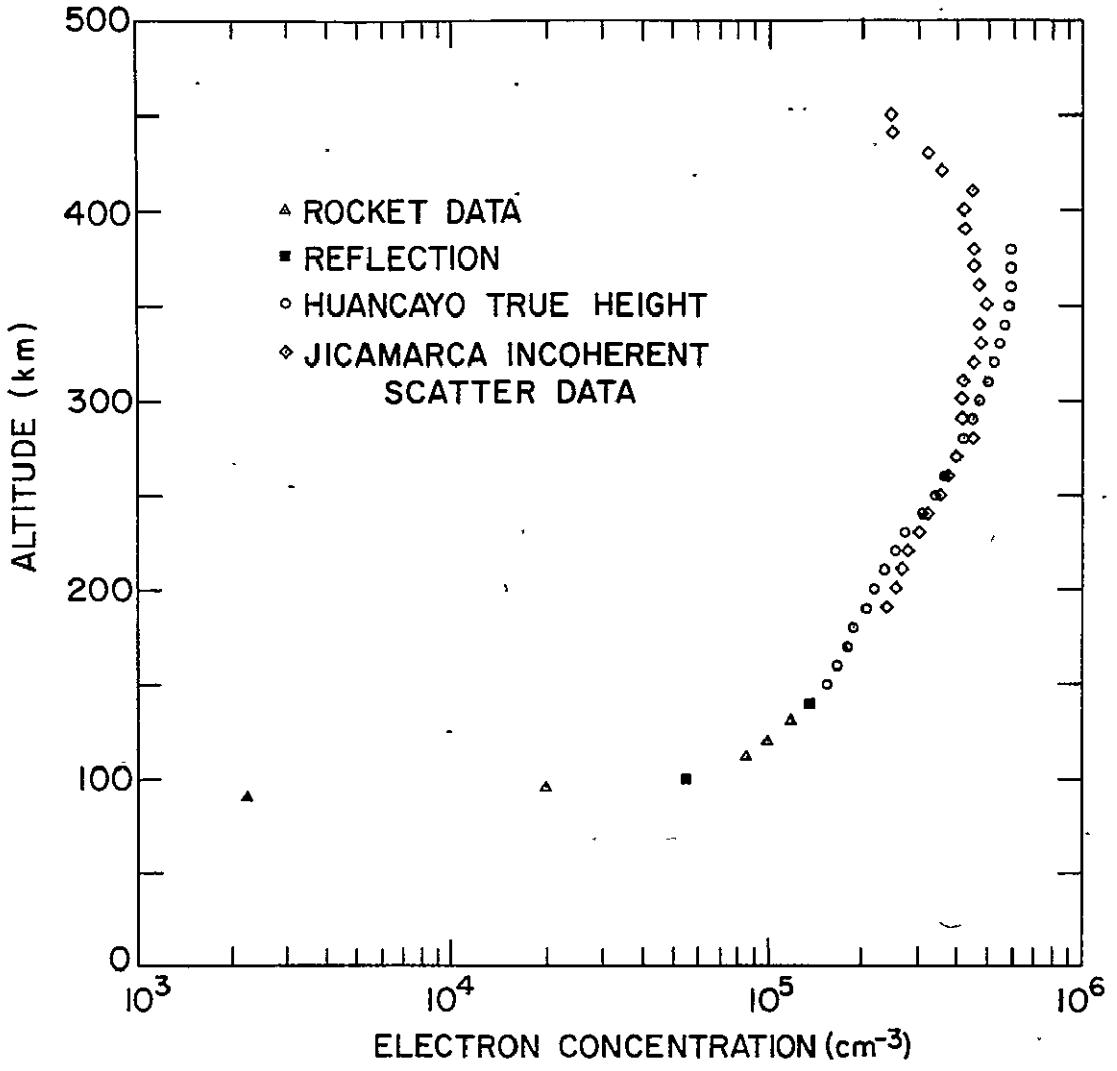

Figure 4.4 Comparison of electron concentration profiles from the rocket experiments on Nike Apache 14.532; from the Jicamarca incoherent-scatter facility; and from true-height analysis of Huancayo ionograms.

irregularities in the size range 0.5 to 15 m are present. Figure 4.5 gives an example of the appearance of the chart record. Here, frequency band 6 (683-1025 Hz) is illustrated corresponding to electron-density fluctuations in the size range 1.2 to 1.7 m (nominal for a rocket velocity of 1.2 km s^{-1}).

$E(f)$, the rms amplitude of $\Delta N/N$ in a specific band divided by the bandwidth, is plotted versus altitude for all eight bands of interest in Figure 4.6. In the high frequency bands the noise signal has a broad maximum between 105 and 115 km with a rapid decrease at lower altitudes and a more gradual decrease at higher altitudes. In the low frequency bands the variation is parallel to that of the high frequency bands for altitudes of 105 km and above but shows a marked difference at lower altitudes. The irregularity amplitudes do not decrease sharply as in the high frequency case but actually increase towards 95 km.

This change can also be observed in the spectral index n, given by the power law $E(f) \propto f^n$. The spectral index n is obtained by a least-squares-fit as illustrated in Figure 4.7 for data at 110 km. In this case $n = -0.478$ with a correlation coefficient of 0.995. Correlation coefficients for the least-squares-fit lines were found to be better than 0.980 from 95 to 160 km showing the accuracy of the power law. The change in character of the irregularities is seen in the variation of the spectral index with altitude, Figure 4.8. Between 105 and 155 km the spectral index is -0.51 ± 0.01. Below 105 km much larger (negative) values are seen showing the presence of much larger scale-size irregularities in relation to smaller scale-size irregularities. This change in spectral index is taken to be indicative of different mechanisms generating the irregularities: those at 105 km and above occur in the region of the electrojet current and are probably due to plasma instabilities; those below 105 km are probably associated with turbulence in the neutral atmosphere.

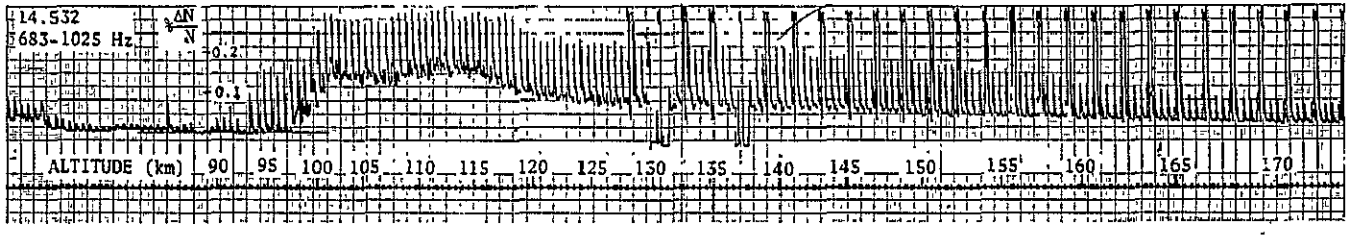

Figure 4.5 Amplitude of electron-density fluctuations in the size range 1.2 to 1.7 m observed on Nike Apache 14.532. The large vertical spikes result from interference from other instrumentation in the payload.

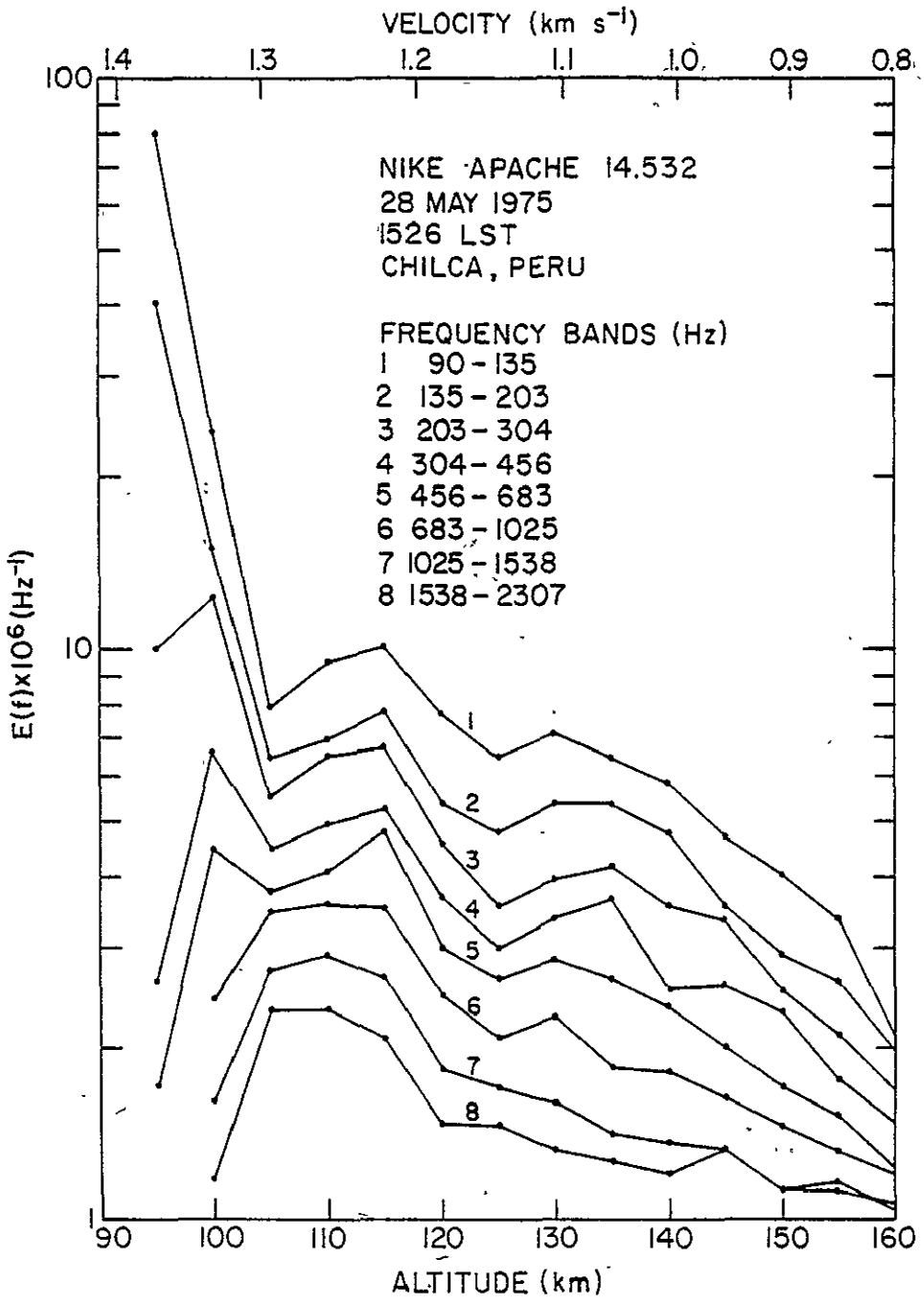

Figure 4.6 The rms amplitude of irregularities in eight frequency bands as a function of altitude and of velocity of the rocket.

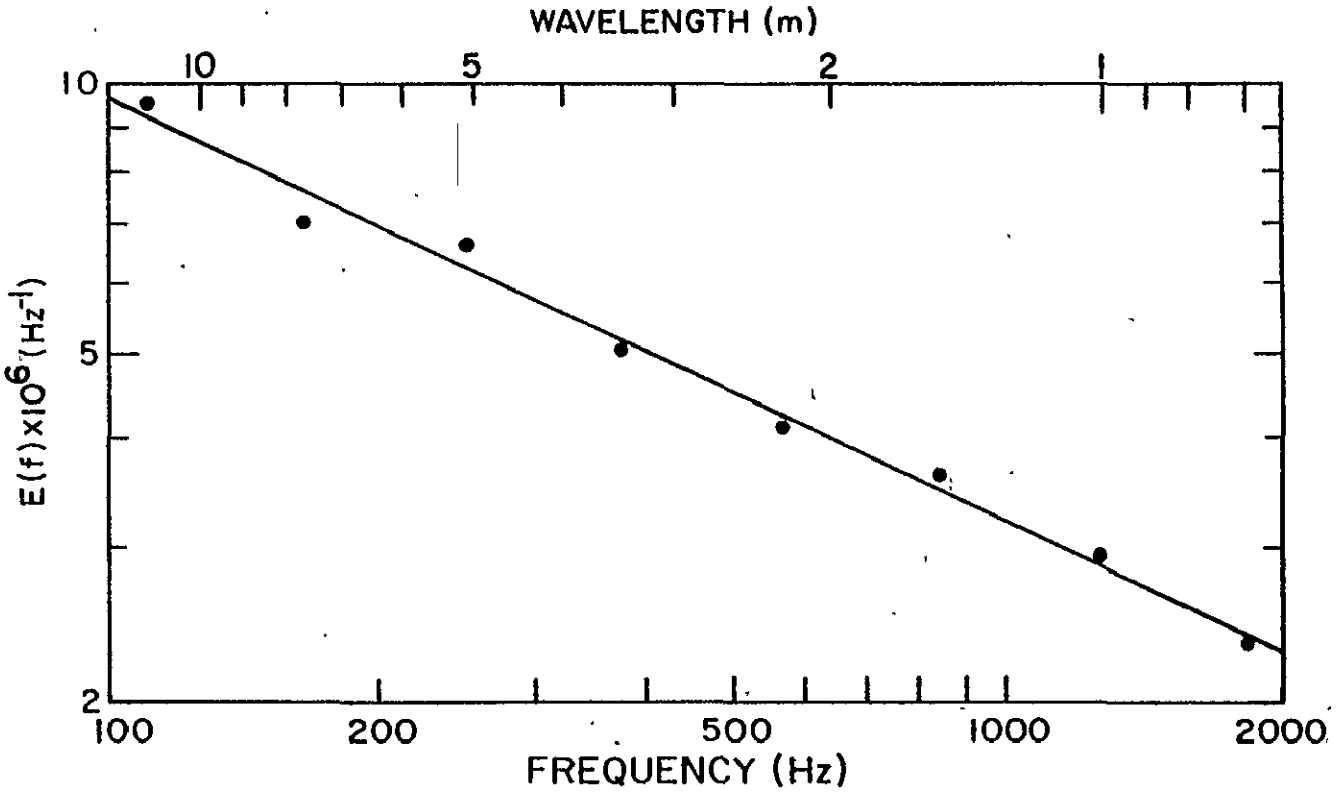

Figure 4.7 Spectrum of irregularities at 110 km altitude as a function of frequency and of wavelength.

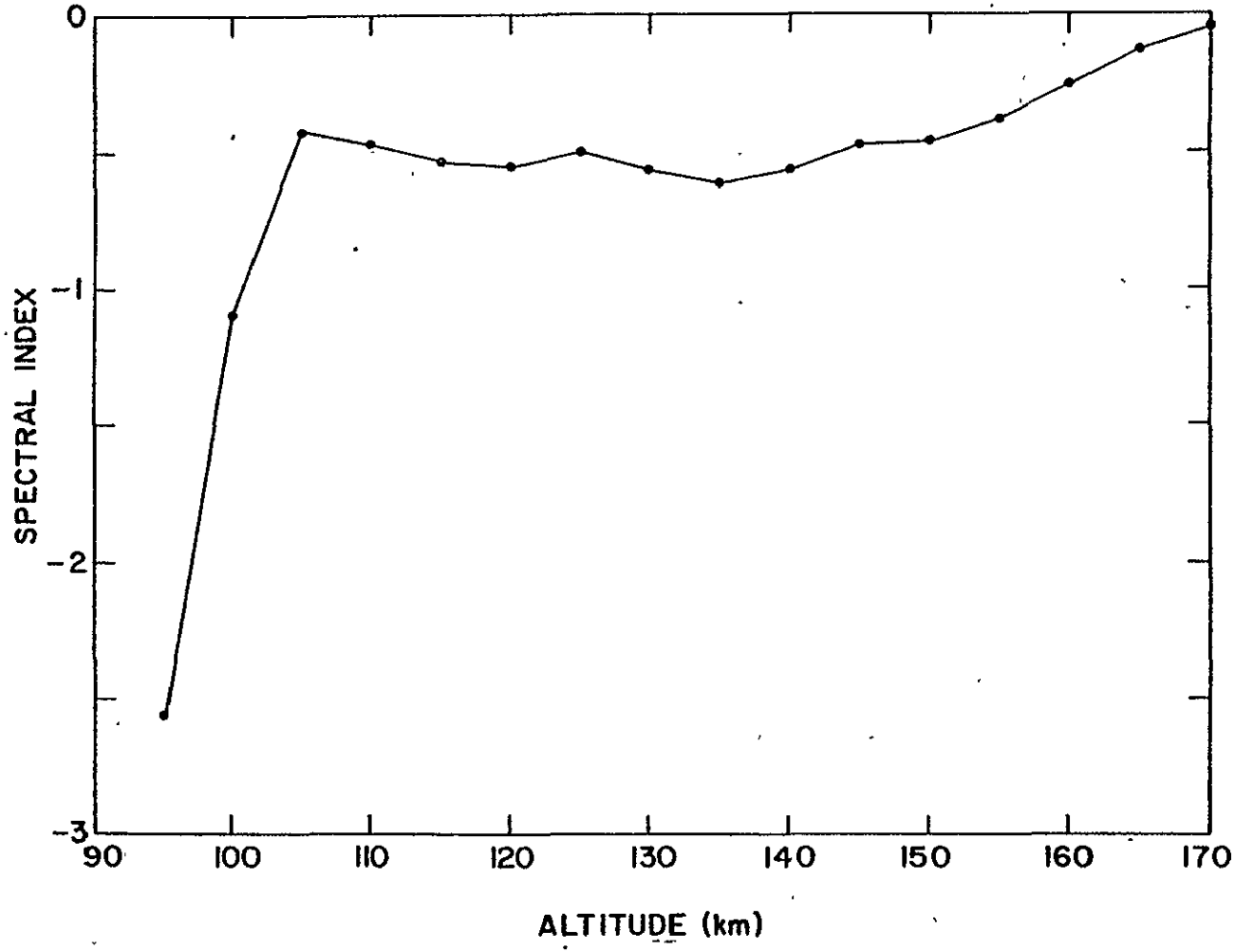

Figure 4.8 Spectral index as a function of altitude.

4.2.3 *Effect of filter response.* In Section 3.4.3 the characteristics of the bandpass filter were discussed. It was noted that leakage of signal from adjoining bands would affect amplitudes and may affect the spectral index. It will now be shown that for the data described in Section 4.2.2 the error in the spectral index is negligible from this cause. To verify that the obtained result of $n = -0.5$ is essentially correct, assume that such a distribution actually exists. The relationship $E(f) = A\ f^{-0.5}$ represents a spectrum decreasing in amplitude at 3 dB/octave. When this signal is combined with the 24 dB/octave slopes of the bandpass filter, the result can be thought of as a modified filter acting on a signal of spectral index zero. This modified filter would have a low frequency rolloff of 21 dB/octave and a high frequency rolloff of 27 dB/octave. Thus the signals from adjacent bands produce a small increase in amplitude in the band being measured but, more importantly, that increase is the same fraction for all bands. As a result, the amplitudes are all increased by the same relative amount and the spectral relationship of -0.5 remains constant. This holds true until the spectral index approaches -4 (or +4) which is equivalent to the 24 dB/octave rolloff of the filter. At this point, the apparent spectral index will not be correct.

A numerical study of this explanation verifies its accuracy for spectral indexes of -0.5 and -2.0. In each case values of $E(f)$ were calculated at each of the midband frequencies. The effects of imperfect filtering were taken into account by assuming from the filter frequency response plots that 0.48 of the two immediately adjacent bands and 0.1 of the next bands leak in. The results are plotted in Figures 4.9 and 4.10. Line 1 in each depicts a theoretical spectral index of -0.5 and -2.0 respectively. The actual filter response assuming the various signals add as the square root of the sum of the squares is shown as line 2. The spectral index remains the same

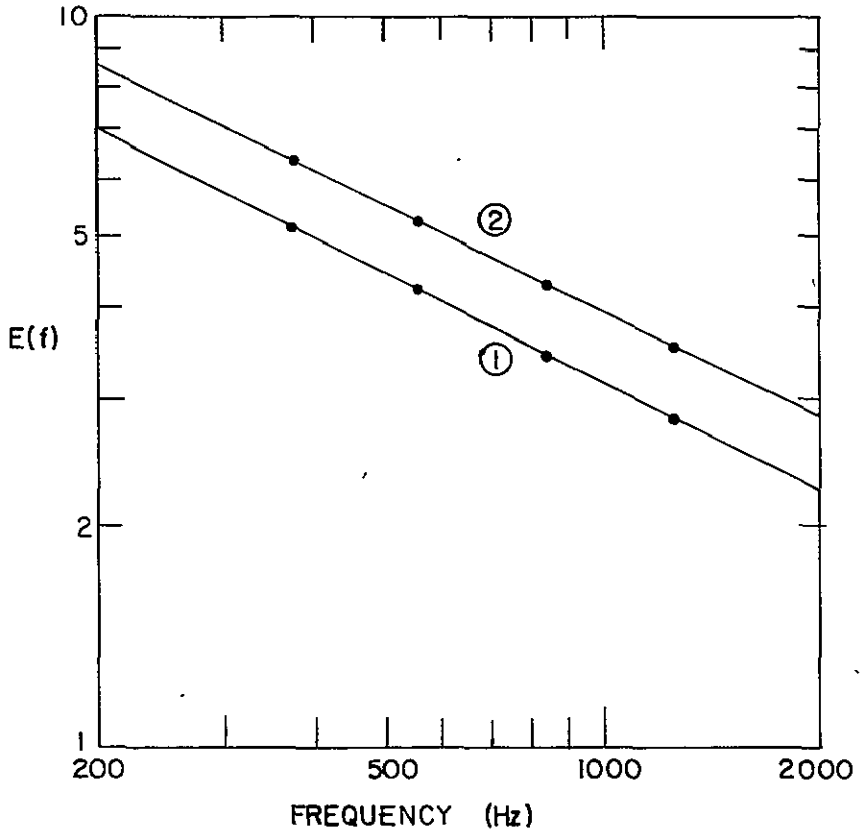

Figure 4.9 The effect of filter response on a spectrum having an index of -0.5. Line 1 is the assumed spectrum; line 2 is the calculated spectrum resulting from non-ideal response of the band-pass filter.

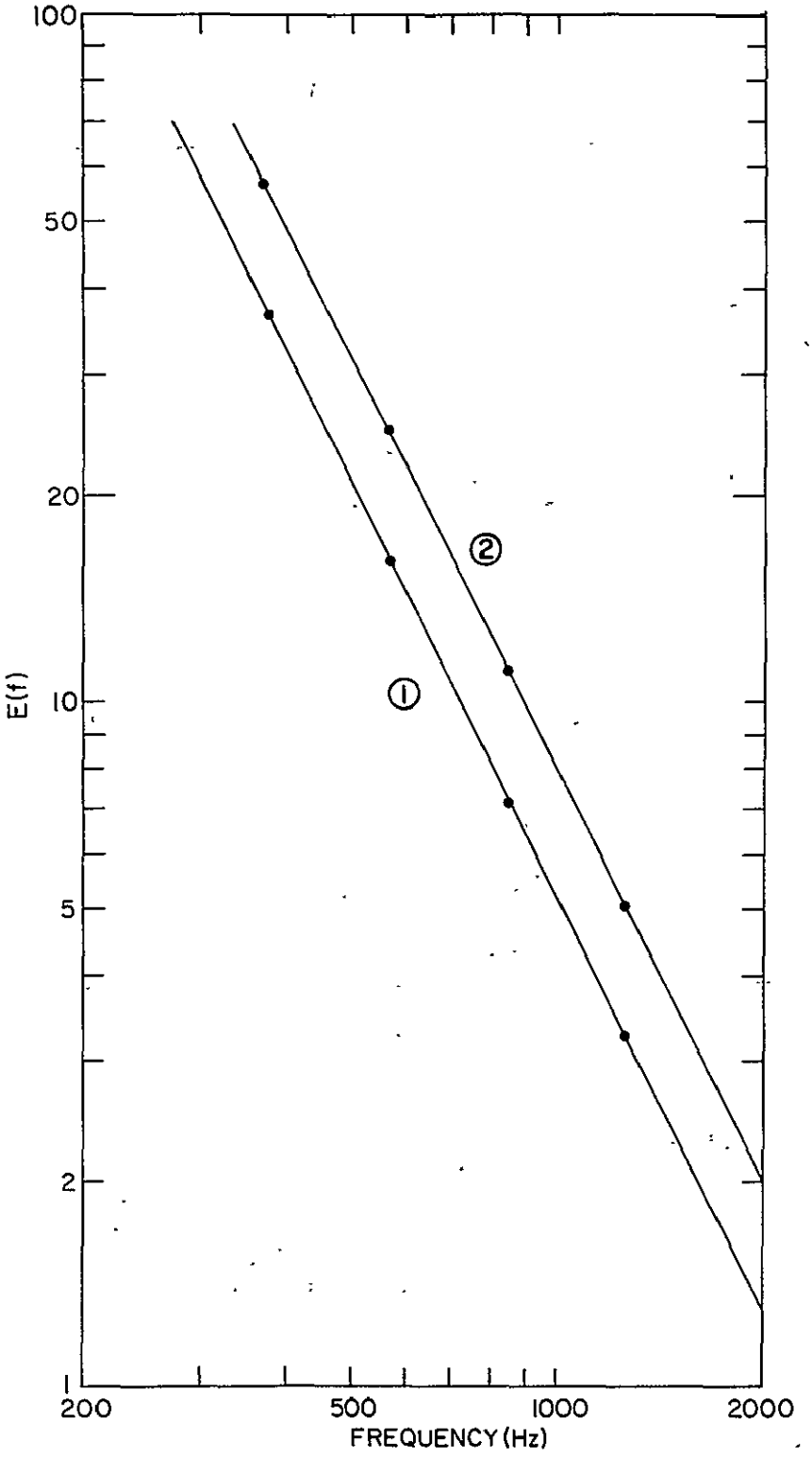

Figure 4.10 The effect of filter response on a spectrum having an index of -2.0. Line 1 is the assumed spectrum, line 2 is the calculated spectrum resulting from non-ideal response of the band-pass filter.

but the amplitudes increase by about 20% for the spectral index of -0.5 and about 60% for the spectral index of -2.0. The conclusion is that for the Peru data, with a spectral index between 0 and -2.5, little error exists in the spectral index due to imperfect filter response. The amplitudes will be overestimated, however, and a correction should be applied.

4.2.4 *Comparison with other observations.* *Prakash et al.* [1972] have conducted many rocket flights at Thumba, India at the geomagnetic equator to measure electron density and the associated fine structure. They have found during the daytime that small-scale irregularities (1 m to 15 m) start at about 95 km and continue up to rocket apogee at about 190 km. Figures 4.11 and 4.12 display irregularity and electron-density data from two daytime flights, 10.37 and 10.38. The peak amplitudes of the irregularities occur at 105 km corresponding to the peak of the electrojet current at Thumba. This is a narrower peak than was observed in Peru with Nike Apache 14.532 where a broader maximum between 105 and 115 km was found (see Figure 4.6). The data are in agreement, however, in the gradual decrease in amplitude towards the higher altitudes and sharp decrease towards lower altitudes. The conclusion is that much similarity exists between the Indian and Peruvian profiles of irregularity amplitude.

The spectral index n is displayed for 10.38 in Figure 4.13. The spectral index is seen to be large and negative at 95 km but then rapidly changes to a value of +1 at 100 km. Flight 14.532 shows a similar trend (see Figure 4.8) but the change ends at 105 km at n = -0.5 where it remains for the majority of the flight. In the Indian launch, n is zero between 110 km and 135 km after which it increases to about 0.5. The apparent discrepancy between the observations taken in India and those in Peru has not been explained. It might be noted that there is a considerable difference in the

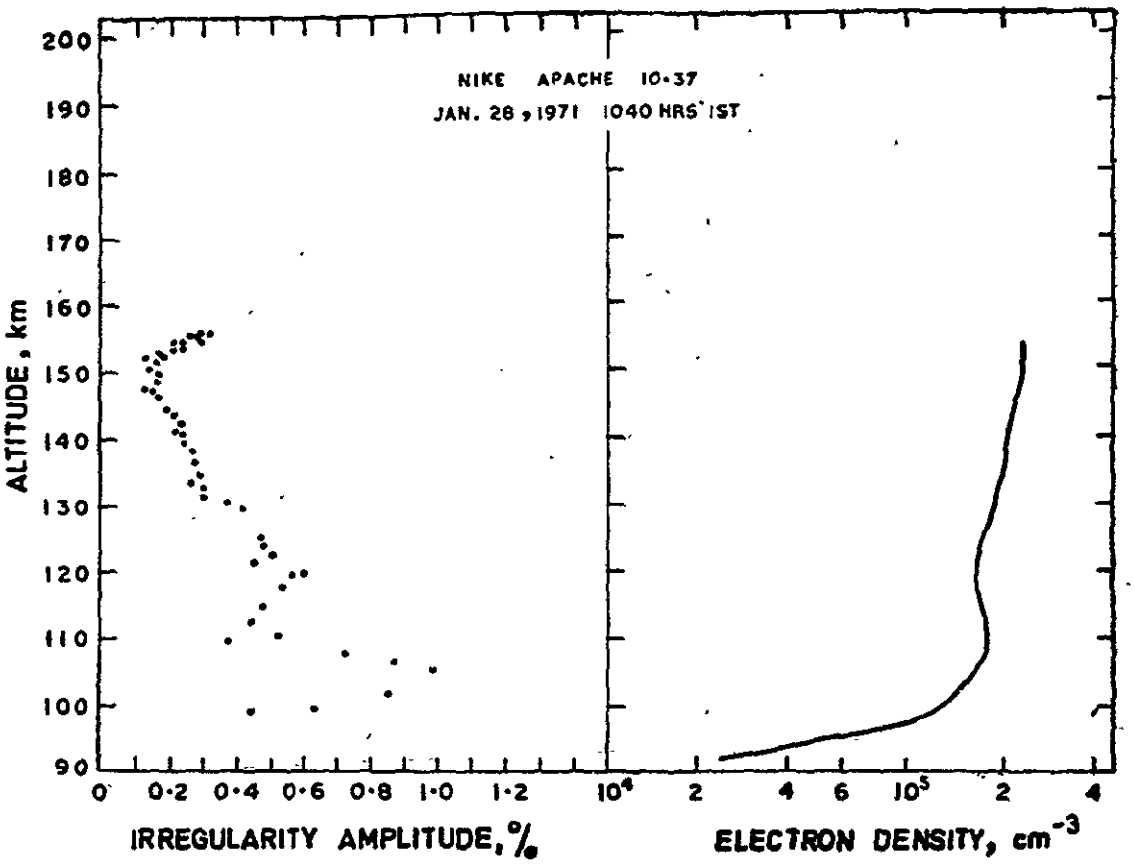

Figure 4.11 Amplitude of 1 to 15 m ionization irregularities detected on flight 10.37 at 1040 hrs IST on 28 January 1971. Also shown is the electron-density profile obtained from the on-board Langmuir probe and resonance probe experiments [*Prakash et al.*, 1972].

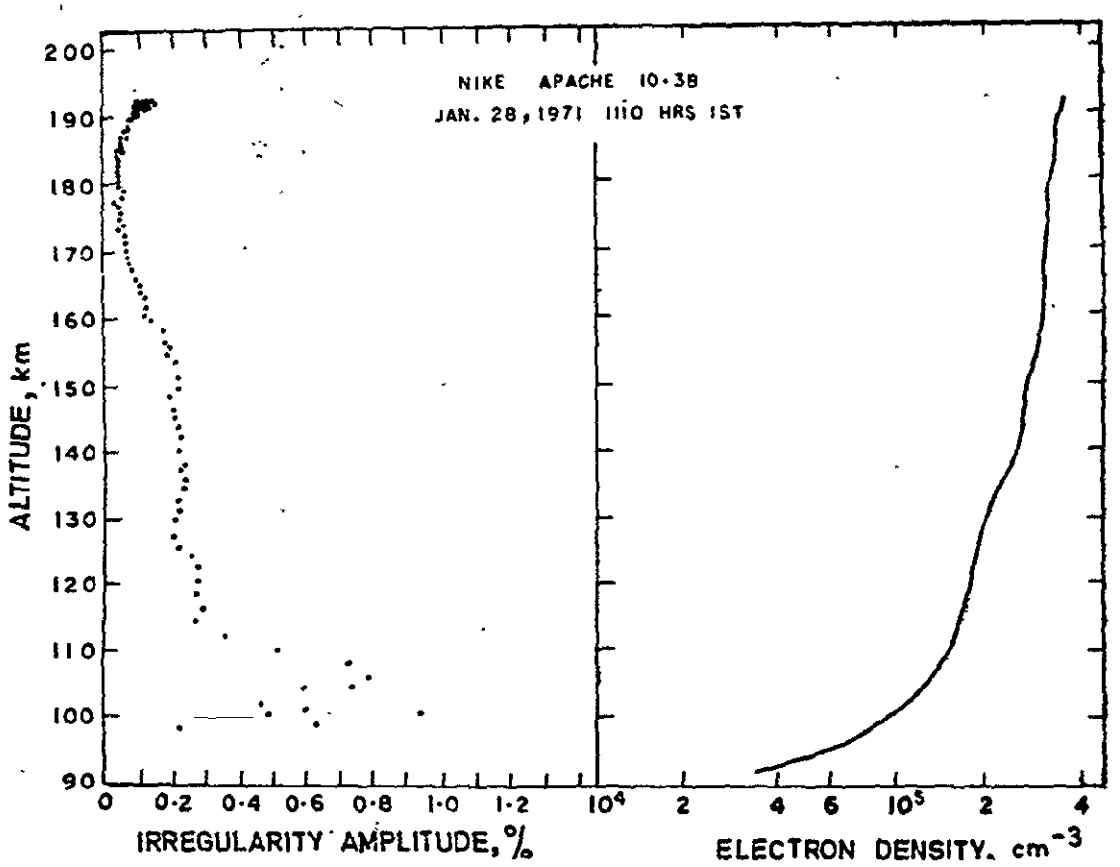

Figure 4.12 Amplitude of 1 to 15 m ionization irregularities detected on flight 10.38 at 1110 hrs IST on 28 January 1971. Also shown is the electron-density profile obtained from the on-board Langmuir probe experiment. [*Prakash et al.*, 1972]

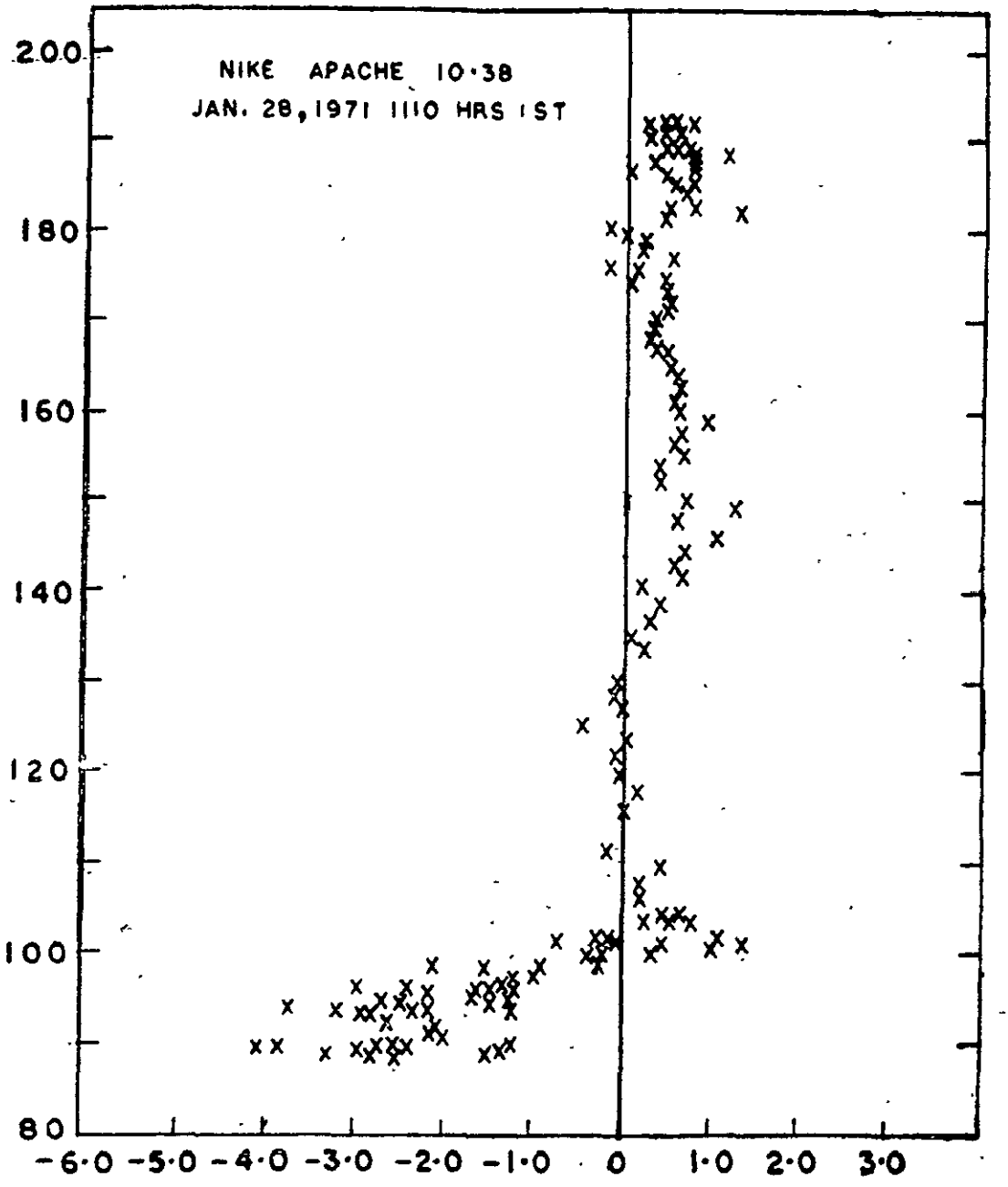

Figure 4.13 Spectral index n obtained from $E(k) \propto k^n$ for the 1 to 15 m irregularities of flight 10.38. The results for flight 10.37 were similar to those of 10.38 [*Prakash et al.*, 1972].

time of day of the observations: the Indian data are before noon; the Peru data are in the afternoon.

Using the 50 MHz Jicamarca radar capable of detecting only 3-m irregularities, *Fejer et al.* [1975] have made extensive studies of the electrojet region. They have found that during the day echoes are observed between 93 and 113 km, with a single maximum in the echo strength at approximately 103 km (Figure 4.14). The thinness of this region is in contrast with that of the rocket observations both in India and Peru. Fejer et al. believe that Prakash's data may be rather marginal and close to the noise level at the higher altitudes (above 120 km). They also state that the radar measurement having a dynamic range of the order of 60 dB is much more sensitive than the rocket measurement. Apparently irregularities as strong as the rocket studies indicate above 120 km would have given very strong radar signals, which are not observed. The chart record from Nike Apache 14.532 for band 4 (304-456 Hz corresponding to 3-4 m scale sizes) is shown in Figure 4.15. It is seen that the irregularities start at about 93 km and peak at 101 km with a magnitude of 0.15%. The irregularity amplitude then drops to about 0.10%. Above 115 km there is a slow decrease to the apparent noise floor at 170 km. The rocket data from Peru, like that from India, are in contradiction with those of Fejer et al. and no explanation is apparent. In contrast to what Fejer et al. remark about Prakash's data, data from the Peru launch appears clearly and is not lost in the noise. A small noise floor voltage is observed before the irregularities begin and after they end but this should have little effect on the data as it is taken into account in calculating $E(f)$.

4.3 *Nighttime Observations*

4.3.1 *Electron-density profiles.* Nike Apache 14.524 was launched from

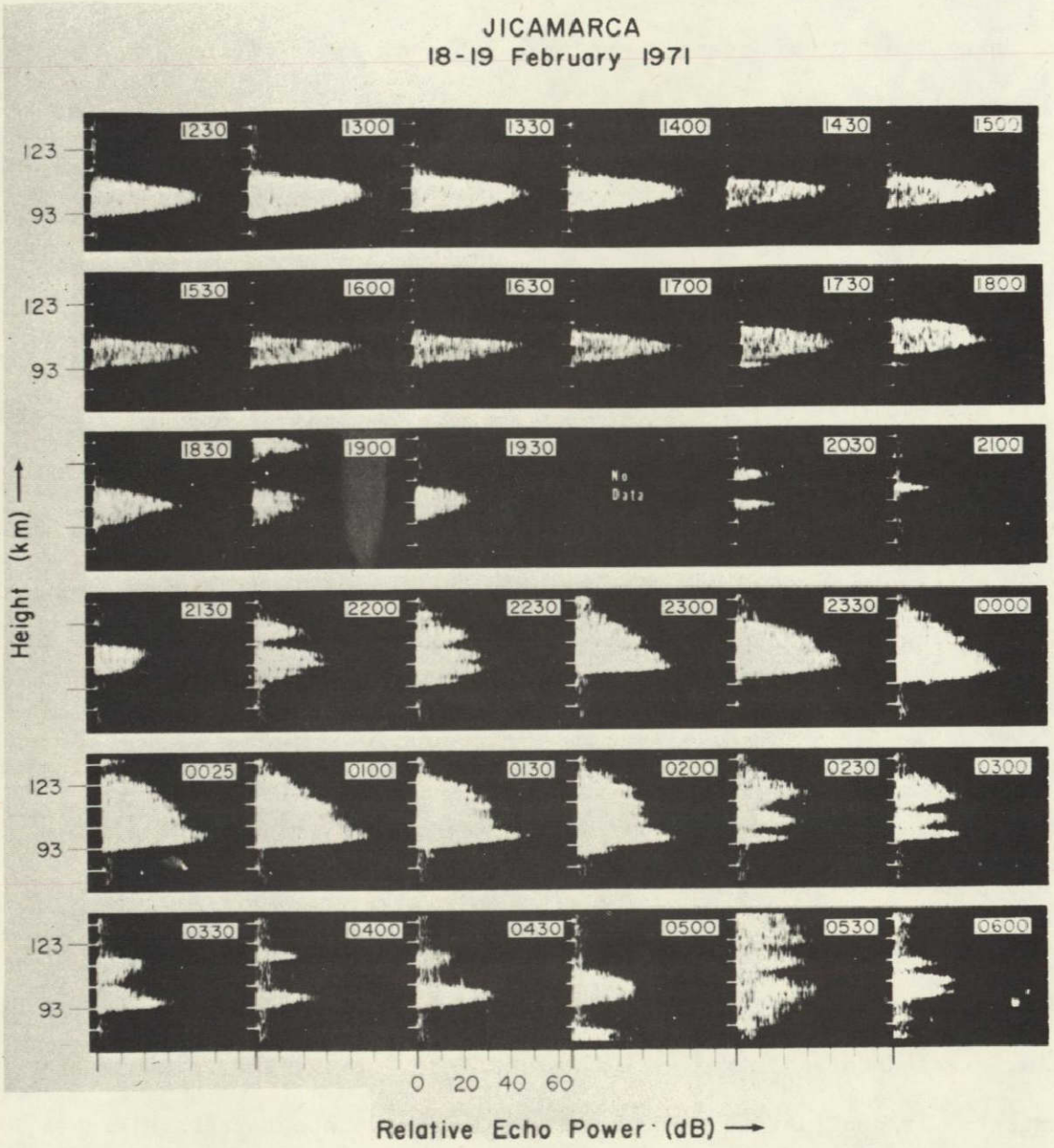

Figure 4.14 Power backscattered from the electrojet at 50 MHz. The large vertically directed incoherent scatter antenna at Jicamarca was used. Spread *F* comtaminated the data between 0405 and 0550 and perhaps at 1900. The times are local times (75°W or EST) [*Fejer et al.*, 1975].

the Chilca Range on 29 May 1975 at 2336 LST. Rocket apogee was 189 km. Magnetic activity was low with a Kp index of 2+. Huancayo ionograms, Figure 4.16 and the *f*-plot, Figure 4.17, show that spread *F* was not present at launch time. The launch of Nike Apache 14.525 took place at 0011 LST on 2 June 1975. Rocket apogee was 188 km. The Kp index was 5; this represents disturbed magnetic conditions. Huancayo ionograms near launch time are shown in Figure 4.18. Spread *F* was present throughout the entire night of 1-2 June as seen by the Huancayo *f*-plot, Figure 4.19.

The propagation experiment did not give any useful data on electron density. True-height analysis of Huancayo ionograms was possible for the first night but was done only above 200 km. True-height analysis was not possible on the second night because of spread *F*. Accordingly, the calibration factors from the daytime flight were used in the probe current calibration for both nighttime flights.

The electron-density profiles from the two nighttime rocket flights are shown in Figures 4.20 and 4.21 respectively. The profile for 29 May 1975 exhibits a sharp positive gradient above 80 km with few variations to a broad peak between 100 and 110 km. The density then rapidly falls off by an order of magnitude to a trough at about 135 km. Many large-scale fluctuations are seen in this negative gradient. Above 140 km, the density smoothly increases to 155 km. At greater altitudes the electron density is nearly constant.

The electron-density profile for the second night flight is in marked contrast to that just described. The lower boundary of the ionosphere is somewhat higher. Above a broad peak between 95 and 105 km there is a gradual decrease to a minimum at about 125 km then a rather steady increase in to rocket apogee.

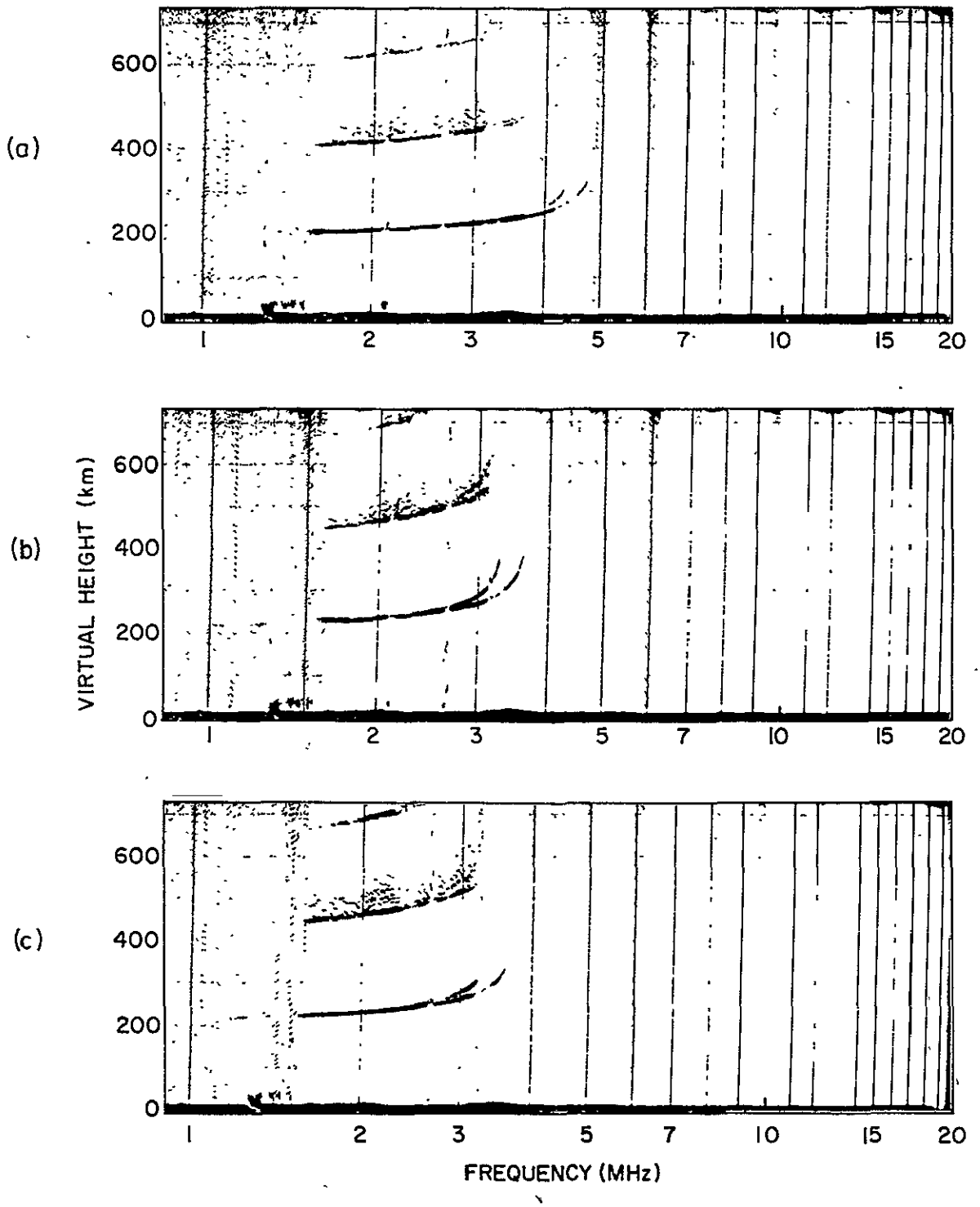

Figure 4.16 Ionograms recorded at (a) 2300, (b) 2330, and (c) 2400 LST, 29 May 1975 at Huancayo. Nike Apache 14.524 was launched at 2336 LST from the Chilca rocket range. [Data obtained from WDC-A for Solar Terrestrial Physics].

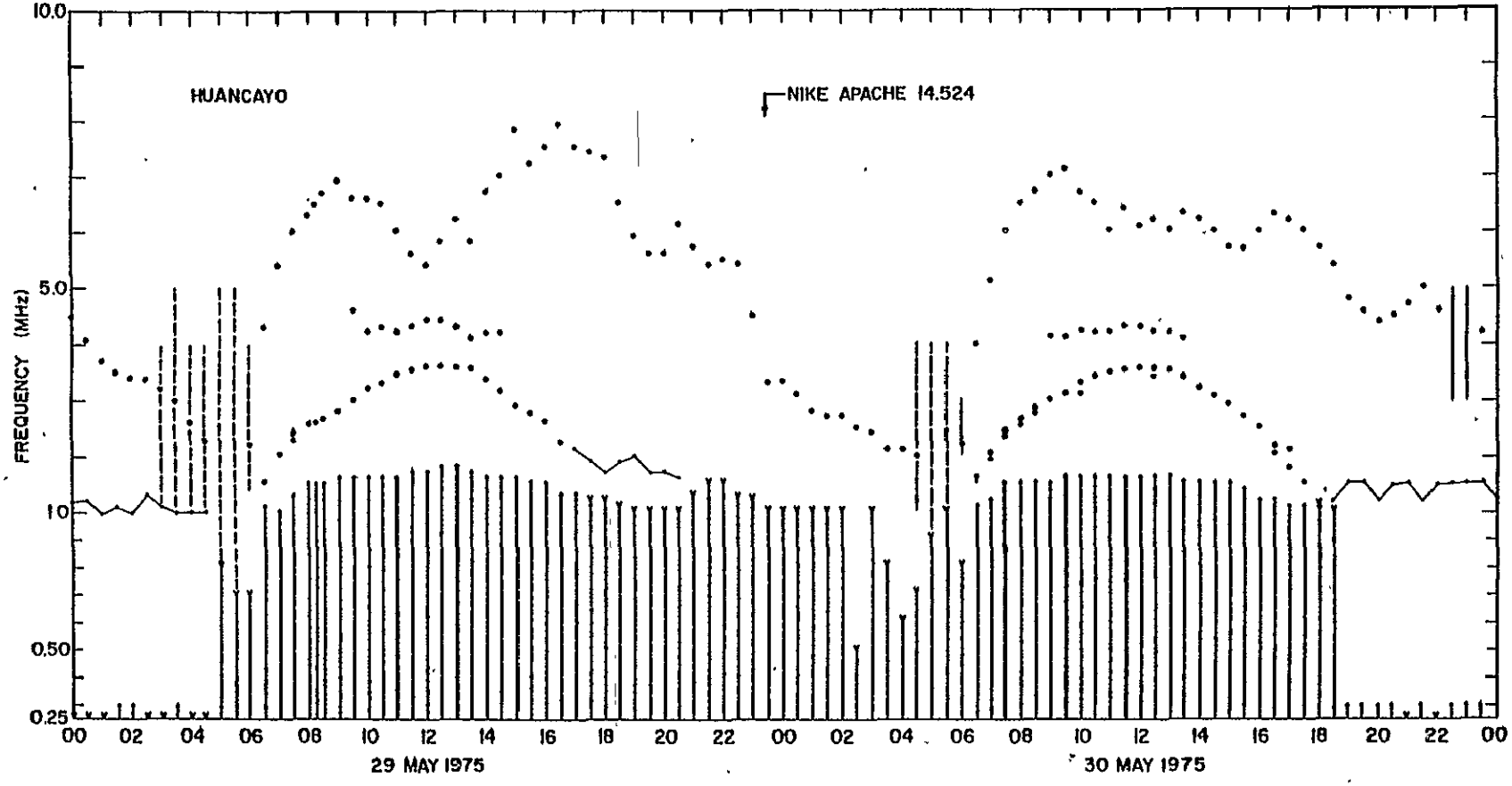

Figure 4.17 Huancayo f-plots for 29 and 30 May 1975. The launch time of Nike Apache 14.524 is indicated. [Data obtained from WDC-A for Solar Terrestrial Physics].

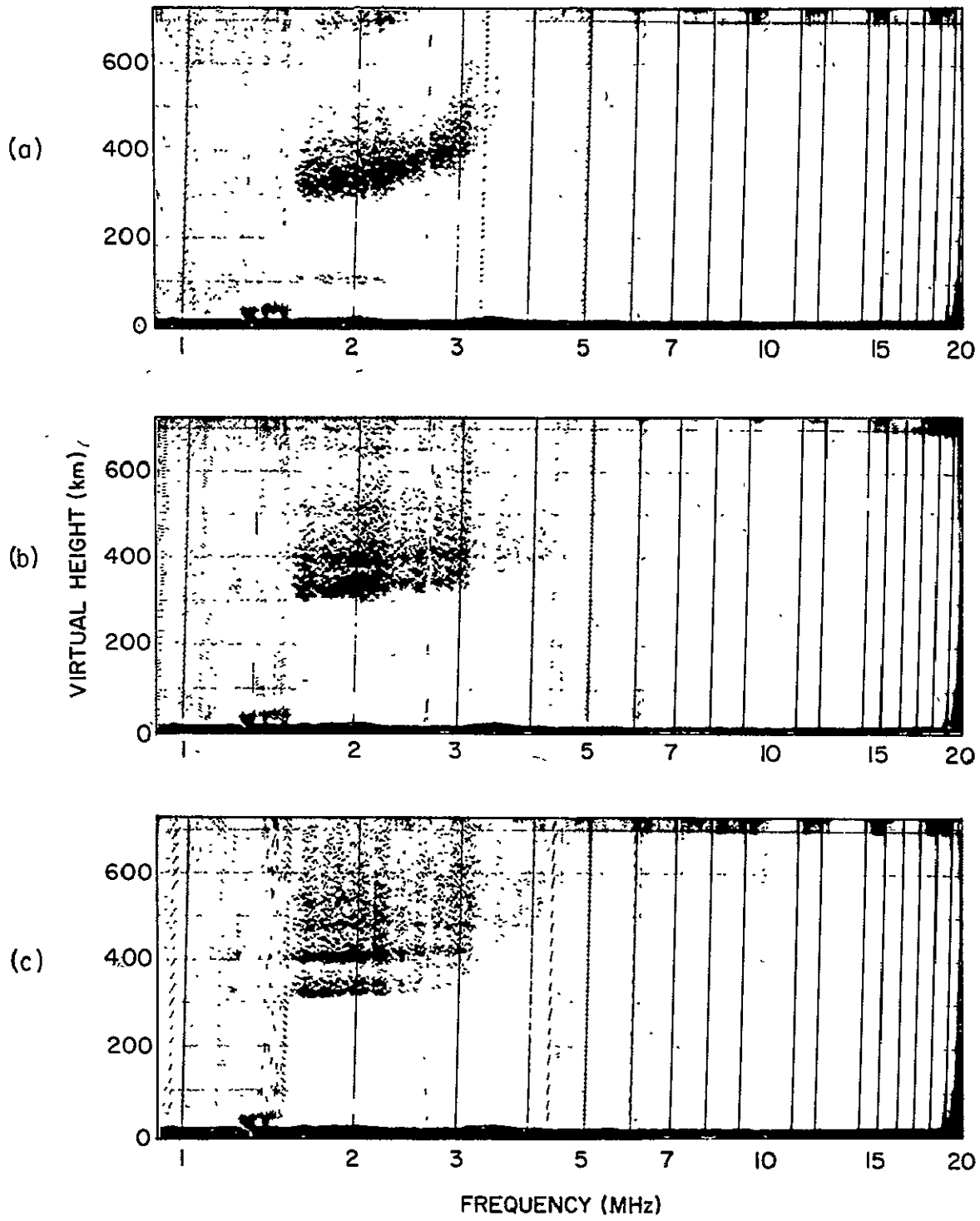

Figure 4.18 Ionograms recorded (a) at 2330 and (b) at 2400 LST, 1 June 1975; and (c) at 0030 LST, 2 June 1975 at Huancayo. Nike Apache 14.525 was launched at 0011 LST, 2 June 1975 from the Chilca rocket range. [Data obtained from WDC-A for Solar Terrestrial Physics].

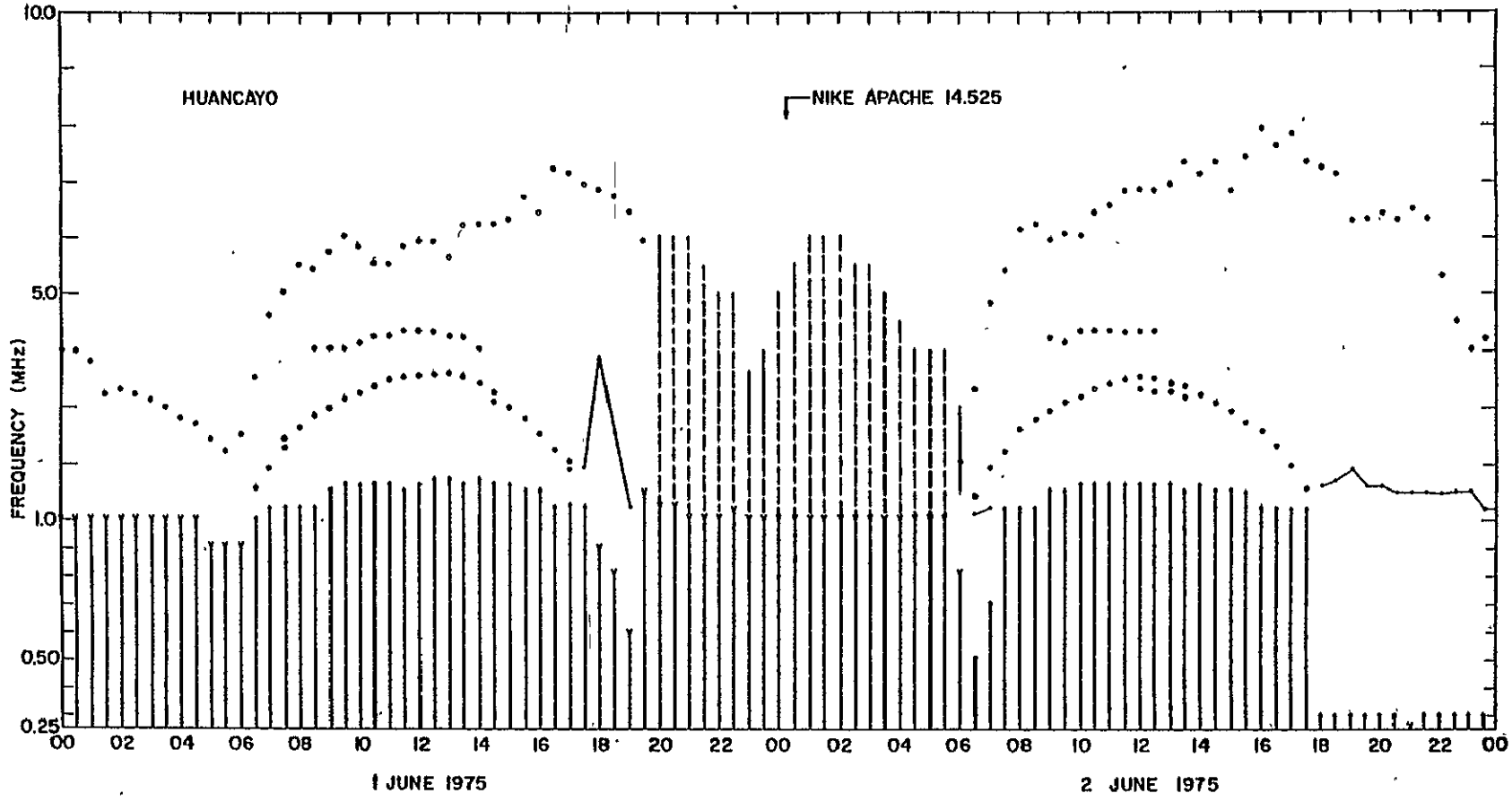

Figure 4.19 Huancayo *f*-plots for 1 and 2 June 1975. The launch time of Nike Apache 14.525 is indicated. [Data obtained from WDC-A for Solar-Terrestrial Physics].

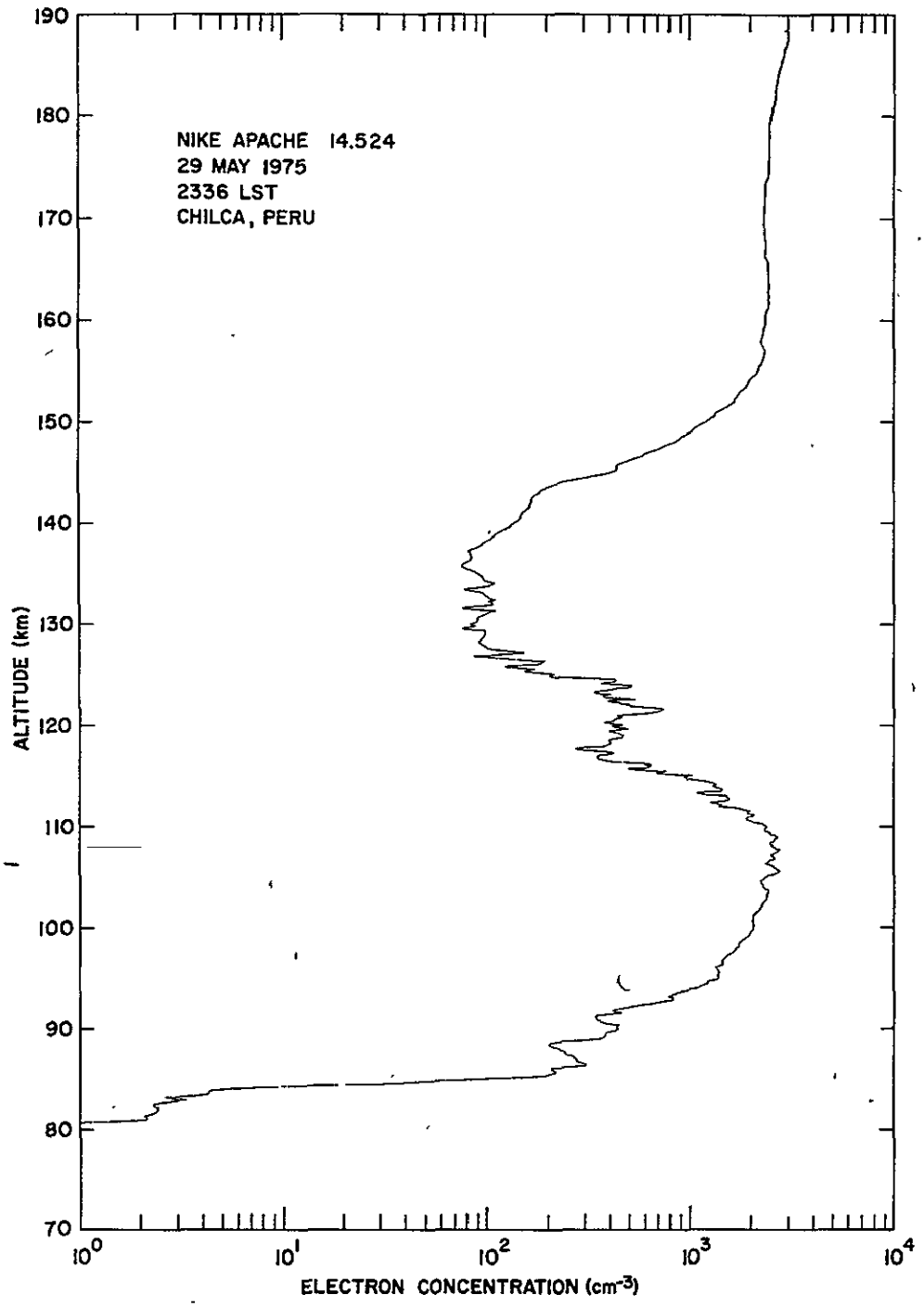

Figure 4.20 Electron concentration profile from Nike Apache 14.524. Huancayo ionograms show the absence of spread F at this time.

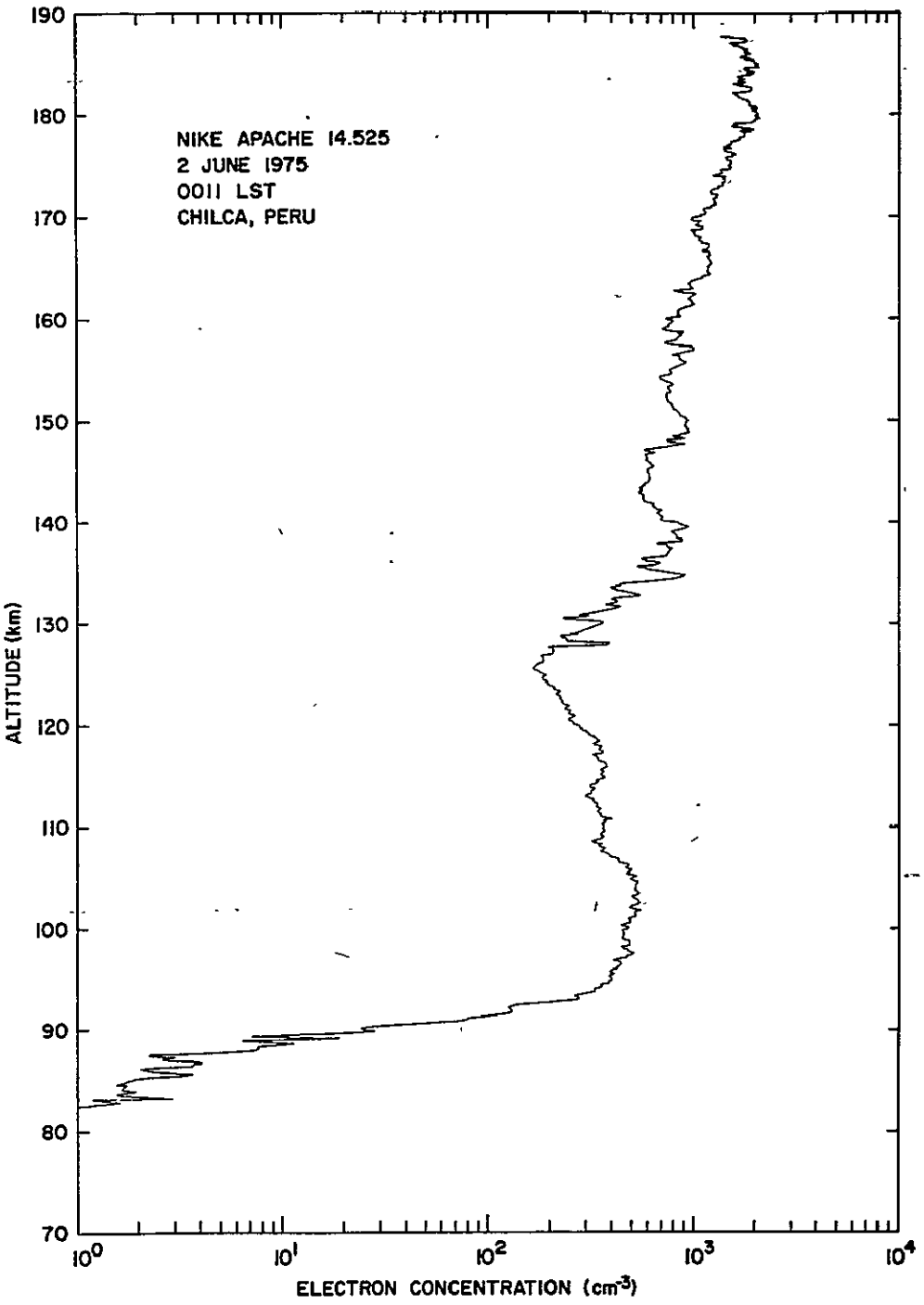

Figure 4.21 Electron concentration profile from Nike Apache 14.525. Huancayo ionograms show the presence of spread *F* at this time.

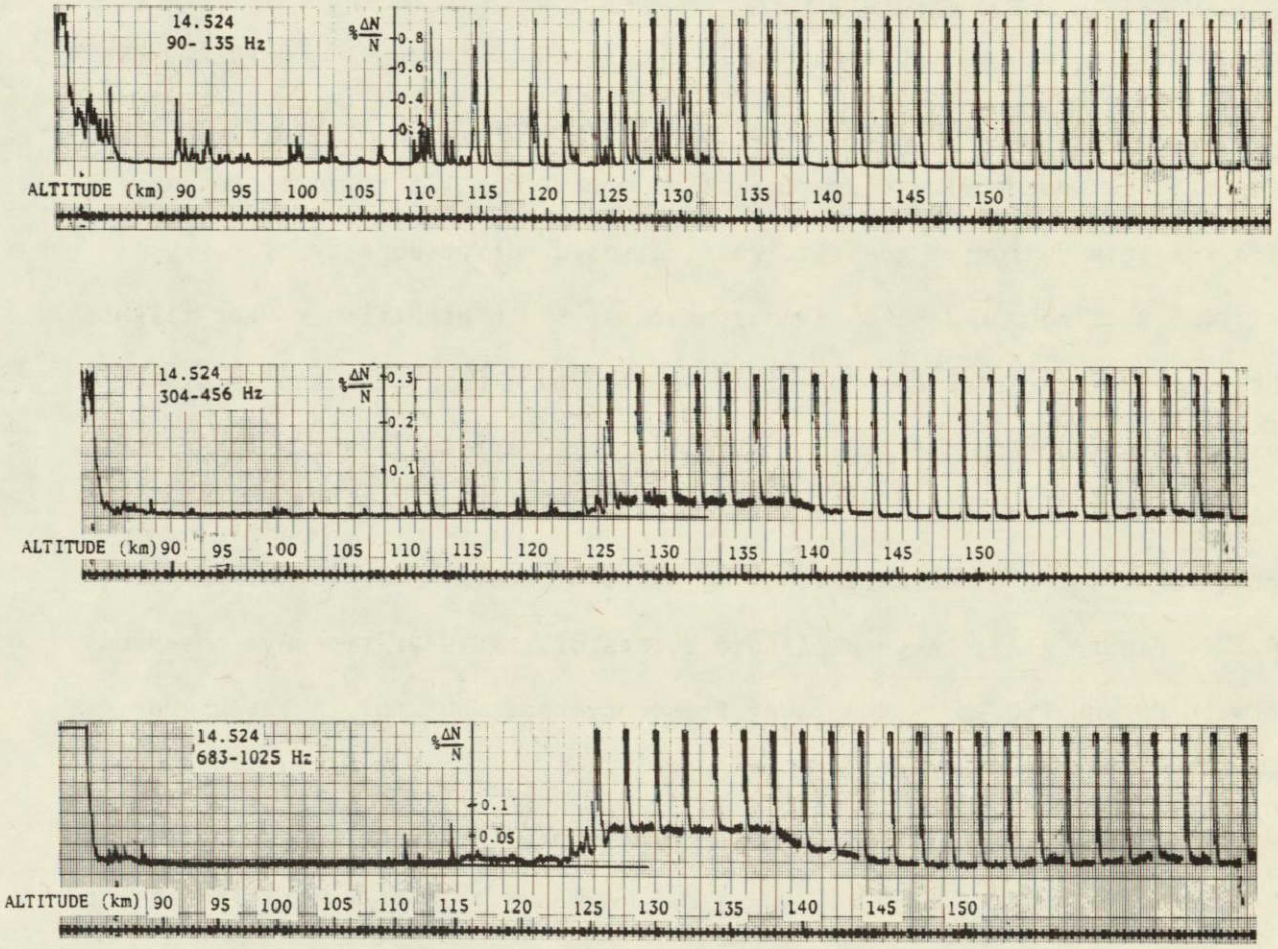

Figure 4.22 Irregularities in the frequency bands 1(90 to 135 Hz), 4(305 to 456 Hz) and 6(683 to 1025 Hz) observed on Nike Apache 14.524. The periodic large excursions at altitudes above 127 km result from the voltage sweep of the probe.

In addition to the major differences in the general features of these two midnight profiles there are obvious differences in the magnitude and altitudes of occurrence of the small-scale irregularities. (Recall that these profiles show structure >300 m). In the profile from the first night the irregularities are most pronounced in the altitude range of 110 to 135 km, a region of negative gradient of electron density. On the second night, however, the most obvious irregularities occur from 125 km to rocket apogee (188 km) in a region of positive gradient of electron density.

4.3.2 *Electron-density fine structure.* Both nighttime rocket flights were analyzed for electron-density fine structure using the analog system described in Section 3.4 and also used for the daytime flight. In neither case could a spectral index be determined due to the erratic nature of the irregularities. In the data from the first nighttime flights, Nike Apache 14.524, Figure 4.22, large amplitude bursts of irregularities are observed between 90 and 130 km in the lower frequency bands but not in the higher bands. At the same time that these noise spikes are diminishing, a broad region of irregularities begins to appear in the two higher bands between 125 and 145 km. As a result, band 1 (90 to 135 Hz) contains only bursts of irregularities while band 8 (1538 to 2307 Hz) shows a continuum of small-scale irregularities over a 20 km range (125 to 145 km). In relation to the electron-density profile, Figure 4.20, the small-scale irregularities correspond very well to the valley between 125 and 145 km. The larger scale bursts cannot be tied to specific large fluctuations but lie in the region where some moderate to large fluctuations exist.

The data from the second nighttime flight, Nike Apache 14.525, show a different type of irregularity structure. In the low frequency bands, Figure 4.23, bursts are observed between 90 and 107 km and between 130 and

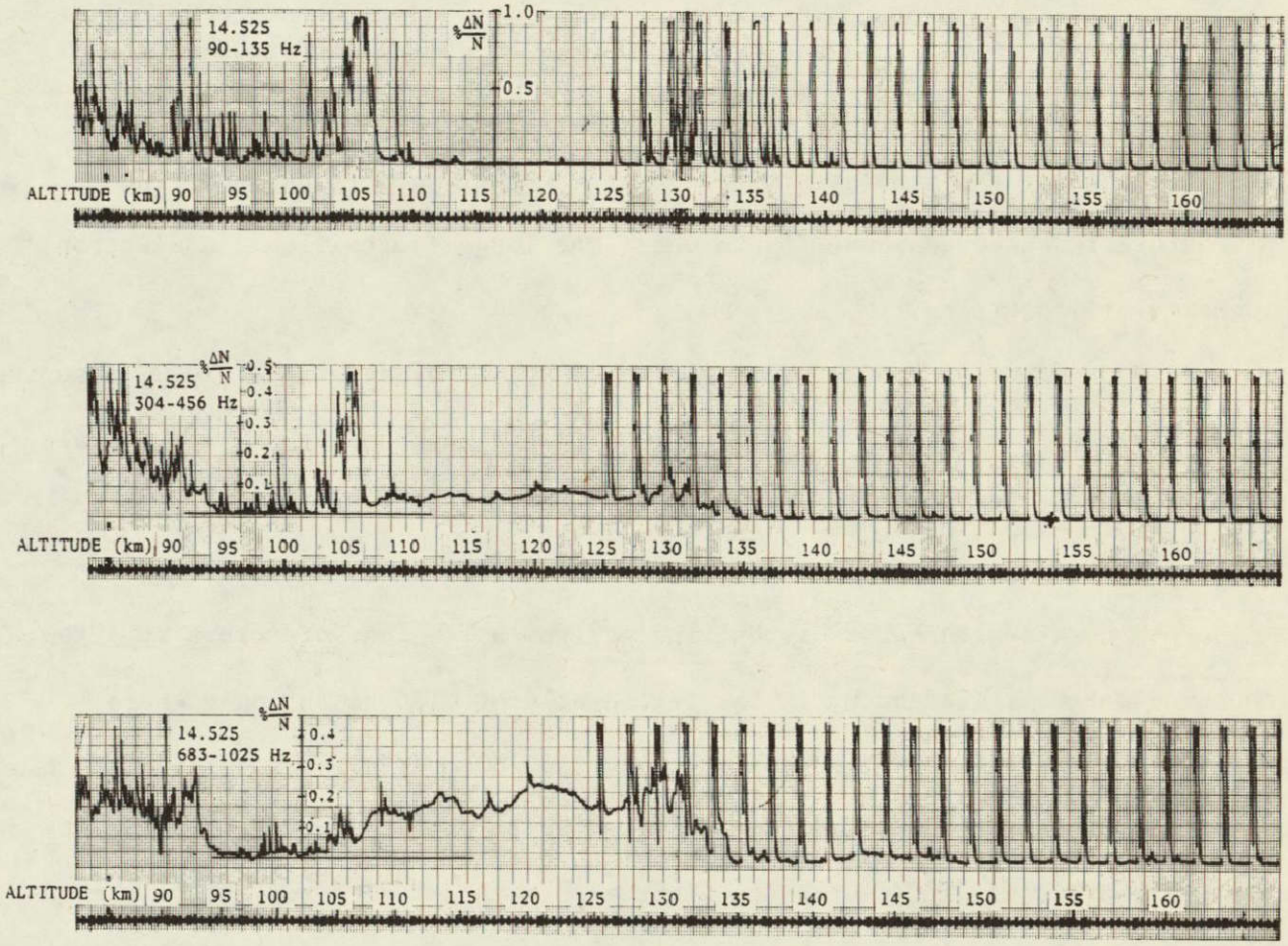

Figure 4.23 Irregularities in the frequency bands 1(90 to 135 Hz), 4(305 to 456 Hz) and 6(683 to 1025 Hz) observed on Nike Apache 14.525. The periodic large excursion at altitudes above 125 km result from the voltage sweep of the probe.

140 km. At 105 km a large burst is observed with an amplitude of 1% in band 1 (90 to 135 Hz). As the frequency increases, the magnitude of the bursts decreases and a continuous structure forms in the region from 105 to 135 km. The irregularities of greatest amplitude here are found in bands 4, 5, and 6 corresponding to scale sizes of about 1 to 4 m. Referring to the electron-density profile of Figure 4.21, fluctuations are apparent at the altitudes where the fine structure occurs. Rather surprisingly no fine structure is observed above 135 km where the large fluctuations in electron density are occurring.

4.3.3 *Comparison with other observations.* *Prakash et al.* [1972] describe the result of a nighttime flight and report that both small- and large-scale irregularities are present only in regions where the background electron-density profile exhibits a negative gradient. The irregularities occur in discrete bursts with burst widths ranging from a few tens of meters to a few hundred meters. They occur in the region of 90 to 130 km but only where there is a negative electron-density gradient. Comparing this data to the two Peru nighttime flights, some similarities can be observed. The Peru flights do exhibit bursts of fine structure but also have extended regions of irregularities irrespective of the sign and magnitude of the gradient of electron density.

Nighttime observations of 3-m irregularities with the 50 MHz backscattering radar at Jicamarca by *Fejer et al.* [1975] show a strongly layered structure. Large local power variations are observed, especially below about 100 km, with no apparent changes in the upper part. According to these authors recombination becomes negligible at night because of the much lower electron densities. This fact, together with the very jagged nature of the nighttime electron-density profile, leads to increased instability at night and

5. SUMMARY, SUGGESTIONS FOR FUTURE WORK, AND CONCLUSIONS

5.1 *Summary*

The equatorial electrojet is a 700-km wide current system centered on the magnetic dip equator. This electrojet is contained in the *E* region with a maximum current at about 105 to 110 km. The electrojet current flows eastward during the day, beginning at sunrise, reaching a peak at noon and decreasing towards sunset. Many studies have been made of this phenomenon including: magnetic field measurements using ground-based, rocket and satellite instrumentation; radio-wave experiments using ionosonde and VHF radar; and *in situ* observations of electron-density irregularities using rocket-borne probes.

Electron-density irregularities resulting from plasma instabilities generated by the electrojet cause a radio-wave scattering phenomenon in the *E* region, equatorial sporadic *E*, frequently seen in daytime ionograms. VHF radar experiments at 50 MHz show two distinct varieties of irregularities, type I and type II. They also show that type II irregularities are the irregularities recorded as equatorial sporadic *E*.

Prakash has shown the first *in-situ* evidence of irregularities obtained by instrumentation on rockets launched from Thumba, India near the dip equator. Through the use of various experiments, Prakash has identified several different types of irregularities. These studies have greatly helped in postulating the causative mechanisms of the ionization irregularities.

Three Nike Apache rockets instrumented by the Aeronomy Laboratory were launched in May and June 1975 from the Chilca Range, Peru close to the magnetic dip equator. The instrumentation of each payload included a dc probe experiment to measure electron density and its fine structure. This fine-structure experiment was designed to observe electron-density irregu-

larities in the size range of 0.5 to 15 m. Because of the high velocity of the rocket these irregularities appear as noise on the probe current in the frequency range 90 to 2300 Hz.

A data reduction system using a variable bandpass filter, precision ac-dc converter, and chart recorder was used to analyze these irregularities. By adjusting the filter for eight different frequency bands, the spectral nature of the irregularities was determined. The data can be represented by a power law $E(f) \propto f^n$ where $E(f)$ is the rms amplitude of $\Delta N/N$ in a specified band divided by the bandwidth, f is the frequency, and n is the spectral index. For the daytime flight, in the high frequency bands the noise signal had a broad maximum between 105 and 115 km with a rapid decrease at lower altitudes and a more gradual decrease to higher altitudes. In the low frequency bands the variation is parallel to that of the high frequency bands for altitudes of 105 km and above but shows a marked difference at lower altitudes. This change is observed in the spectral index n. Between 105 and 155 km the spectral index is -0.51 ± 0.01. Below 105 km much larger (negative) values are seen. This difference appears to be due to a difference in generating mechanisms of the irregularities.

The other two flights were conducted near local midnight. The structure of the irregularities was erratic with bursts of irregularities at the low frequencies being seen above about 90 km. At the higher frequencies the bursts were not apparent but continuous regions of irregularities appeared in both cases. No spectral index could be obtained for these night flights.

5.2 *Suggestions for Future Work*

The fine structure experiment used in the Peru launches was successful but several improvements could be made in the present system. The most important is that of providing more gain in the rocket-borne ac

amplifier. Originally it was thought that irregularities greater than 1% would be observed. This led to the design of an ac amplifier capable of measuring $\Delta N/N$ up to 7%. Irregularities of amplitudes this large were not observed and the gain of the amplifier could safely be increased by a factor of 2. This stronger data signal would help eliminate some of the noise problems encountered at the highest frequencies. Since the data signal decreases at approximately 3 dB/octave, another possibility for improvement of the circuit is to provide pre-emphasis in the ac amplifier. A pre-emphasis of 3 or 6 dB/octave would increase the high frequency components and provide a higher signal-to-noise ratio in an area of the spectrum where noise is more prevalent. De-emphasis of the data signal could easily be incorporated in the data reduction process.

A problem that appeared on the daytime flight was interference from the resonance probe. This occurred through perturbations of the vehicle potential relative to the plasma. The probe caused noise spikes every one-half second in the fine structure data which hindered the data analysis. Elimination of this interference would be very helpful.

In the present data reduction system, the greatest improvement would be in the variable bandpass filter. A rolloff outside the bandpass on the order of 36 dB/octave or greater would significantly reduce leakage from adjacent bands in order that the amplitude of the irregularities be more accurately measured.

Two digital techniques involving computer algorithms exist which could possibly aid in the data reduction process. In both of these processes the data is sampled at greater than the Nyquist frequency (typically 5 kHz for the fine structure experiment). The first is a fast Fourier transform (FFT) which processes data samples obtained during a discrete time interval. The

output is composed of discrete linearly-spaced frequency components and is the Fourier transform for that time span. The frequency resolution obtained is proportional to the number of data samples read in. A possible problem exists with noise spikes (such as due to the resonance probe) which would have to be avoided for accurate results.

Perhaps more appropriate to the fine structure data for calculating the power spectrum is the nested variance technique [*Owens*, 1977]. This method is possibly superior to the FFT in this case because it gives spectral estimates logarithmically-spaced in frequency, it takes less computing time, and it easily accommodates gaps in the data. The nested variance technique appears to be suitable for this type of data analysis and should be seriously investigated.

There are also possibilities for partially processing the signal in the payload. With the advent of complex integrated circuits, spectrum analyzers on a chip now exist. These chips use charge-coupled devices and produce the power spectral density of the input signal. In one such, 512 time samples are used as inputs with the resulting output an equal number of frequency coefficients. Processing time is 250 μs once the samples are taken. The coefficients would then be telemetered to the ground where they would be recorded and analyzed for a spectral index. A main advantage would be the elimination of the possibility of telemetry noise from the fine structure data. In addition a microprocessor in the payload could be used to obtain the spectral index which would then be transmitted. This on-board analyzer has much potential and should be looked into as a possible replacement and/or addition to the present system.

5.3 *Conclusions*

The University of Illinois fine structure experiment and its associated

analog data reduction system has provided more insight into the composition of the electrojet. The experimental set-up has been described in detail with the idea that the fine structure experiment could be accurately repeated in the future. The observations show a definite association between the daytime irregularities and the equatorial electrojet. Comparison of these results with those of the Indian rocket studies and the VHF radar studies show many similarities but also several major discrepancies. To resolve these differences, more research will have to be done in order to obtain a better understanding of the electrojet and its associated *E*-region irregularities.

REFERENCES

Balsley, B. B. [1969], Some characteristics of non-two-stream irregularities in the equatorial electrojet, *J. Geophys. Res. 74*, 2333-2347.

Balsley, B. B. and D. T. Farley [1971], Radar studies of the electrojet at three frequencies, *J. Geophys. Res. 76*, 8341-8351.

Balsley, B. B.; G. Haerendel and R. A. Greenwald [1972], Equatorial spread *F*: Recent observations and a new interpretation, *J. Geophys. Res. 77*, 5625-5628.

Balsley, B. B.; A. Rey and R. F. Woodman [1976], On the plasma instability mechanisms responsible for E_{sq}, *J. Geophys. Res. 81*, 1391-1396.

Beer, T. [1974], On the dynamics of equatorial spread *F*, *Australian J. Physics 27*, 391-400.

Bowles, K. L. and R. Cohen [1962], A study of radio wave scattering from sporadic *E* near the magnetic equator, *Ionospheric Sporadic-E* (edited by E. K. Smith and S. Matsushita), Pergamon Press, Oxford, 51-77.

Bowles, K. L.; B. B. Balsley and R. Cohen [1963], Field-aligned *E*-region irregularities identified with acoustic plasma waves, *J. Geophys. Res. 68*, 2485-2501.

Burrows, K. [1970], The day-to-day variability of the equatorial electrojet in Peru, *J. Geophys. Res. 75*, 1319-1323.

Burrows, K. and T. S. G. Sastry [1976], Rocket measurements of current distribution in a normal and an intense equatorial electrojet, *J. Atmos. Terr. Phys. 38*, 307-311.

Cahill, L. J., Jr. [1959], Investigation of the equatorial electrojet by rocket magnetometer, *J. Geophys. Res. 64*, 489-503.

Cain, J. C., A. Onwumechilli, P. M. Mayaud, and E. Oni [1973], Summary and future work, *J. Atmos. Terr. Phys. 35,* 1281-1282.

Cain, J. C. and R. E. Sweeney [1973], The Pogo data, *J. Atmos. Terr. Phys. 35,* 1231-1247.

Chapman S. [1952], The earth's magnetism, *Arch. Meteoro. Geophys. Bioklim.A4,* 368.

Clemesha, B. R. and R. W. H. Wright [1966], A survey of equatorial spread *F*, *Spread F and Its Effects upon Radiowave Propagation and Communication* (edited by P. Newman), Technivision, Maidenhead, England, 3-27.

Cole, K. D. [1974], Energetics of and a source of energy for equatorial spread-*F* events, *J. Atmos. Terr. Phys 36,* 1099-1102.

Davis, T. N., K. Burrows and J. D. Stolarik [1967], A latitude survey of the equatorial electrojet with rocket-borne magnetometers, *J. Geophys Res. 72,* 1845-1861.

Egedal, J. [1947], The magnetic diurnal variation of the horizontal force near the magnetic equator, *Terr. Mag. Atmos. Elect. 52,* 449.

Egedal, J. [1948], Daily variation of the horizontal magnetic force at the magnetic equator, *Nature 161,* 443-444.

Farley, D. T. [1971], Radio wave scattering from the ionosphere, *Methods of Experimental Physics -- Vol. 9, Plasma Physics* (edited by R. H. Lovberg and H. R. Griem), 139-186.

Farley, D. T., B. B. Balsley, R. F. Woodman and J. P. McClure [1970], Equatorial spread *F*: Implications of VHF radar observations, *J. Geophys. Res. 75,* 7199-7216.

Fejer, B. G., D. T. Farley, B. B. Balsley and R. F. Woodman [1975], Vertical structure of the VHF backscattering region in the equatorial electrojet and the gradient drift instability, *J. Geophys. Res. 80,* 1313-1324.

Fillinger, R. W., E. A. Mechtly and E. K. Walton [1976], Analysis of sounding rocket data from Punta Chilca, Peru, *Aeron. Rep. No. 73*, Aeron. Lab., Dep. Elec. Eng., Univ. Ill., Urbana-Champaign.

Forbush, S. E. and M. Casaverde [1961], Equatorial electrojet in Peru, *Carnegie Institution of Washington Publication 620*, Washington, DC.

Hanson, W. B., J. P. McClure and D. L. Sterling [1973], On the cause of equatorial spread *F*, *J. Geophys. Res. 78*, 2353-2356.

Hirao, K. and K. Oyama [1970], An improved type of electron temperature probe, *J. Geomag. Geoelect. 22*, 393-402.

Knecht, R. W. and R. E. McDuffie [1962], On the width of the equatorial E_s belt, *Ionospheric Sporadic E* (edited by E. K. Smith and S. Matsushita), Pergamon Press, 215-218.

Matsushita, S. [1951], Intense E_s ionization near the magnetic equator, *J. Geomag. Geoelect. 3*, 44.

Maynard, N. C. [1967], Measurements of ionospheric currents off the coast of Peru, *J. Geophys. Res. 72*, 1863-1875.

Mechtly, E. A., S. A. Bowhill, L. G. Smith and H. W. Knoebel [1967], Lower ionosphere electron density and collision frequency from rocket measurements of Faraday rotation, differential absorption and probe current, *J. Geophys. Res. 72*, 5239-5245.

Mechtly, E. A., P. E. Monro, N. Golshan, and R. S. Sastry [1970], Fortran programs for calculating lower ionosphere electron densities and collision frequencies from rocket data, *Aeron. Rep. No. 37*, Aeron Lab., Dep. Elec. Eng., Univ. Ill., Urbana-Champaign.

Morse, F. A., B. C. Edgar, H. C. Koons, C. J. Rice, W. J. Heikkila, J. H. Hoffman, B. A. Tinsley, J. D. Winningham, A. B. Christensen, R. F. Woodman, J. Pomalaza, and N. R. Teixeira [1977], Equion, an equatorial ionospheric irregularity experiment, *J. Geophys. Res. 82*, 578-592.

National Semiconductor Corporation [1972], *Linear Applications Handbook*, AN31-12, LB8-1 and LB8-2.

Onwumechilli, A. [1967], Geomagnetic variations in the equatorial zone, *Physics of Geomagnetic Phenomena* (edited by S. Matsushita and W. H. Campbell), Academic Press, New York, 425-507.

Owens, A. J. [1977], The nested variance power spectrum, *J. Geophys. Res. 82*, 3315-3318.

Piggott, W. R. and K. Rawer [1972] (editors), URSI Handbook of Ionogram Interpretation and Reduction, 2nd edition, *Report UAG-22 from World Data Center A for Solar-Terrestrial Physics*.

Prakash S. and B. H. Subbaraya [1967], Langmuir probe for the measurement of electron density and electron temperature in the ionosphere, *Rev. Sci. Inst. 38*, 1132.

Prakash, S., B. H. Subbaraya and S. P. Gupta [1968], A study of the equatorial *E*-region during evening twilight using a Langmuir probe, *J. Atmos. Terr. Phys. 30*, 1193-1202.

Prakash, S., S. P. Gupta, and B. H. Subbaraya [1969a], Irregularities in the equatorial *E* region over Thumba, India, *Radio Sci. 4*, 791-796.

Prakash, S., B. H. Subbaraya and S. P. Gupta [1969b], A study of the lower ionosphere over the geomagnetic equator at Thumba using a Langmuir and plasma probe, *Space Res. IX*, 237-245.

Prakash, S., S. P. Gupta, and B. H. Subbaraya [1970], A study of the irregularities in the night time equatorial *E*-region using a Langmuir probe and plasma noise probe, *Planet. Space Sci. 18,* 1307-1318.

Prakash, S., B. H. Subbaraya, and S. P. Gupta [1971a], Investigation of the daytime lower ionosphere over the equator using Langmuir and plasma noise probe, *J. Atmos. Terr. Phys. 33,* 129-135.

Prakash, S., S. P. Gupta and B. H. Subbaraya [1971b], Experimental evidence for cross-field instability in the equatorial ionosphere, *Space Res. XI,* 1139-1145.

Prakash, S., S. P. Gupta, and B. H. Subbaraya [1971c], Cross field instability and ionization irregularities in the equatorial *E* region, *Nature Physical Science 230,* 170-171.

Prakash, S., S. P. Gupta, B. H. Subbaraya and C. L. Jain [1971d], Electrostatic plasma instabilities in the equatorial electrojet, *Nature Physical Science 233,* 56-58.

Prakash, S., B. H. Subbaraya, and S. P. Gupta [1972], Rocket measurements of ionization irregularities in the equatorial ionosphere at Thumba and identification of plasma instabilities, *Ind. J. Radio Space Phys. 1,* 72-80.

Prakash, S., S. P. Gupta, B. H. Subbaraya, and H. S. S. Sinha [1973], A review of the in situ measurements of *E* region irregularities, *COSPAR,* Konstanz, Germany.

Prakash, S., S. P. Gupta, H. S. S. Sinha and T. R. Rao [1976], Ionization irregularities in the *E* region during counter electrojet, *Space Res. XVI,* Akademie-Verlag, Berlin.

Richmond, A. D. [1973], Equatorial electrojet -- I. Use of the model to study the equatorial ionosphere, *J. Atmos. Terr. Phys. 35,* 1105-1118.

Röttger, J. [1973], Wave-like structures of large-scale equatorial spread-*F* irregularities, *J. Atmos. Terr. Phys. 35,* 1195-1206.

Schutz, S. R., L. G. Smith, and H. D. Voss [1975], Electron heating rates in the *E* and lower *F* regions, *Radio Sci. 10,* 289-296.

Shuman, B. M. [1970], Rocket measurements of the equatorial electrojet, *J. Geophys. Res. 75,* 3889-3901.

Singer, S. F., E. Maple, and W. A. Bowen, Jr. [1951], Evidence for ionospheric current from rocket experiments near geomagnetic equator, *J. Geophys. Res. 56,* 265-281.

Smith, L. G. [1967], Langmuir probes for measurements in the ionosphere, Revised version of Tech. Manual Series, *COSPAR Bulletin No. 17* (edited by K. Maeda).

Smith, L. G., R. K. Zimmerman, K. Hirao, K. Oyama, and C. Calderon [1978], Electron temperature in the equatorial *E* region measured by two rocket experiments and by incoherent scatter, *Space Res. 18,* 265-268.

Voss, H. D. and L. G. Smith [1974], Design and calibration of a rocket-borne electron spectrometer for investigation of particle ionization in the nighttime midlatitude *E* region, *Aeron. Rep. No. 62,* Aeron. Lab., Dep. Elec. Eng., Univ. Ill., Urbana-Champaign.

Voss, H. D. and L. G. Smith [1977], Energetic particles and ionization in the nighttime middle and low latitude ionosphere, *Aeron. Rep. No. 78,* Aeron. Lab., Dep. Elec. Eng., Univ. Ill., Urbana-Champaign.